# THE GROWTH IMPLICATIONS OF WOMEN'S REPRODUCTIVE FREEDOM

Yimei Zou*

February 2026

**Abstract**

I study the growth and welfare implications of women's reproductive freedom, defined as the ability to control the timing and incidence of childbearing. I develop and quantify a continuous-time overlapping-generations growth model in which women choose fertility over the life cycle as a stochastic dynamic decision, subject to reproductive aging, contraception effectiveness, and child penalties on human capital accumulation. The irreversibility of motherhood makes first births qualitatively different from subsequent births and creates an age-dependent incentive to delay entry into motherhood. In equilibrium, individual fertility choices shape the joint distribution of population over age and income, while endogenous intergenerational human capital spillovers generate sustained growth in output per capita. Calibrating the model to U.S. data from 1961–2019, I show that the post-1961 improvements in contraception effectiveness account for 44% of the increase in female labor supply and 32% of the rise in female labor productivity during this period. Aggregate welfare gains from these improvements amount to 28–37% of lifetime consumption, depending on the social discount rate. Projections further show that, conditional on the same long-run population growth target, policies that reduce motherhood career penalties dominate restrictions on reproductive freedom in terms of productivity and welfare.

**Keywords**: Endogenous Growth, Overlapping Generations, Fertility, Contraception, Human Capital, Child Penalty
**JEL Codes**: E24, J11, J13, O40

*Institute for International Economic Studies (IIES), Stockholm University. Email: yimei.zou@iies.su.se. I thank Timo Boppart, Per Krusell, Kieran Larkin, Kurt Mitman, Joshua Weiss, and seminar participants at IIES and Nordic Summer Symposium in Macroeconomics for feedback.

# 1 INTRODUCTION

Over the past six decades, the adoption of modern contraception has expanded alongside sharp increases in female educational attainment and labor force participation (Goldin 2024). While celebrating women's advancements in education and the workplace, many countries also worry about below-replacement fertility and population decline, leading to renewed interest in policies that lift birth rates. Together, these developments raise fundamental macroeconomic questions: how does improved control over fertility shape long-run growth and welfare, and how do the growth and welfare consequences differ across policies that raise births by expanding family-friendliness versus restricting reproductive choice?

To answer these questions, I build an endogenous growth model that incorporates individual optimization of childbearing and human capital accumulation over a realistic life cycle. On the micro level, the model delivers a closed-form individual fertility policy that depends continuously on age and differs by whether the woman already has children. The timing of childbearing, especially of first birth, is therefore the key margin through which contraception and policy instruments shape individual fertility choices. On the macro level, endogenous intergenerational human capital spillovers generate sustained productivity growth. Aggregation admits a transparent mapping from individual fertility choices to aggregate dynamics of population, productivity, and welfare along the full transition path. Together, these features make the model a suitable framework for examining—both theoretically and quantitatively—the growth and welfare implications of women's reproductive freedom, defined as the ability to control the timing and incidence of childbearing.

Figure 1 empirically motivates the model's focus on fertility timing. There are two takeaways. First, within a given year, fertility rates differ sharply across ages and by whether women have previously given birth. Second, the secular shift since the 1960s reflects not only lower total fertility but also substantial postponement of childbearing, especially first births. Viewed through the lens of Figure 1, contraception enables women not only to choose family size but also to time births. Such control over fertility timing has implications for economic growth because (i) reproductive years overlap prime ages for human capital accumulation and (ii) childbearing imposes penalties on women's human capital progression (e.g., Cortés and Pan 2023; Kleven et al. 2025).

Motivated by these birth patterns across ages and motherhood statuses, I model fertility as a stochastic dynamic optimization problem over the life cycle. Children are discrete random variables, arriving according to a non-homogeneous Poisson process whose intensity the woman controls. Fertility planning is subject to the biological constraint of reproductive aging and the technological constraint of contraception effectiveness, which governs the utility cost of suppressing fertility below a biologically determined natural level.[1] Fertility choices also shape women's human

[1] Throughout, contraception effectiveness is not meant to capture the monetary price of a particular method or its

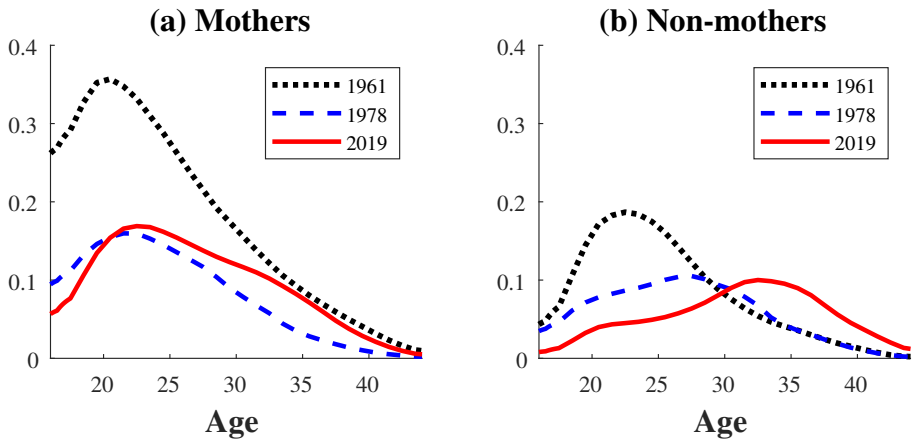



Figure 1: AGE-SPECIFIC FERTILITY RATES BY MOTHERHOOD STATUS, UNITED STATES

*Notes:* "Mothers" refer to women who have previously borne children and "non-mothers" those who have not. The age-specific fertility rate by motherhood status is a ratio where the numerator is the number of children born to women of a given age and motherhood status and the denominator is the number of women of that age and motherhood status. Details on data construction are given in Online Appendix B.1.

capital, the growth rate of which follows a two-state Markov process. Higher current child-arrival intensity and the entry into motherhood raise, respectively in a transient and a permanent way, the likelihood of being in the low-growth state, capturing the career costs of childbearing.

The life-cycle block yields a closed-form characterization of the optimal fertility schedule as an age-dependent arrival intensity of children. Crucially, the optimal schedule differs for women with children (mothers) and without children (non-mothers). Delaying the first birth carries an option value because entry into motherhood is irreversible and shifts the woman into a state with worse conditions for human capital growth. Accordingly, the fertility schedules of mothers and non-mothers are separated by an age-dependent wedge that captures how the net value of keeping the first-birth option unexercised varies over the life cycle. The closed-form solution also makes transparent how fertility responds to changes in incentives. Improvements in contraception effectiveness alone tend to lower fertility; however, when combined with reductions in the career impacts of motherhood, they can instead primarily reallocate births over the life cycle, delaying timing rather than reducing completed fertility. Furthermore, policies that raise the relative attractiveness of motherhood, such as alleviating long-term child penalties, encourage first births in particular, suggesting a potential solution for low-fertility economies facing rising childlessness.

At the aggregate level, output is produced from human-capital-augmented labor, supplied inelastically by working-age individuals, and a government levies an income tax to finance the consumption of those outside the working age. The aggregate state of the economy is the joint distribution of the population over ages, human capital, growth states, and motherhood statuses. Sustained

clinical failure rate. It summarizes the overall effectiveness of fertility control in practice, encompassing access and real-world frictions that shape whether individuals can obtain and consistently use modern contraception.

growth in output per capita arises from intergenerational human capital spillovers, modeled as a pure externality whereby successive cohorts draw their initial human capital from a distribution that shifts rightward over time at a rate increasing in the high-growth share of the working-age population. Individual fertility choices thus shape not only population distribution but also, through the aggregate high-growth share, the intensity of human capital spillovers. Although the model features a rich cross-sectional distribution of human capital, the aggregate output path is pinned down by four age-dependent objects—the population age density, the non-mother share, the high-growth share by motherhood status, and the conditional mean human capital—each of which maps one-to-one onto an observable empirical counterpart. This aggregation result helps with model discipline and keeps the quantitative analysis interpretable.

What is the theoretical relationship, both in the short and in the long run, between population growth and aggregate productivity growth? The answer depends on how births are distributed across ages and motherhood statuses, on the equilibrium population age structure, and on the forces driving fertility changes. First births play a qualitatively different role from subsequent births because they entail irreversible entry into motherhood, thereby altering the population distribution between mothers and non-mothers. Furthermore, increases in fertility generate not only within-age reallocations across growth states and motherhood statuses, but also shifts in the population age structure. This age-structure channel has positive growth impact when high-growth statuses are disproportionately concentrated among younger workers: a younger workforce then mechanically increases the overall share of high-growth workers, raising aggregate growth. In addition, policies that reduce the career penalties of motherhood have a direct pro-growth effect by reallocating women toward the high-growth state, over and above their impact on fertility. By contrast, pro-natal policies targeting contraception affect aggregate dynamics solely through changes in fertility.

I then take the model to U.S. female data over 1961–2019 and discipline it using the joint evolution of age-specific fertility rates by motherhood status and age-specific means of relevant socioeconomic outcomes. The high-growth state is proxied by schooling or full-time work, representing a regime of rapid human capital accumulation. The calibration targets transitional dynamics and exploits the model's analytical mapping between primitives and observable moments to identify key structural parameters sequentially. The short- and long-term career impacts of motherhood are first recovered from high-growth shares by age, leveraging differential loading across ages and motherhood statuses for identification. Contraception effectiveness is then backed out directly from observed fertility rates using the closed-form fertility policy. The degree of intergenerational human capital spillovers is separately identified by targeting the 2019 income-by-age profile, whose shape is in part governed by how fast mean entry human capital improves across cohorts. The inferred parameter paths imply a roughly fourfold increase in contraception effectiveness since 1961, alongside substantial declines in both the short- and long-term career impacts

of motherhood.

Using the calibrated model, I conduct counterfactual exercises to quantify the contribution of post-1961 improvements in contraception effectiveness to economic growth and welfare. Rising contraception effectiveness explains a substantial share of the 1961–2019 gains in female labor market outcomes, accounting for 44% of the increase in mean hours worked and 32% of the rise in output per hour averaged over informative counterfactual bounds. Welfare gains from expanded reproductive freedom vary sharply across cohorts and are largest for those born around 2000, who benefit from accumulated contraception improvements and human capital spillovers while largely avoiding the higher dependency ratios associated with rapid population aging. Aggregate welfare gains remain sizable, equivalent to a 28–37% increase in lifetime consumption, depending on the social discount rate.[2] A welfare decomposition shows that these gains arise mainly because improved fertility control reduces births and hence near-term dependency burdens that would otherwise crowd out resources for immediate cohorts.

Finally, I use the model to project future demographic and economic trajectories and to compare pro-natal interventions that operate through different margins. Under a continuation of 2019 conditions, the economy converges to a long-run equilibrium with population growth of −0.69% per year and aggregate productivity growth of 1.17% per year. I then consider three stylized interventions introduced in 2025—reducing the short- and long-term career impacts of motherhood versus scaling back contraception effectiveness—each calibrated to achieve the same long-run population growth rate of 0.88% per year (roughly the U.S. average since 2000). Conditional on the same long-run demographic target, the choice of policy instrument matters decidedly for productivity and welfare. Reducing the long-term career impact of motherhood yields the most favorable paths for aggregate productivity and cohort-specific welfare, whereas restricting reproductive freedom produces the least favorable outcomes. All pro-natal interventions considered generate transitional productivity losses relative to laissez-faire, reaching 4–6% by the 2080s. Moreover, policy-induced baby booms can create intergenerational inequality, as higher dependency burdens temporarily depress consumption for near-term cohorts before larger cohorts enter the workforce. Therefore, the desirability of pro-natal policies hinges on how societies trade off transitional costs against long-run gains.

This paper contributes to the literature on modern economic growth with endogenous population (e.g., Becker and Barro 1988; Barro and Becker 1989; Galor and Weil 1996; de la Croix and Doepke 2003; Greenwood et al. 2005; Jones 2022). This literature typically either abstracts away from cross-sectional age heterogeneity or resorts to stylized life cycle representations. As a result, the fertility decision in this literature generally focuses on the number of children, without timing

[2] Aggregate welfare is evaluated using the $\mathcal{A}$-*Efficiency* criterion of Golosov et al. (2007), which assigns no welfare weights to those unborn in one of the allocations being compared.

consideration. Models that feature a fertility timing decision typically do so with low-dimensional choice variables.[3] By contrast, this paper treats childbearing as a stochastic dynamic optimization problem in which women continuously control the arrival intensity of children. The resulting life-cycle fertility choice is a policy function rather than a scalar or a small vector, allowing the model to replicate the empirical age distribution of births while highlighting a distinct mechanism for postponing births: the irreversibility of motherhood in the presence of labor market risks and persistent impacts of children on women's human capital trajectories.

More broadly, growth models with stylized life cycle representations cannot capture the slow-moving nature of population age distribution, and are therefore less suited for quantitative analysis of transitional dynamics. With age advancing continuously with calendar time, the present framework delivers a tight mapping from theory to age-by-year data on fertility and women's labor market outcomes, enabling policy evaluation along full transition paths.

This paper is also related to the quantitative macroeconomic literature studying the joint determination of fertility and labor market outcomes over women's life cycle, under income risks and child-related career penalties (e.g., Sommer 2016; Adda et al. 2017; Eckstein et al. 2019). I complement this literature by embedding a rich life-cycle optimization block into an endogenous growth framework, showing how individual fertility outcomes and human capital trajectories aggregate across cohorts to generate tractable dynamics of output and productivity along demographic transitions.

Finally, this paper contributes to the broader literature on the economic implications of women's reproductive freedom in modern high-income societies. A large empirical literature estimates the causal effects of improved access to contraception and abortion on women's fertility behavior, educational attainment, and labor market outcomes (e.g., Goldin and Katz 2002; Bailey 2006, 2010; Bailey et al. 2012; Myers 2017). In particular, Gallen et al. (2025) provide direct reduced-form support for the mechanism at the core of this paper: exploiting quasi-random unplanned pregnancies among users of long-acting reversible contraceptives in Sweden, they show that the timing of pregnancy, especially unintended early first births, has large and persistent career consequences through disrupted human capital accumulation.

I complement the reduced-form evidence with a structural framework that rationalizes why birth timing matters and maps individual-level fertility control into aggregate economic outcomes, enabling growth accounting and policy experiments. Choi (2017) and Seshadri and Zhou (2022) also adopt structural approaches to study the aggregate effects of reproductive freedom, either in a stationary environment or with a stylized life cycle representation. This paper complements their

[3]For example, Iyigun (2000), d'Albis et al. (2018), and Abad et al. (2025) consider a two-period reproductive window, in which women allocate births between an "early" and a "late" period; d'Albis et al. (2010) and de la Croix and Licandro (2013) model fertility timing as a one-time choice of when to enter motherhood.

work with a unified framework in which realistic life-cycle behavior and non-stationary aggregate dynamics jointly determine the contribution of contraception-enabled shifts in fertility timing to the post-1961 rise in female labor supply and productivity.

The rest of the paper proceeds as follows. Section 2 presents the model and the theoretical results. Section 3 conducts the quantitative analyses. Section 4 concludes.

# 2 THEORY

In this section, I set up the model and establish its theoretical properties both on and off the balanced growth path. Derivations and proofs are provided in Online Appendix A.

## 2.1 THE MODEL

Time is continuous and extends indefinitely. The economy is populated by a continuum of finitely lived agents whose total mass is endogenously determined in equilibrium through individual fertility choices. Abstracting from couple formation, I assume all agents are female. An individual of age $a \in [0, \bar{a}]$ faces an exogenous Poisson death intensity $\xi(a)$, where $\bar{a} < \infty$ is the maximum age. An individual born at calendar time $t$ is referred to as being of cohort $t$. There is no migration.

**Children** Children are modeled as a discrete individual state variable. Let $n(a, t+a)$ denote the number of children ever born to a woman of age $a$ and cohort $t$ at calendar time $t+a$. The quantity of children $n(a, t+a)$ follows a non-homogeneous Poisson process, independent across individuals, with arrival rate $\lambda(a, t+a)$ and unit jump size. The Poisson arrival rate of children $\lambda(a, t+a)$ is a choice variable of the individual, reflecting the intensity of fertility effort.

**Human capital** Nested within the lifespan is the working-life interval $\left[\underline{a}^w, \bar{a}^w\right] \subset [0, \bar{a}]$. Let $z(a, t+a)$ denote the human capital of a cohort-$t$ woman of age $a$ at calendar time $t+a$. Individuals below the minimum working age $\underline{a}^w$ have zero human capital. Upon entering the labor market, a cohort-$t$ individual draws initial human capital $z\left(\underline{a}^w, t+\underline{a}^w\right)$ from a distribution $f\left(x, t+\underline{a}^w\right)$, where $x = \log z$. The log human capital distribution $f$ is continuous and time-dependent, with support $(-\infty, \infty)$. For $a \in \left[\underline{a}^w, \bar{a}^w\right]$, human capital evolves according to

$$\frac{dz(a, t+a)}{da} = \left[\mu(a, t+a) - \eta(a)\right] z(a, t+a).$$

Human capital accumulation is stochastic through a two-state Markov chain $\mu(a, t+a) \in \{\mu_H, \mu_L\}$, with $\mu_H > \mu_L \geq 0$. Let $i \in \{H, L\}$ denote an individual's human capital growth type. A high-growth individual switches to the low-growth state with intensity $\phi(a) + \gamma\lambda(a, t+a) + \theta\mathbb{I}_{n>0}$,

where $\gamma, \theta > 0$ and $\mathbb{I}$ denotes the indicator function. A low-growth individual switches to the high-growth state with intensity $\psi(a) - \gamma\lambda(a, t+a) - \theta\mathbb{I}_{n>0}$.

These transition intensities have three components. The baseline terms $\phi(a)$ and $\psi(a)$ capture age-specific labor market risks unrelated to fertility decisions. The term $\gamma\lambda(a, t+a)$ captures how current fertility effort worsens human-capital-growth prospects. I refer to $\gamma$ as the *short-term career impact of motherhood*.[4] The term $\theta\mathbb{I}_{n>0}$ captures persistent human capital scarring after entry into motherhood, independent of current fertility effort. I refer to $\theta$ as the *long-term career impact of motherhood*.[5] Together, these career impacts increase the high-to-low transition intensity and decrease the low-to-high transition intensity relative to the baseline rates $\phi(a)$ and $\psi(a)$.

Since the transition intensities between growth states depend on reproductive history, an individual's motherhood status matters for her decision-making. I therefore distinguish motherhood status $j \in \{M, N\}$, where $M$ denotes mothers and $N$ non-mothers.[6] At age $\underline{a}^w$, a share $\sigma \in (0,1)$ of entering workers starts in the high-growth state, with the remainder in the low-growth state. In addition, human capital depreciates deterministically at rate $\eta(a)$. Once individuals pass the retirement age $\bar{a}^w$, human capital is destroyed. Thus $z(a, t+a) = 0$ for $a \notin \left[\underline{a}^w, \bar{a}^w\right]$.

**Consumption** There is no saving technology in this economy. Cohort-$t$ individuals receive a tax-financed stipend $s(t+a)$ from the government when they are below the minimum working age. During working ages, individuals supply labor inelastically. A worker of growth type $i$ supplies $1 - \mathbb{I}_{i=L}\epsilon$ units of labor to a final good producer with linear technology. Thus $\epsilon \in (0,1)$ captures a static labor supply penalty associated with the low-growth state, in addition to the dynamic penalty from slower human capital accumulation. Wages are normalized to one and labor income is taxed at rate $\tau$. After retirement, cohort-$t$ individuals receive a tax-financed pension equal to a fraction $\upsilon$ of their pre-tax earnings at retirement age $\bar{a}^w$. Consumption over the life cycle of cohort-$t$ individuals is therefore

$$c(a, t+a) = \begin{cases} s(t+a) & \text{if } a \in \left[0, \underline{a}^w\right), \\ (1 - \mathbb{I}_{i=L}\epsilon)(1-\tau) z(a, t+a) & \text{if } a \in \left[\underline{a}^w, \bar{a}^w\right], \\ \upsilon(1-\tau)^{-1} c(\bar{a}^w, t+\bar{a}^w) & \text{if } a \in (\bar{a}^w, \bar{a}]. \end{cases}$$

[4] Summarizing a transient impact of childbearing, $\gamma$ may proxy real-world mechanisms such as temporary reductions in hours or job search intensity during pregnancy and postpartum; health constraints around childbirth; and employer responses to pregnancy and breastfeeding. For expositional simplicity, I refer to $\gamma$ as the short-term career impact of *motherhood*, although in the model it operates through contemporaneous fertility effort and thus can affect women before the first birth.

[5] Encapsulating a persistent impact tied to motherhood status, $\theta$ may reflect real-world mechanisms such as lasting losses in experience and promotion opportunities following career interruptions; permanent switches to more flexible but lower-growth jobs or occupations; and durable employer beliefs about mothers' availability and commitment.

[6] By definition, $j = M$ if the woman has borne children ($n > 0$) and $j = N$ if she has not ($n = 0$).

**Preference** Individuals derive utility from consumption and children, and incur a utility cost of fertility control. Flow utility is given by

$$u_{ij}(a, t+a) = \log c(a, t+a) + \zeta n(a, t+a) - \chi_j(a, \lambda(a, t+a)), \tag{1}$$

where the utility cost of fertility control is

$$\chi_j(a, \lambda(a, t+a)) = \begin{cases} \frac{1}{2\kappa_j(a)} [\beta(a) - \lambda(a, t+a)]^2 & \text{if } \lambda(a, t+a) \leq \beta(a), \\ \infty & \text{if } \lambda(a, t+a) > \beta(a). \end{cases} \tag{2}$$

I refer to $\beta(a)$ as the *natural fertility rate*: an age-specific primitive corresponding to the arrival intensity of children absent any fertility control effort, reflecting biological fecundability. The medical literature suggests that $\beta(a)$ varies non-monotonically with age, peaking in the early twenties and declining from the thirties onward, a pattern often referred to as the "biological clock".[7] To facilitate the theoretical analysis, I introduce the following assumption on $\beta(a)$.

ASSUMPTION 1. *The natural fertility rate is a function* $\beta : [0, \bar{a}] \to [0, \infty)$ *such that* $\beta(a) = 0$ *for all* $a \notin [\underline{a}^w, \bar{a}^r)$*, where* $\bar{a}^r$ *is the reproductive horizon satisfying* $\underline{a}^w < \bar{a}^r \leq \bar{a}^w$*. On* $[\underline{a}^w, \bar{a}^r)$*,* $\beta$ *is strictly positive and continuously differentiable, with* $\lim_{a \uparrow \bar{a}^r} \beta(a) = 0$*.*

Assumption 1 implies that the natural fertility rate is positive only on $[\underline{a}^w, \bar{a}^r) \subseteq [\underline{a}^w, \bar{a}^w]$, which keeps the model focused on the central economic tradeoff: the tension between childbearing and human capital accumulation. Reducing fertility below $\beta(a)$ entails a convex utility cost that is decreasing in $\kappa_j(a)$. I refer to $\kappa_j(a)$ as *contraception effectiveness*: a reduced-form shifter that governs how costly it is—in utility terms—for an individual to suppress births below the natural fertility rate, given real-world frictions.[8] The model abstracts from fertility enhancement—such as assisted reproductive technology (e.g., IVF)—by imposing an infinite utility cost for choosing a child-arrival intensity above $\beta(a)$. I introduce regularity conditions on the remaining age-dependent primitives in Assumption 2.

ASSUMPTION 2. *The mortality function* $\xi : [0, \bar{a}] \to [0, \infty)$ *is continuously differentiable on* $[0, \bar{a})$*, with* $\lim_{a \uparrow \bar{a}} \xi(a) = \infty$*. The baseline transition intensity functions* $\phi, \psi : [\underline{a}^w, \bar{a}^w] \to [0, \infty)$*, the human capital depreciation function* $\eta : [\underline{a}^w, \bar{a}^w] \to [0, \infty)$*, and the contraception effectiveness function* $\kappa_j : [0, \bar{a}] \to (0, \infty)$*,* $j \in \{M, N\}$*, are continuously differentiable.*

[7] A review of the medical literature on female reproductive aging can be found in Broekmans et al. (2007).

[8] $\kappa_j(a)$ should not be interpreted narrowly as the clinical efficacy of any particular contraceptive method. Instead, it summarizes *the overall effectiveness of fertility control in practice*, encompassing method reliability and ease of use as well as real-world frictions—such as legal constraints and medical delivery barriers, physical and mental health burdens from adherence, and partner dynamics and social norms—that shape whether individuals can obtain and consistently use modern contraception.

**Aggregation** Aggregate output equals the total efficient labor supplied by working-age individuals:

$$Y(t) = \int_{\underline{a}^w}^{\bar{a}^w} \int_{-\infty}^{\infty} \sum_j \sum_i (1 - \epsilon \mathbb{I}_{i=L}) e^x l_{ij}(x, a, t) \, dx da, \tag{3}$$

where $l_{ij}(x, a, t)$ denotes the endogenous mass of workers at time $t$ of age $a$, log human capital $x = \log z$, growth type $i \in \{H, L\}$ and motherhood status $j \in \{M, N\}$. Let $p(a, t)$ denote the mass of age-$a$ individuals at time $t$. For $a \in [\underline{a}^w, \bar{a}^w]$, $p(a, t) = \sum_j \sum_i \int_{-\infty}^{\infty} l_{ij}(x, a, t) \, dx$. A balanced government budget implies

$$\begin{aligned} \tau Y(t) = s(t) & \int_0^{\underline{a}^w} p(a, t) \, da \\ & + \upsilon \int_{\bar{a}^w}^{\bar{a}} \int_{-\infty}^{\infty} \sum_j \sum_i (1 - \epsilon \mathbb{I}_{i=L}) e^x l_{ij}(x, \bar{a}^w, t - a + \bar{a}^w) e^{-\int_{\bar{a}^w}^{a} \xi(a') da'} dx da, \end{aligned} \tag{4}$$

so income tax revenue equals the consumption of those outside working ages.

**Intergenerational spillovers** I model intergenerational human capital spillovers as improvements of the entry distribution $f$, from which labor market entrants draw their initial log human capital at age $\underline{a}^w$. Specifically, $f$ follows a traveling-wave law of motion:

$$\frac{\partial f(x, t)}{\partial t} + \varphi \mathcal{H}(t) \frac{\partial f(x, t)}{\partial x} = 0, \tag{5}$$

where $\varphi > 0$ and $\mathcal{H}(t)$ is the share of high-growth types among the working-age population:

$$\mathcal{H}(t) = \frac{\int_{\underline{a}^w}^{\bar{a}^w} \int_{-\infty}^{\infty} \sum_j l_{Hj}(x, a, t) \, dx da}{\int_{\underline{a}^w}^{\bar{a}^w} p(a, t) \, da}. \tag{6}$$

The law of motion implies that the shape of $f$ is stable while its location shifts rightward over time, so successive cohorts enter the labor market with higher initial human capital on average. The endogenous drift rate $\varphi \mathcal{H}(t)$ captures, in reduced form, the idea that economies with a larger fraction of high-growth workers cultivate and transmit know-how more intensively, raising the human capital of future cohorts at a faster rate.[9] These intergenerational spillovers are the source of sustained growth in output per capita in the model.

[9] The specification (5) is intended to capture the development and diffusion of human-capital-relevant know-how (e.g., teaching quality, managerial practices, occupational norms), not the production of new ideas via R&D. The exposure of a typical entrant to such know-how is plausibly governed by workforce composition—the prevalence of high-growth workers in schools and workplaces—more than by aggregate headcount. I therefore abstract from the scale effects emphasized in R&D-based frameworks such as Jones (2022) to keep the mechanism focused.

## 2.2 LIFE-CYCLE OPTIMIZATION

I solve the life-cycle problem for an individual from an arbitrary cohort, suppressing the calendar-time index to lighten notation when doing so causes no confusion. I decompose the problem into the working and non-working ages, and analyze each segment separately. Exploiting the utility specification, I apply a guess-and-verify argument to solve for affine value functions, which deliver interior fertility policy rules in near closed form. These expressions provide a transparent mapping from model primitives to fertility incentives and support analytical comparative statics.

**The working life** To streamline notation, let $\omega_{HL,j}(a)$ and $\omega_{LH,j}(a)$ denote the high-to-low and low-to-high transition intensities between human capital growth states for an age-$a$ worker with motherhood status $j \in \{M, N\}$ as described in Section 2.1:

$$\omega_{HL,j}(a) \equiv \phi(a) + \gamma\lambda_{Hj}(a) + \theta\mathbb{I}_{j=M} \qquad \text{and} \qquad \omega_{LH,j}(a) \equiv \psi(a) - \gamma\lambda_{Lj}(a) - \theta\mathbb{I}_{j=M}, \tag{7}$$

where the potential dependence of the chosen fertility effort $\lambda_{ij}(a)$ on individual types $i$ and $j$ is made explicit.

During working life, the value function $V_{iM}(x, n, a)$ of an age-$a$ mother with $n$ children, log human capital $x$, and growth type $i \in \{H, L\}$ solves the Hamilton-Jacobi-Bellman (HJB) equation

$$\begin{aligned}[\rho + \xi(a)]\, V_{iM}(x, n, a) = \max_{0 \le \lambda_{iM}(a) \le \beta(a)} & u_{iM}(a) + [\mu_i - \eta(a)] \frac{\partial V_{iM}(x, n, a)}{\partial x} + \frac{\partial V_{iM}(x, n, a)}{\partial a} \\ & + \lambda_{iM}(a) \left[V_{iM}(x, n+1, a) - V_{iM}(x, n, a)\right] \\ & + \omega_{ii',M}(a) \left[V_{i'M}(x, n, a) - V_{iM}(x, n, a)\right], \quad i' \neq i, i' \in \{H, L\}, \end{aligned} \tag{8}$$

where $\rho > 0$ is the discount rate and $u_{iM}$ the flow utility specified by (1).[10] The individual's continuation value derives from instantaneous utility, deterministic human capital accumulation and aging, the arrival of an additional child with intensity $\lambda_{iM}(a)$, and the switch to the other growth state with intensity $\omega_{ii',M}(a)$. For $a \in [\bar{a}^r, \bar{a}^w]$, $\beta(a) = 0$ and therefore $\lambda_{iM}(a) = 0$ by the feasibility constraint. For $a \in \left[\underline{a}^w, \bar{a}^r\right)$, the interior first-order condition for $\lambda_{iM}(a)$ is

$$\frac{\beta(a) - \lambda_{iM}(a)}{\kappa_M(a)} + V_{iM}(x, n+1, a) - V_{iM}(x, n, a) = \gamma\left[V_{HM}(x, n, a) - V_{LM}(x, n, a)\right]. \tag{9}$$

The left-hand side of (9) is the marginal cost of suppressing fertility: the direct utility cost of birth control plus the forgone continuation value from an additional child. The right-hand side is the marginal benefit: by lowering the child-arrival intensity, the individual tilts transition rates toward the high-growth state; the gain equals the continuation-value premium of being high-growth,

[10] In (8), given $i' \neq i$, $\omega_{ii',M}(a)$ corresponds to $\omega_{HL,M}(a)$ when $(i, i') = (H, L)$ and to $\omega_{LH,M}(a)$ when $(i, i') = (L, H)$. Analogous mapping from $\omega_{ii',N}(a)$ to $\omega_{HL,N}(a)$ or $\omega_{LH,N}(a)$ applies to non-mothers' HJB (10).

$V_{HM}(x,n,a) - V_{LM}(x,n,a)$, scaled by the short-term career impact parameter $\gamma$.

For a non-mother of age $a$, log human capital $x$, and growth type $i \in \{H,L\}$, the value function $V_{iN}(x,a)$ solves the HJB equation

$$\begin{aligned}[\rho + \xi(a)]\, V_{iN}(x,a) = &\max_{0\le\lambda_{iN}(a)\le\beta(a)} u_{iN}(a) + [\mu_i - \eta(a)]\,\frac{\partial V_{iN}(x,a)}{\partial x} + \frac{\partial V_{iN}(x,a)}{\partial a} \\ &+ \lambda_{iN}(a)\,[V_{iM}(x,1,a) - V_{iN}(x,a)] \\ &+ \omega_{ii',N}(a)\,[V_{i'N}(x,a) - V_{iN}(x,a)], \quad i' \neq i, i' \in \{H,L\}. \end{aligned} \tag{10}$$

Compared to (8), the key difference here is that a first birth changes the individual's motherhood status from $j = N$ to $j = M$, in addition to raising the number of children $n$ by one. Again, the feasibility constraint implies $\lambda_{iN}(a) = 0$ for $a \in [\bar{a}^r, \bar{a}^w]$. For $a \in \left[\underline{a}^w, \bar{a}^r\right)$, the interior first-order condition for $\lambda_{iN}(a)$ is

$$\frac{\beta(a) - \lambda_{iN}(a)}{\kappa_N(a)} + V_{iM}(x,1,a) - V_{iN}(x,a) = \gamma\,[V_{HN}(x,a) - V_{LN}(x,a)]. \tag{11}$$

Relative to mothers, the marginal cost-benefit tradeoff for non-mothers also captures the discrete change in continuation value that comes from entering motherhood. Crucially, entry into motherhood is irreversible: individuals do not transition from $j = M$ back to $j = N$.

**Outside working life** For $a \notin \left[\underline{a}^w, \bar{a}^w\right]$, Assumption 1 implies $\beta(a) = 0$, so the feasible and hence optimal child-arrival intensity is $\lambda(a) = 0$. Outside working ages, the individual has no human capital and experiences no birth; her continuation value evolves only through deterministic aging. In retirement, $a \in (\bar{a}^w, \bar{a}]$, the value function $V^O(c,n,a)$ of an individual with $n$ children and pension-financed consumption $c$ solves

$$[\rho + \xi(a)]\, V^O(c,n,a) = \log c + \zeta n + \frac{\partial V^O(c,n,a)}{\partial a}, \tag{12}$$

with terminal condition $V^O(c,n,\bar{a}) = 0$ and value matching at $\bar{a}^w$:

$$\lim_{a\downarrow\bar{a}^w} V^O(\upsilon(1 - \mathbb{I}_{i=L}\epsilon)e^x, n, a) = V_{iM}(x,n,\bar{a}^w), \quad i \in \{H,L\}; \tag{13}$$

$$\lim_{a\downarrow\bar{a}^w} V^O(\upsilon(1 - \mathbb{I}_{i=L}\epsilon)e^x, 0, a) = V_{iN}(x,\bar{a}^w), \quad i \in \{H,L\}. \tag{14}$$

Before working life, $a \in \left[0, \underline{a}^w\right)$, a cohort-$t$ individual's value function $V^{\mathcal{Y}}(a, t+a)$ solves

$$[\rho + \xi(a)]\, V^{\mathcal{Y}}(a,t+a) = \log s(t+a) + \frac{\partial V^{\mathcal{Y}}(a,t+a)}{\partial a}, \tag{15}$$

with value matching at $\underline{a}^w$:

$$\lim_{a \uparrow \underline{a}^w} V^{\mathcal{Y}}(a, t+a) = \int_{-\infty}^{\infty} \left[\sigma V_{HN}\left(x, \underline{a}^w, t+\underline{a}^w\right) + (1-\sigma) V_{LN}\left(x, \underline{a}^w, t+\underline{a}^w\right)\right] f\left(x, t+\underline{a}^w\right) dx. \tag{16}$$

The right-hand side of (16) is the cohort-$t$ individual's expected continuation value at labor market entry, integrating over the initial human capital draw $x \sim f\left(\cdot, t+\underline{a}^w\right)$ and over the initial growth state, which is high with probability $\sigma$.

**Optimal fertility schedule** The HJB equations (8) and (10), together with the value matching conditions (13)–(14), deliver a transparent characterization of the individual's interior fertility policy during reproductive ages. In particular, I can express the optimal fertility schedule in closed form as a function of age and motherhood status, up to the solution of an auxiliary terminal value problem stated below.

PROPOSITION 1. *An interior optimal fertility schedule on $\left[\underline{a}^w, \bar{a}^r\right)$, if it exists, depends only on age $a$ and motherhood status $j \in \{M, N\}$ and can be written as*

$$\lambda_j(a) = \beta(a) - \kappa_j(a)\left[\gamma \widehat{\Psi}(a) + \Phi(a)\mathbb{I}_{j=N} - \zeta \Pi(a)\right], \tag{17}$$

*where*

$$\Pi(a) = \int_a^{\bar{a}} e^{-\int_a^{a'}[\rho+\xi(a'')]da''} da', \tag{18}$$

$$\begin{aligned}\widehat{\Psi}(a) = &\int_a^{\bar{a}^w} e^{-\int_a^{a'}[\rho+\xi(a'')+\phi(a'')+\psi(a'')]da''}\left[(\mu_H-\mu_L)\Pi(a') - \log(1-\epsilon)\right] da' \\ &- e^{-\int_a^{\bar{a}^w}[\rho+\xi(a'')+\phi(a'')+\psi(a'')]da''}\Pi(\bar{a}^w)\log(1-\epsilon),\end{aligned} \tag{19}$$

*and $\Phi(a)$ solves the terminal value problem*

$$\begin{aligned}\Phi'(a) = &\frac{\kappa_M(a)}{2}\left[\gamma\widehat{\Psi}(a) - \zeta\Pi(a)\right]^2 - \frac{\kappa_N(a)}{2}\left[\gamma\widehat{\Psi}(a) + \Phi(a) - \zeta\Pi(a)\right]^2 \\ &+ \left[\rho + \xi(a) + \beta(a)\right]\Phi(a) - \theta\widehat{\Psi}(a),\end{aligned} \tag{20}$$

$$\Phi(\bar{a}^r) = \int_{\bar{a}^r}^{\bar{a}^w} e^{-\int_{\bar{a}^r}^{a'}[\rho+\xi(a'')]da''}\theta\widehat{\Psi}(a')\,da'. \tag{21}$$

PROOF: See Online Appendix A.1.

The proof of Proposition 1 follows a guess-and-verify strategy. Given the flow utility specification in (1), the value functions admit an affine representation in log human capital and in the number of children, which yields an explicit characterization of the interior fertility policy. To sharpen the analytical results, I impose sufficient conditions on the model primitives—collected in Assumption

OA1 in Online Appendix A.2—to ensure that the interior fertility policy $\lambda_j(a)$, $j \in \{M, N\}$, given by Proposition 1 exists for all reproductive ages. Corollary 1 then formally establishes existence of the interior policy by showing that the terminal value problem (20)–(21) admits a unique solution $\Phi(a)$ satisfying $\zeta\Pi(a) - \gamma\widehat{\Psi}(a) < \Phi(a) < \zeta\Pi(a) - \gamma\widehat{\Psi}(a) + \frac{\beta(a)}{\kappa_N(a)}$ for all $a \in \left[\underline{a}^w, \bar{a}^r\right)$.[11]

COROLLARY 1. *Under Assumptions 1–2 and OA1, there exists an interior solution $\lambda_j(a)$ for $j \in \{M, N\}$ and all $a \in \left[\underline{a}^w, \bar{a}^r\right)$, given by (17)–(21) in Proposition 1.*
PROOF: See Online Appendix A.2.

Let us pause to interpret the optimal fertility schedule in Proposition 1. The term $\zeta\Pi(a)$ is the discounted lifetime utility from an additional child. In the proof of Proposition 1, I show that $\widehat{\Psi}(a) = V_{HM}(x, n, a) - V_{LM}(x, n, a) = V_{HN}(x, a) - V_{LN}(x, a)$. Thus, $\widehat{\Psi}(a)$ is the continuation-value premium of the high-growth state relative to the low-growth state; it is strictly positive on $\left[\underline{a}^w, \bar{a}^w\right]$ because $\mu_H > \mu_L$ and $\epsilon \in (0, 1)$. The expression (19) of $\widehat{\Psi}(a)$ makes clear two sources of loss from being in the low-growth state: a static income loss from reduced hours and a dynamic income loss from slower human capital accumulation. The continuation-value premium $\widehat{\Psi}(a)$ increases with the human capital growth differential $\widehat{\mu} \equiv \mu_H - \mu_L$ and the hours reduction $\epsilon$, and decreases with the baseline transition intensities $\phi(a)$ and $\psi(a)$.

For mothers, the terms $\zeta\Pi(a)$ and $\gamma\widehat{\Psi}(a)$ summarize the cost-benefit trade-off behind $\lambda_M(a)$. For non-mothers, $\lambda_N(a)$ also depends on an age-specific wedge $\Phi(a)$. As shown in the proof of Proposition 1, $\Phi(a)$ gives the continuation-value differential—conditional on growth type—between remaining a non-mother and being a mother, net of the utility from children per se: $\Phi(a) = V_{iN}(x, a) - V_{iM}(x, n, a) + \zeta n\Pi(a)$, for $i \in \{H, L\}$. I refer to $\Phi(a)$ as the *motherhood-status value differential*. Two forces generate this differential. First, the transition into motherhood is irreversible. Second, beyond the utility from children, motherhood differs from the non-mother status through (i) the persistent career penalty $\theta\widehat{\Psi}(a)$ and (ii) differences in the utility cost of fertility control, which arise both because contraception effectiveness may differ by motherhood status and because mothers and non-mothers may optimally choose different fertility schedules.

**Comparative statics** Proposition 1 enables an analytical characterization of how individual policy functions vary with model primitives (scalar parameters and functions). Table 1 reports the comparative statics of the optimal fertility schedules, $\lambda_j(a)$ for $j \in \{M, N\}$, and their key components: the discounted expected remaining lifetime $\Pi(a)$, the continuation-value premium of being in the high-growth state $\widehat{\Psi}(a)$, and the motherhood-status value differential $\Phi(a)$.[12] The first five

[11] I focus on the interior candidate policy characterized in Proposition 1. Rather than pursue a general uniqueness theorem for the full HJB system, I establish in Corollary 1 that the interior fertility policy of Proposition 1 exists throughout reproductive ages, which is sufficient for the analysis in this paper.

[12] In cases where the primitive of interest is a function, I use functional derivatives (pointwise perturbations) for the comparative statics; this is equivalent to asking how outcomes vary under a small local change in the primitive

primitives govern the human capital process and the labor market environment. The next two, $\bar{a}$ and $\xi$, are demographic primitives that shape life expectancy. The last two, $\kappa_M$ and $\kappa_N$, govern contraception effectiveness. Because the fertility policy rules admit almost closed-form representations, many comparative statics can be signed directly. This makes clear which primitives operate through which margin, providing a transparent link between the theory and the quantitative analyses in Section 3.

TABLE 1: KEY COMPARATIVE STATIC RESULTS OF THE OPTIMAL FERTILITY SCHEDULE

| | $\Pi(a)$ | $\widehat{\Psi}(a)$ | $\lambda_M(a)$ | $\Phi(a)$ | $\lambda_N(a)$ |
|---|---|---|---|---|---|
| *Effect of an increase in:* | | | | | |
| $\gamma$ | 0 | 0 | $-$ | $\pm$ | $\pm$ |
| $\theta$ | 0 | 0 | 0 | $+$ | $-$ |
| $\widehat{\mu}$ | 0 | $+$ | $-$ | $\pm$ | $\pm$ |
| $\epsilon$ | 0 | $+$ | $-$ | $\pm$ | $\pm$ |
| $\bar{a}^w$ | 0 | $\pm$ | $\pm$ | $\pm$ | $\pm$ |
| $\bar{a}$ | $+$ | $+$ | $\pm$ | $\pm$ | $\pm$ |
| $\xi$ *at age* $a' \in [a, \bar{a})$ | $-$ | $-$ | $\pm$ | $\pm$ | $\pm$ |
| $\kappa_N$ *at age* $a' \in [a, \bar{a}^r)$ | 0 | 0 | 0 | $+$ | $-$ |
| $\kappa_M$ *at age* $a$ | 0 | 0 | $-$ | $-$ | $+$ |
| $\kappa_M$ *at age* $a' \in (a, \bar{a}^r)$ | 0 | 0 | 0 | $-$ | $+$ |

*Notes:* Each entry reports the sign of the partial derivative (or functional derivative, when the primitive is a function) of the column variable with respect to the row primitive. Focusing on nontrivial cases, comparative statics are conducted over restricted age domains for these variables: $\Pi(a)$ over $[0, \bar{a})$, $\Phi(a)$ over $\left[\underline{a}^w, \bar{a}^w\right)$, and $\lambda_j(a)$ over $\left[\underline{a}^w, \bar{a}^r\right)$ for $j \in \{M, N\}$. Ambiguous signs are denoted by "$\pm$". Proofs are in Online Appendix A.3.

First, let us consider mothers' responses. The optimal fertility rate for mothers, $\lambda_M(a)$, decreases with the short-term career impact of motherhood $\gamma$, the human capital growth differential $\widehat{\mu}$, and the hours reduction $\epsilon$ in the low-growth state. An increase in each of these primitives raises the opportunity cost of children, summarized by the term $\gamma\widehat{\Psi}(a)$. By contrast, the long-term career impact of motherhood $\theta$ does not affect mothers' fertility choices: for mothers, $\theta$ shifts the high-to-low and low-to-high transition intensities between growth states symmetrically, leaving the high-growth premium $\widehat{\Psi}(a)$ and hence the opportunity cost of children $\gamma\widehat{\Psi}(a)$ unchanged.

Changing the retirement age $\bar{a}^w$ has an ambiguous effect on mothers' fertility effort, because it affects the opportunity cost of children through two channels that work in opposite directions. Specifically, the continuation-value gap $\widehat{\Psi}(a)$ accounts for not only low-state earning losses during working ages, but also the reduction in pensions, which are proportional to the exiting labor income. For a fixed maximum age $\bar{a}$, a higher $\bar{a}^w$ extends the working life and shortens retirement, so the net effect on $\widehat{\Psi}(a)$ is a priori unclear.

function. The formal definition of functional derivative is given in Online Appendix A.3.

Longer life expectancy—through either a higher $\bar{a}$ or lower mortality $\xi$—has an ambiguous effect on mothers' fertility planning, because it raises both the benefit and the opportunity cost of children through lower mortality-driven discounting. A longer expected horizon increases $\Pi(a)$, raising the discounted lifetime utility from an additional child. At the same time, it raises $\widehat{\Psi}(a)$, because the income losses associated with being in the low-growth state are weighted more in continuation value.

With respect to contraception technology, the optimal fertility rate for mothers $\lambda_M(a)$ is decreasing in the own-age, own-motherhood-status contraception effectiveness, namely $\kappa_M$ at age $a' = a$, but it does not respond to $\kappa_N$ or to $\kappa_M$ at ages $a' > a$. The irrelevance of $\kappa_N$ follows from motherhood being an absorbing state. The lack of a forward-looking response to $\kappa_M$ reflects that, conditional on age and motherhood status, fertility choices do not vary by human capital growth state; hence $\kappa_M$ does not enter the continuation-value premium $\widehat{\Psi}(a)$ between the high- and low-growth states.

In contrast to the relatively straightforward fertility responses of mothers, fertility planning for non-mothers is complicated by the irreversibility of entering motherhood. Although the motherhood-status value differential $\Phi(a)$ has no closed-form expression, its comparative statics can still be signed analytically. In particular, $\Phi(a)$ increases in the long-term career impact of motherhood $\theta$ and in non-mothers' contraception effectiveness, and decreases in mothers' contraception effectiveness: a higher $\theta$, more effective contraception for non-mothers, and less effective contraception for mothers all make the non-mother status more attractive relative to motherhood. Moreover, the dependence of $\Phi(a)$ on contraception effectiveness is forward-looking: $\Phi(a)$ responds to changes in $\kappa_N$ and $\kappa_M$ at all current and future reproductive ages $a' \in [a, \bar{a}^r)$. By contrast, the remaining primitives affect women both outside and inside motherhood and therefore have an ambiguous effect on $\Phi(a)$.

The heterogeneous fertility responses across motherhood status have important policy implications. First, relative to mothers, non-mothers respond to a different set of incentives when choosing fertility effort during the working life. In particular, non-mothers respond to changes in the long-term career impact of motherhood $\theta$, reducing fertility effort when $\theta$ rises, whereas mothers do not. Non-mothers also respond in a forward-looking manner to changes in contraception effectiveness for both motherhood statuses, whereas mothers respond only to changes in own-motherhood-status contraception effectiveness at current age. In particular, improving contraception effectiveness for mothers spills over to non-mothers by making motherhood relatively more attractive, thereby lowering the motherhood-status value differential $\Phi(a)$ and encouraging fertility among women who have not yet had children.

Second, for primitive changes that affect all women, non-mothers' fertility responses are more nuanced in direction. For the primitives in Table 1, mothers' fertility responses have unambiguous

signs, except for primitives governing retirement age and life expectancy. For non-mothers, by contrast, responses are also ambiguous with respect to labor market conditions (captured by $\gamma$ and $\epsilon$) and the human capital process (captured by $\widehat{\mu}$), reflecting the fact that the motherhood-status value differential $\Phi(a)$ can move in either direction in response to changes in $\gamma$, $\epsilon$, or $\widehat{\mu}$. These differences in fertility planning between women with and without children are especially relevant for economies where low total fertility rate is driven by a rising incidence of lifelong childlessness.

## 2.3 DISTRIBUTIONAL DYNAMICS

Having solved the individual life-cycle problem, I now characterize the economy's distributional dynamics. A direct approach would track the full cross-sectional density $l_{ij}(x, a, t)$ of workers over log human capital $x$, age $a$, growth type $i \in \{H, L\}$ and motherhood status $j \in \{M, N\}$. I instead proceed by separating the sources of non-stationarity and introducing summary statistics that are useful for aggregation. I first show that, under the optimal fertility schedules from Section 2.2, demographic dynamics—summarized by the population age density $p(a, t)$—can be analyzed separately from the cross-sectional human capital distribution. I then summarize workforce composition with two statistics in closed form: the age-specific shares of non-mothers and the age-specific high-growth shares by motherhood status. Finally, I normalize human capital by the entering cohort's average, yielding a normalized distribution net of the aggregate productivity drift and therefore suitable for characterizing the long-run equilibrium.

**The Kolmogorov forward equations** For non-mothers, the worker density $l_{iN}(x, a, t)$ for growth type $i \in \{H, L\}$ evolves according to the Kolmogorov forward equation (KFE):

$$\frac{\partial l_{iN}(x,a,t)}{\partial t} + \frac{\partial l_{iN}(x,a,t)}{\partial a} = -\xi(a)\, l_{iN}(x,a,t) - [\mu_i - \eta(a)] \frac{\partial l_{iN}(x,a,t)}{\partial x} - \omega_{ii',N}(a)\, l_{iN}(x,a,t) + \omega_{i'i,N}(a)\, l_{i'N}(x,a,t) - \lambda_N(a)\, l_{iN}(x,a,t), \quad i' \neq i, \; i' \in \{H, L\}, \tag{22}$$

with boundary conditions at $a = \underline{a}^w$:

$$l_{iN}\left(x, \underline{a}^w, t\right) = \left[\sigma \mathbb{I}_{i=H} + (1-\sigma)\, \mathbb{I}_{i=L}\right] f(x,t)\, p\left(\underline{a}^w, t\right), \tag{23}$$

and initial condition $l_{iN}(x, a, 0) = l^0_{iN}(x, a)$. Conditions (23) reflect that all individuals enter working life without children (since the optimal child-arrival intensity is zero for $a < \underline{a}^w$), start in the high-growth state with probability $\sigma$, and draw initial log human capital from the entry distribution $f(x, t)$. The left-hand side of (22) reflects that, in addition to calendar time $t$, the density shifts along the $a$-dimension as individuals age at unit speed. On the right-hand side of (22), $l_{iN}(x, a, t)$ loses mass through mortality at rate $\xi(a)$, switches from growth state $i$ to $i'$ at rate $\omega_{ii',N}(a)$, and entry into motherhood at rate $\lambda_N(a)$; it gains mass from switches from growth

state $i'$ to $i$ at rate $\omega_{i'i,N}(a)$. The log human capital drift term $\mu_i - \eta(a)$ shifts mass along the $x$-dimension.

For mothers, the worker density $l_{iM}(x,a,t)$ for growth type $i \in \{H,L\}$ satisfies

$$\frac{\partial l_{iM}(x,a,t)}{\partial t} + \frac{\partial l_{iM}(x,a,t)}{\partial a} = -\xi(a) l_{iM}(x,a,t) - [\mu_i - \eta(a)] \frac{\partial l_{iM}(x,a,t)}{\partial x} - \omega_{ii',M}(a) l_{iM}(x,a,t) + \omega_{i'i,M}(a) l_{i'M}(x,a,t) + \lambda_N(a) l_{iN}(x,a,t), \quad i' \neq i, \; i' \in \{H,L\}, \tag{24}$$

with boundary condition $l_{iM}\left(x, \underline{a}^w, t\right) = 0$ and initial condition $l_{iM}(x,a,0) = l^0_{iM}(x,a)$. Relative to the KFE for non-mothers, here first births generate an inflow $\lambda_N(a) l_{iN}(x,a,t)$ into $l_{iM}(x,a,t)$, as first-time mothers transition irreversibly from $j = N$ to $j = M$. Subsequent births do not alter motherhood status $j$ and therefore do not enter the evolution of $l_{iM}(x,a,t)$.

For the whole population, the age density $p(a,t)$ evolves according to

$$\frac{\partial p(a,t)}{\partial t} + \frac{\partial p(a,t)}{\partial a} = -\xi(a) p(a,t), \tag{25}$$

with initial condition $p(a,0) = p^0(a)$.[13] Since the economy is closed to migration, there are no inflows to $p(a,t)$ for $a > 0$ and outflows arise only from mortality. Equation (25) is accompanied by the boundary condition at birth $p(0,t) = b(t)$, where $b(t)$ is the inflow of newborns at time $t$:

$$b(t) = \alpha \int_{\underline{a}^w}^{\bar{a}^r} \int_{-\infty}^{\infty} \sum_j \sum_i \lambda_j(a) l_{ij}(x,a,t) \, dx da. \tag{26}$$

In (26), $\alpha$ is the female share of newborns used to map total birth data to the model's female-only population. For working ages $a \in \left[\underline{a}^w, \bar{a}^w\right]$, the population age density equals the marginal of the worker density: $p(a,t) = \sum_j \sum_i \int_{-\infty}^{\infty} l_{ij}(x,a,t) \, dx$.

**Demographic dynamics** The cross-sectional density of workers $l_{ij}(x,a,t)$ is an equilibrium outcome shaped by demographic forces (births and deaths) and economic forces (human capital accumulation and labor market transitions). In general, $l_{ij}(x,a,t)$ need not converge to a stationary distribution because two distinct sources of non-stationarity are at work: changing cohort sizes and ongoing productivity growth. It is thus useful to decompose the non-stationary dynamics into a demographic component and a productivity component. Formally, demographic dynamics are summarized by the population age density $p(a,t)$, while productivity dynamics are summarized by the conditional human capital distribution $\ell_{ij}(x,a,t)$ defined as

$$\ell_{ij}(x,a,t) \equiv \frac{l_{ij}(x,a,t)}{\int_{-\infty}^{\infty} l_{ij}(x,a,t) \, dx}, \tag{27}$$

[13] KFE (25) is also known as the McKendrick-von Foerster equation of age-structured population dynamics.

which is the probability density of $x$ conditional on age $a$, growth type $i$, and motherhood status $j$.[14] The model permits the decoupling of demographic dynamics from productivity dynamics, because individual fertility policies $\lambda_j(a)$ do not depend on human capital.[15]

To characterize demographic dynamics, I define the age-specific share of non-mothers

$$\Omega(a,t) \equiv \frac{\int_{-\infty}^{\infty} \sum_i l_{iN}(x,a,t)\,dx}{p(a,t)}, \tag{28}$$

with initial condition $\Omega^0(a) = \sum_i \int_{-\infty}^{\infty} l_{iN}^0(x,a)\,dx/p^0(a)$. Lemma 1 characterizes $\Omega(a,t)$ explicitly in terms of primitives and previously defined objects.

LEMMA 1. *The share of non-mothers among workers of age $a$ at time $t$ is*

$$\Omega(a,t) = \left[\mathbb{I}_{a-t\leq \underline{a}^w} + \Omega^0(a-t)\,\mathbb{I}_{a-t>\underline{a}^w}\right] e^{-\int_{\max\{\underline{a}^w,a-t\}}^{a} \lambda_N(a')da'}.$$

PROOF: See Online Appendix A.4.

The expression in Lemma 1 has an intuitive interpretation. Motherhood is an absorbing state, and entry into motherhood occurs at the age-specific hazard rate $\lambda_N(a)$; hence $\Omega(a,t)$ is the probability that an age-$a$ woman at time $t$ has not yet entered motherhood, with the initial condition adjusted for whether she was already of working age at $t=0$. Using $\Omega(a,t)$ to rewrite the mass of newborns (26), the boundary condition for the population KFE (25) becomes

$$p(0,t) = \alpha \int_{\underline{a}^w}^{\bar{a}^r} \{\lambda_N(a)\,\Omega(a,t) + \lambda_M(a)\,[1-\Omega(a,t)]\}\,p(a,t)\,da. \tag{29}$$

Since Proposition 1 and Lemma 1 express $\lambda_j(a)$, for $j \in \{M,N\}$, and $\Omega(a,t)$ in terms of primitives, the demographic block of the model—summarized by $p(a,t)$—is entirely pinned down by the linear partial differential equation (25) together with the non-local boundary condition (29) and the initial condition $p(a,0) = p^0(a)$.[16]

**Productivity dynamics** I now turn to productivity dynamics. To analyze the evolution of the conditional human capital distribution $\ell_{ij}(x,a,t)$ defined in (27), it is useful to summarize the composition of growth types by age and motherhood status. For $j \in \{M,N\}$, I define $h_j(a,t)$ as

[14] Because the mass of mothers is zero at $a = \underline{a}^w$, $\ell_{iM}(x,a,t)$ is well-defined only for $a \in (\underline{a}^w, \bar{a}^w]$. By contrast, $\ell_{iN}(x,a,t)$ is well-defined for all $a \in [\underline{a}^w, \bar{a}^w]$.

[15] There is coupling in the other direction: productivity dynamics depend on demographic dynamics through intergenerational human capital spillovers outlined in (5)–(6).

[16] The demographic block of this model has the same mathematical structure as the Lotka-McKendrick model of age-structured population dynamics, except that fertility is endogenous here: the fertility rates $\lambda_j(a)$ are micro-founded from individual life-cycle optimization and therefore responsive to economic incentives, rather than being exogenous model inputs. For a systematic treatment of the Lotka-McKendrick framework, see Iannelli and Milner (2017).

the share of high-growth types among individuals with age $a$ and motherhood status $j$:

$$h_j(a,t) \equiv \frac{\int_{-\infty}^{\infty} l_{Hj}(x,a,t)\,dx}{\int_{-\infty}^{\infty} \sum_i l_{ij}(x,a,t)\,dx}, \tag{30}$$

with initial condition $h_j^0(a) = \int_{-\infty}^{\infty} l_{Hj}^0(x,a)\,dx / \int_{-\infty}^{\infty} \sum_i l_{ij}^0(x,a)\,dx$.[17] Since individual fertility policies depend only on age and motherhood status, the KFEs (22) and (24) imply closed form expressions for $h_j(a,t)$, as shown by Lemma 2.

LEMMA 2. *The shares of high-growth types by age a and motherhood status at time t are*

$$\begin{aligned} h_N(a,t) &= \left[\sigma \mathbb{I}_{a-t\leq \underline{a}^w} + h_N^0(a-t)\,\mathbb{I}_{a-t>\underline{a}^w}\right] e^{-\int_{\max\{\underline{a}^w,a-t\}}^{a}[\phi(a')+\psi(a')]da'} \\ &\quad + \int_{\max\{\underline{a}^w,a-t\}}^{a} e^{-\int_{a'}^{a}[\phi(a'')+\psi(a'')]da''}\omega_{LH,N}(a')\,da', \\ h_M(a,t) &= h_N(a,t) + \int_{\max\{\underline{a}^w,a-t\}}^{a} e^{-\int_{a'}^{a}\left[\phi(a'')+\psi(a'')+\frac{\lambda_N(a'')\Omega(a'',t-a+a'')}{1-\Omega(a'',t-a+a'')}\right]da''}\left[\omega_{LH,M}(a')-\omega_{LH,N}(a')\right]da'. \end{aligned}$$

PROOF: See Online Appendix A.5.

Unlike $\Omega(a,t)$ in Lemma 1, which has the straightforward "survival under a hazard" interpretation, the expressions for $h_N(a,t)$ and $h_M(a,t)$ reflect two-way switching between growth states and—for $h_M(a,t)$—one-way entry into motherhood. For non-mothers, $h_N(a,t)$ accounts for (i) individuals who remain in the high-growth state throughout $\left[\underline{a}^w, a\right]$ and (ii) individuals who switch growth states but are in the high-growth state at age $a$. Entry into motherhood does not directly affect $h_N(a,t)$: because the first-birth hazard $\lambda_N(a)$ is independent of growth type, it scales the high-growth and total non-mother densities proportionally, leaving their ratio $h_N(a,t)$ unchanged. For mothers, $h_M(a,t)$ reflects not only growth-type switching within motherhood, but also the inflow of new mothers from the non-mother pool. This inflow affects the numerator and denominator of $h_M(a,t)$ asymmetrically, because it brings in women whose high-growth share may differ from that of existing mothers. Lemma 2 shows explicitly the determinants of the high-growth share wedge $h_M(a,t) - h_N(a,t)$ across motherhood status.

Lemmas 1–2 allow me to characterize analytically how childbearing reallocates women across human capital growth states. Table 2 summarizes the comparative statics of $h_j(a,t)$ for $j \in \{M,N\}$ with respect to fertility rates. The high-growth share $h_j(a,t)$ is decreasing in the own-motherhood-status fertility rate $\lambda_j(a')$ for $a' \leq a$, whenever the short-term career impact of motherhood $\gamma > 0$. Cross-motherhood-status effects are asymmetric: mothers' fertility effort does not affect $h_N(a,t)$, because entry into motherhood is irreversible; by contrast, $\lambda_N(a')$ for $a' \leq a$ affect $h_M(a,t)$

[17] Because the mass of mothers is zero at $a = \underline{a}^w$, $h_M(a,t)$ is well-defined only for $a \in \left(\underline{a}^w, \bar{a}^w\right]$. By contrast, $h_N(a,t)$ is well-defined for all $a \in \left[\underline{a}^w, \bar{a}^w\right]$.

through the growth-state composition of new mothers, with the direction a priori ambiguous. Finally, for the primitives in Table 1, all effects on $h_j(a,t)$ operate through fertility rates, except for $\gamma$ and $\theta$, which also enter the transition structure directly and therefore affect the growth state distributions even holding fertility rates fixed.[18]

TABLE 2: KEY COMPARATIVE STATIC RESULTS OF GROWTH STATE DISTRIBUTION

| | $h_M(a,t)$ | $h_N(a,t)$ |
|---|---|---|
| *Effect of an increase in:* | | |
| $\lambda_M$ *at age* $a' \leq a$ | $-$ | $0$ |
| $\lambda_N$ *at age* $a' \leq a$ | $\pm$ | $-$ |

*Notes:* Each entry reports the sign of the functional derivative of the column variable with respect to the row function at point $a'$. Focusing on nontrivial cases, comparative statics are conducted over restricted age domain $\left(\underline{a}^w, \bar{a}^w\right]$ for $h_j(a,t)$. Ambiguous signs are denoted by "$\pm$". Proofs are in Online Appendix A.6.

Since the entry distribution $f(x,t)$ shifts over time according to (5), it is convenient to measure human capital relative to the current labor market entrants. I define the geometric-mean human capital of entering workers $\mathcal{Z}_{\underline{a}^w}(t)$, the normalized log human capital $\tilde{x}$, and the normalized conditional human capital distribution $\tilde{\ell}_{ij}(\tilde{x},a,t)$ respectively as

$$\mathcal{Z}_{\underline{a}^w}(t) \equiv e^{\int_{-\infty}^{\infty} x f(x,t)dx}, \tag{31}$$

$$\tilde{x} \equiv \log\left[\frac{z}{\mathcal{Z}_{\underline{a}^w}(t)}\right] = x - \log \mathcal{Z}_{\underline{a}^w}(t), \tag{32}$$

$$\tilde{\ell}_{ij}(\tilde{x},a,t) \equiv \ell_{ij}\left(\tilde{x} + \log \mathcal{Z}_{\underline{a}^w}(t), a, t\right) = \ell_{ij}(x,a,t). \tag{33}$$

This human capital normalization removes the common rightward drift induced by intergenerational spillovers: $\mathcal{Z}_{\underline{a}^w}(t)$ grows at the same rate as the traveling-wave shift of $f(x,t)$, so the normalized entry distribution $\tilde{f}(\tilde{x},t) \equiv f\left(\tilde{x} + \log \mathcal{Z}_{\underline{a}^w}(t), t\right)$ is stationary. Lemma 3 establishes these claims formally and shows that the normalized entry distribution can be written in terms of the initial entry distribution $f^0$, under the regularity conditions imposed by Assumption 3.[19]

ASSUMPTION 3. *The initial entry distribution of log human capital,* $f^0 : \mathbb{R} \to [0,\infty)$*, is a continuously differentiable probability density with finite first moment, satisfying* $\lim_{|x|\to\infty} |x| f^0(x) = 0$*,* $\int_{-\infty}^{\infty} \left|f^{0\prime}(x)\right| dx < \infty$*, and* $\int_{-\infty}^{\infty} e^x f^0(x)\, dx < \infty$*.*

LEMMA 3. *Under Assumption 3, the geometric-mean human capital of entering workers* $\mathcal{Z}_{\underline{a}^w}(t)$

[18] Holding fertility fixed, $\bar{a}^w$ affects $h_j(a,t)$ only at $a = \bar{a}^w$ but not at other ages.

[19] Assumption 3 imposes mild smoothness and tail conditions on $f^0$, ensuring finite average log human capital, finite aggregate output (since human capital $z = e^x$), and vanishing boundary terms in integration-by-parts arguments used below. These conditions are satisfied by common parametric specifications such as the normal, logistic, and Laplace distributions, among others.

*satisfies*

$$\log \mathcal{Z}_{\underline{a}^w}(t) = \int_{-\infty}^{\infty} x f^0(x)\, dx + \varphi \int_0^t \mathcal{H}(t')\, dt', \tag{34}$$

*where $\mathcal{H}(t)$ is the aggregate high-growth share defined in (6). The partial differential equation (5) with initial condition $f(x,0) = f^0(x)$ admits the traveling-wave solution*

$$f(x,t) = f^0\left(x - \varphi \int_0^t \mathcal{H}(t')\, dt'\right). \tag{35}$$

*The normalized entry distribution $\tilde{f}(\tilde{x},t)$ is stationary:*

$$\tilde{f}(\tilde{x},t) = \tilde{f}(\tilde{x}) = f^0\left(\tilde{x} + \int_{-\infty}^{\infty} x f^0(x)\, dx\right). \tag{36}$$

PROOF: See Online Appendix A.7.

In Online Appendix A.8, I show that the normalized conditional human capital distribution $\tilde{\ell}_{ij}(\tilde{x},a,t)$ for growth type $i \in \{H,L\}$ and motherhood status $j \in \{M,N\}$ evolves according to

$$\begin{aligned}\frac{\partial \tilde{\ell}_{ij}(\tilde{x},a,t)}{\partial t} + \frac{\partial \tilde{\ell}_{ij}(\tilde{x},a,t)}{\partial a} = &-\left[\mu_i - \eta(a) - \varphi \mathcal{H}(t)\right] \frac{\partial \tilde{\ell}_{ij}(\tilde{x},a,t)}{\partial \tilde{x}} \\ &+ \omega_{i'i,j}(a) \frac{Q_{i'j}(a,t)}{Q_{ij}(a,t)} \left[\tilde{\ell}_{i'j}(\tilde{x},a,t) - \tilde{\ell}_{ij}(\tilde{x},a,t)\right] \\ &+ \mathbb{I}_{j=M} \frac{\lambda_N(a)\,\Omega(a,t)}{1-\Omega(a,t)} \frac{Q_{iN}(a,t)}{Q_{iM}(a,t)} \left[\tilde{\ell}_{iN}(\tilde{x},a,t) - \tilde{\ell}_{iM}(\tilde{x},a,t)\right],\end{aligned} \tag{37}$$

where $i' \neq i$, $i' \in \{H,L\}$, and $Q_{ij}(a,t)$ is the share of growth type $i$ among workers with age $a$ and motherhood status $j$:

$$Q_{ij}(a,t) = \left\{h_j(a,t)\, \mathbb{I}_{i=H} + \left[1 - h_j(a,t)\right] \mathbb{I}_{i=L}\right\}. \tag{38}$$

Equation (37) is accompanied by the (limit) boundary condition at $a = \underline{a}^w$:

$$\tilde{\ell}_{iN}(\tilde{x}, \underline{a}^w, t) = \lim_{a \downarrow \underline{a}^w} \tilde{\ell}_{iM}(\tilde{x},a,t) = \tilde{f}(\tilde{x}), \tag{39}$$

and initial condition $\tilde{\ell}^0_{ij}(\tilde{x},a) = l^0_{ij}(x,a) / \int_{-\infty}^{\infty} l^0_{ij}(x,a)\, dx$. The first term on the right-hand side of (37) captures drift in relative log human capital, $\mu_i - \eta(a) - \varphi \mathcal{H}(t)$, i.e., individual accumulation net of the economy-wide shift in labor market entrants' human capital induced by intergenerational spillovers. The aggregate high-growth share $\mathcal{H}(t)$, defined in (6), can be written as

$$\mathcal{H}(t) = \int_{\underline{a}^w}^{\bar{a}^w} \left\{h_N(a,t)\,\Omega(a,t) + h_M(a,t)\left[1 - \Omega(a,t)\right]\right\} \frac{p(a,t)}{\int_{\underline{a}^w}^{\bar{a}^w} p(a,t)\, da} da, \tag{40}$$

so it is a population-weighted average of the age-specific high-growth shares $h_j(a,t)$ by motherhood status $j \in \{M,N\}$, with weights determined jointly by the population age density $p(a,t)$ and the age-specific shares of non-mothers $\Omega(a,t)$. Since $p(a,t)$ is pinned down by the KFE (25) with non-local boundary condition (29), $\mathcal{H}(t)$ generally has no closed-form expression. Finally, unlike the unnormalized worker density $l_{ij}(x,a,t)$, the normalized conditional distribution $\tilde{\ell}_{ij}(\tilde{x},a,t)$ factors out (i) changes in cohort size and (ii) the common rightward drift in entrants' human capital induced by intergenerational spillovers. This normalization separates aggregate growth forces—demographic and productivity-wise—from within-cohort distributional dynamics, making $\tilde{\ell}_{ij}(\tilde{x},a,t)$ the natural object for studying long-run stationary distributional outcomes.

## 2.4 Aggregation

This section builds the bridge from the model's individual-level and distributional objects to aggregate outcomes. I first define a dynamic equilibrium and establish its well-posedness. I then show that, although the model features a rich distribution of individual human capital, the aggregate outcomes studied in the quantitative analyses depend on this distribution only through a set of age-dependent conditional moments.

**Aggregate variables** Total population $P(t)$ and the working-age population $P^w(t)$ are given by

$$P(t) = \int_0^{\bar{a}} p(a,t)\,da, \quad P^w(t) = \int_{\underline{a}^w}^{\bar{a}^w} p(a,t)\,da.$$

Using definitions (27), (28), and (30), aggregate output (3) can be written as

$$Y(t) = \int_{\underline{a}^w}^{\bar{a}^w} y(a,t)\,p(a,t)\,da, \tag{41}$$

with the average output of age-$a$ workers given by

$$y(a,t) = \mathcal{Z}_{\underline{a}^w}(t) \sum_j \sum_i \mathcal{P}_j(a,t)\,\mathcal{Q}_{ij}(a,t)\,(1-\epsilon\mathbb{I}_{i=L}) \int_{-\infty}^{\infty} e^{\tilde{x}}\tilde{\ell}_{ij}(\tilde{x},a,t)\,d\tilde{x}, \tag{42}$$

where the normalization (32)–(33) is applied, $\mathcal{Q}_{ij}(a,t)$ is given by (38), and $\mathcal{P}_j(a,t)$ is the share of motherhood status $j$ among age-$a$ workers:

$$\mathcal{P}_j(a,t) = \left\{[1-\Omega(a,t)]\,\mathbb{I}_{j=M} + \Omega(a,t)\,\mathbb{I}_{j=N}\right\}. \tag{43}$$

Finally, the government budget constraint (4) can be written in terms of $y(a,t)$ and $p(a,t)$ as

$$\tau \int_{\underline{a}^w}^{\bar{a}^w} y(a,t)\,p(a,t)\,da = s(t)\int_0^{\underline{a}^w} p(a,t)\,da + v\int_{\bar{a}^w}^{\bar{a}} y(\bar{a}^w, t-a+\bar{a}^w)\,p(a,t)\,da, \tag{44}$$

which pins down the time-varying transfers $s(t)$ to individuals with age $a < \underline{a}^w$.

**Dynamic equilibrium** Taking stock of the model characterization so far, I now define a dynamic equilibrium of the economy.

DEFINITION 1. *Given initial distributions $p^0$, $f^0$, and $l^0_{ij}$ for $i \in \{H, L\}$ and $j \in \{M, N\}$, a dynamic equilibrium consists of fertility schedule $\lambda_j(a)$, time-varying distributions $p$ and $\tilde{\ell}_{ij}$, and paths $\left\{\mathcal{Z}_{\underline{a}^w}(t), s(t)\right\}_{t=0}^{\infty}$ such that (i) $\lambda_j(a)$ for $a \in \left[\underline{a}^w, \bar{a}^r\right)$ is given by Proposition 1 and $\lambda_j(a) = 0$ for all $a \notin \left[\underline{a}^w, \bar{a}^r\right)$; (ii) $p$ solves (25) with boundary condition (29); (iii) $\left\{\tilde{\ell}_{ij}\right\}_{i,j}$ jointly solve the system given by (37) with boundary conditions (39); (iv) $\mathcal{Z}_{\underline{a}^w}(t)$ is given by Lemma 3; and (v) the balanced-budget condition (44) holds for all $t$.*

Since $\mathcal{Z}_{\underline{a}^w}(t)$ and $s(t)$ are pinned down once the demographic and productivity blocks are determined, existence and uniqueness of a dynamic equilibrium reduce to existence and uniqueness of $p$ and $\tilde{\ell}_{ij}$.[20] Imposing regularity conditions on the initial distributions $p^0$ *and* $l^0_{ij}$ in Assumption OA2, Online Appendix A.9, I establish existence and uniqueness of the resulting equilibrium below.

PROPOSITION 2. *Under Assumptions 1–3 and OA1–2, the economy admits a unique dynamic equilibrium.*

PROOF: See Online Appendix A.9.

Proposition 2 ensures that the equilibrium objects used in the quantitative analysis are well-defined and uniquely pinned down by the model. I describe the idea of the proof here. Because the dynamics of population age density $p$ is independent of the normalized conditional human capital distribution $\tilde{\ell}_{ij}$, I establish existence and uniqueness of $p$ first. Next, taking $p$ as given, I establish existence and uniqueness of $\tilde{\ell}_{ij}$. In both steps, the method of characteristics transforms the relevant KFEs—together with their boundary conditions—into equivalent linear integral equations, for which solution existence and uniqueness follow from fixed-point arguments essentially leveraging the boundedness of fertility rates $\lambda_j$ and growth-state transition intensities $\omega_{HL,j}$ and $\omega_{LH,j}$.

Although the dynamic equilibrium tracks—through $\tilde{\ell}_{ij}(\tilde{x}, a, t)$—the distribution of human capital within each $(a, i, j)$-cell, aggregation uses the distribution $\tilde{\ell}_{ij}$ only through its exponential moment. Let $\mathcal{Z}_{ij}(a, t) \equiv \int_{-\infty}^{\infty} e^x \ell_{ij}(x, a, t)\, dx$ denote the average human capital of workers with age $a$, growth state $i$, and motherhood status $j$. Under the normalization (32)–(33), $\mathcal{Z}_{ij}(a, t)$ can be

[20] All remaining objects used in aggregation—$\Omega(a, t)$, $h_j(a, t)$, $Q_{ij}(a, t)$, $\mathcal{H}(t)$, $\mathcal{P}_j(a, t)$, and $y(a, t)$—are implied by $\lambda_j(a)$, $p(a, t)$, $\tilde{\ell}_{ij}(\tilde{x}, a, t)$, and $\mathcal{Z}_{\underline{a}^w}(t)$ via Lemmas 1–2, (38), (40), and (42)–(43). Furthermore, Definition 1 focuses on interior policy $\lambda_j(a)$ for $a \in \left[\underline{a}^w, \bar{a}^r\right)$ given by Proposition 1; the uniqueness of such interior fertility policy is established in the proof of Corollary 1.

expressed relative to the geometric-mean human capital of entering workers $\mathcal{Z}_{\underline{a}^w}(t)$ as

$$\mathcal{Z}_{ij}(a,t) = \mathcal{Z}_{\underline{a}^w}(t) \int_{-\infty}^{\infty} e^{\tilde{x}} \tilde{\ell}_{ij}(\tilde{x},a,t)\, d\tilde{x}. \tag{45}$$

Substituting (45) into (42), the average output of age-$a$ workers can be written as

$$y(a,t) = \sum_j \sum_i \mathcal{P}_j(a,t)\, \mathcal{Q}_{ij}(a,t)\, (1-\epsilon \mathbb{I}_{i=L})\, \mathcal{Z}_{ij}(a,t). \tag{46}$$

The following lemma isolates the objects needed for aggregation.

LEMMA 4. *The paths* $\left\{p(\cdot,t), \Omega(\cdot,t), h_j(\cdot,t), \mathcal{Z}_{ij}(\cdot,t)\right\}_{t=0}^{\infty}$ *are sufficient for determining the aggregate output path* $\{Y(t)\}_{t=0}^{\infty}$.

PROOF: The claim follows directly from (41) and (46), using the expressions (38) and (43).

Lemma 4 serves two purposes. First, it provides a basis for growth accounting by identifying the margins through which changes in aggregate output $Y(t)$ operate: demographics ($p$), worker composition ($\Omega$ and $h_j$), and average human capital conditional on age, growth type, and motherhood status ($\mathcal{Z}_{ij}$). Second, it guides empirical discipline: for quantitative analyses focused on aggregates, one need not measure the full human capital distributions $\tilde{\ell}_{ij}$. It suffices to discipline the model using this set of age-dependent objects $\left\{p, \Omega, h_j, \mathcal{Z}_{ij}\right\}$, which map one-to-one onto observable data counterparts. This tight mapping from theory to data is what enables the transparent calibration strategy described in Section 3.1.

**Growth accounting** Following Lemma 4, I now decompose changes in output per worker $Y(t)/P^w(t)$ to obtain a growth-accounting identity:

$$\begin{aligned}\frac{d}{dt}\frac{Y(t)}{P^w(t)} = &\underbrace{\int_{\underline{a}^w}^{\bar{a}^w} \left[\frac{\partial y(a,t)}{\partial t} + \frac{\partial y(a,t)}{\partial a}\right] \wp^w(a,t)\, da}_{\text{within-cohort changes}} + \underbrace{\left[y\left(\underline{a}^w,t\right) - \frac{Y(t)}{P^w(t)}\right] \wp^w\left(\underline{a}^w,t\right)}_{\text{entry}} \\ &\underbrace{- \left[y\left(\bar{a}^w,t\right) - \frac{Y(t)}{P^w(t)}\right] \wp^w\left(\bar{a}^w,t\right)}_{\text{retirement}} \underbrace{- \int_{\underline{a}^w}^{\bar{a}^w} \xi(a) \left[y(a,t) - \frac{Y(t)}{P^w(t)}\right] \wp^w(a,t)\, da}_{\text{mortality}},\end{aligned} \tag{47}$$

where $\wp^w(a,t) \equiv p(a,t)/P^w(t)$ is the age profile of workers. The first term is an age-weighted average of within-cohort changes experienced by incumbent workers. In particular, $\frac{\partial y(a,t)}{\partial t} + \frac{\partial y(a,t)}{\partial a}$ captures how the average output of cohort $t-a$ changes as its members age. In this model, within-cohort evolution reflects both shifts in cohort composition across motherhood status and growth types (through $\Omega$ and $h_j$) and changes in the average human capital given a motherhood status and a growth type (through $\mathcal{Z}_{ij}$). The remaining terms in (47) reflect workforce entry and exit; their

magnitudes depend not only on the worker age structure (through $\wp^w$), but also on how productive entrants and exits are relative to the average incumbent. In particular, the entry term is where intergenerational human capital spillovers directly affect output per worker, through the rightward shifting entry human capital distribution $f(x,t)$.

Since workers in the low-growth state reduce hours by a fraction of $\epsilon$, average hours per worker—given by $\mathcal{H}(t) + (1-\epsilon)[1-\mathcal{H}(t)]$—also evolves over time and admits a growth decomposition analogous to (47). Finally, aggregate productivity is defined as output per hour,

$$A(t) \equiv \frac{Y(t)}{\{\mathcal{H}(t) + (1-\epsilon)[1-\mathcal{H}(t)]\} P^w(t)}. \tag{48}$$

This definition implies that changes in output per capita $Y(t)/P(t)$ can be attributed to three sources: changes in the working-age population share $P^w(t)/P(t)$, changes in average hours per worker $\mathcal{H}(t) + (1-\epsilon)[1-\mathcal{H}(t)]$, and changes in aggregate productivity $A(t)$.

## 2.5 THE BALANCED GROWTH PATH

This section characterizes the model's balanced growth path (BGP). I first define the BGP equilibrium and describe the implied stationary distributions. I then study how changes along different fertility margins affect long-run population and productivity growth.

DEFINITION 2. *A BGP equilibrium is a dynamic equilibrium in which (i) total population $P(t)$ and the geometric-mean human capital of entering workers $\mathcal{Z}_{\underline{a}^w}(t)$ grow at constant rates and (ii) the population age profile $\wp(a,t) \equiv p(a,t)/P(t)$ and the normalized conditional human capital distribution $\tilde{\ell}_{ij}(\tilde{x},a,t)$ are stationary: $\wp(a,t) = \wp(a)$ and $\tilde{\ell}_{ij}(\tilde{x},a,t) = \tilde{\ell}_{ij}(\tilde{x},a)$ for $i \in \{H,L\}$ and $j \in \{M,N\}$.*

For a generic initial population age density $p^0$, the economy cannot satisfy the BGP conditions for $t \in [0,\bar{a})$, because cohorts present at $t=0$ still affect population age profile $\wp(a,t)$.[21] I therefore focus on $t \geq \bar{a}$, when the initial population has died out. In this case, Lemmas 1–2 imply that the non-mother shares by age and the high-growth shares by age and motherhood status are time-invariant: $\Omega(a,t) = \Omega(a)$ and $h_j(a,t) = h_j(a)$ for $j \in \{M,N\}$. On the BGP, the constant population growth rate $g_P = P'(t)/P(t)$ shapes the stationary age profile: $\wp(a) = \wp(0)\, e^{-\int_0^a [g_P + \xi(a')]da'}$. Thus, the newborn accounting identity (29) has the following stationary equivalent:

$$\alpha \int_{\underline{a}^w}^{\bar{a}^r} \{\lambda_N(a)\,\Omega(a) + \lambda_M(a)\,[1-\Omega(a)]\}\, e^{-\int_0^a [g_P+\xi(a')]da'} da = 1. \tag{49}$$

[21] The only exception is the knife-edge case in which the economy is initialized with the stationary age profile up to scale: $p^0(a) = P(0)\,\wp(a)$.

Equation (49) implicitly characterizes the BGP population growth rate $g_P$. Moreover, stationarity of $\wp(a)$, $\Omega(a)$, and $h_j(a)$ implies constant aggregate high-growth share on the BGP:

$$\mathcal{H} = \int_{\underline{a}^w}^{\bar{a}^w} \{h_N(a)\,\Omega(a) + h_M(a)\,[1-\Omega(a)]\}\,\wp^w(a)\,da, \tag{50}$$

where $\wp^w(a) = \wp(a) / \int_{\underline{a}^w}^{\bar{a}^w} \wp(a)\,da$ is the stationary age profile of workers. Using (41)–(42), aggregate productivity $A(t)$ defined in (48) can be written as the following on the BGP:

$$A(t) = \frac{\mathcal{Z}_{\underline{a}^w}(t)}{\mathcal{H} + (1-\epsilon)(1-\mathcal{H})} \int_{\underline{a}^w}^{\bar{a}^w} \tilde{y}(a)\,\wp^w(a)\,da,$$

where $\tilde{y}(a) \equiv y(a,t) / \mathcal{Z}_{\underline{a}^w}(t)$ is the average output of age-$a$ workers normalized by the geometric-mean human capital of entering workers $\mathcal{Z}_{\underline{a}^w}(t)$. In particular, $\tilde{y}(a)$ is time-invariant because all cross-sectional objects entering it—namely $\Omega(a)$, $h_j(a)$, and $\tilde{\ell}_{ij}(\tilde{x}, a)$—are stationary. Therefore, $A(t)$ grows at the same rate as $\mathcal{Z}_{\underline{a}^w}(t)$, because all its other determinants—average hours per worker $\mathcal{H} + (1-\epsilon)(1-\mathcal{H})$, worker age profile $\wp^w(a)$, and the normalized average output by age $\tilde{y}(a)$—are stationary on the BGP. Proposition 3 establishes the existence and uniqueness of the BGP equilibrium.

PROPOSITION 3. *There exists a unique BGP equilibrium in which (i) the population growth rate $g_P$ is implicitly given by (49) and (ii) aggregate productivity and hence GDP per capita grow at rate $g_A = \varphi\mathcal{H}$, where $\mathcal{H}$ is given by (50).*
PROOF: See Online Appendix A.10.

The proof follows by evaluating the unique dynamic equilibrium from Proposition 2 under stationarity; the BGP characterization is then reduced to a scalar fixed-point condition for $g_P$. Table 3 summarizes how the BGP population growth rate $g_P$ and productivity growth rate $g_A$ respond to changes in age-specific fertility rate $\lambda_j(a)$ by motherhood status $j \in \{M, N\}$.

TABLE 3: KEY COMPARATIVE STATIC RESULTS OF THE BGP GROWTH RATES

| | $g_P$ | $g_A$ |
|---|---|---|
| *Effect of an increase in:* | | |
| $\lambda_M$ *at age* $a$ | + | ± |
| $\lambda_N$ *at age* $a$ | + | ± |

*Notes:* Each entry reports the sign of the functional derivative of the column variable with respect to the row function at point $a \in [\underline{a}^w, \bar{a}^r)$. Ambiguous signs are denoted by "±". Proofs are in Online Appendix A.11.

Higher fertility for mothers and non-mothers both increase $g_P$, but through qualitatively different channels. In particular, for $j \in \{M, N\}$, let $\delta g_P[\lambda_j] / \delta\lambda_j(a)$ denote the effect on $g_P$ of a local

upward perturbation to the fertility schedule $\lambda_j$ at age $a$, which are given by

$$\frac{\delta g_P[\lambda_M]}{\delta \lambda_M(a)} = \underbrace{\frac{\alpha}{T_b}[1-\Omega(a)]\frac{\wp(a)}{\wp(0)}}_{\text{local boost}}, \tag{51}$$

$$\frac{\delta g_P[\lambda_N]}{\delta \lambda_N(a)} = \underbrace{\frac{\alpha}{T_b}\Omega(a)\frac{\wp(a)}{\wp(0)}}_{\text{local boost}} + \underbrace{\frac{\alpha}{T_b}\int_a^{\bar{a}^r}[\lambda_M(a')-\lambda_N(a')]\Omega(a')\frac{\wp(a')}{\wp(0)}da'}_{\text{non-local effect through motherhood-status reallocation}}, \tag{52}$$

where $T_b$ is the mean age of women at childbirth.[22] An increase in $\lambda_M(a)$ affects $g_P$ only through additional births at age $a$. By contrast, an increase in $\lambda_N(a)$ has both the local birth effect and a non-local reallocation effect because first births move women irreversibly out of the non-mother status. This reallocation effect attenuates the local boost if, over the remaining reproductive window $(a, \bar{a}^r)$, mothers' fertility is lower than that of non-mothers on an age-weighted-average basis, with the age weights determined by the age profile of non-mothers. Finally, the $1/T_b$ term makes transparent that, all else equal, a lower mean age at birth $T_b$ increases the sensitivity of $g_P$ to the fertility rates: more front-loaded childbearing over the life cycle shortens generation length and accelerates the compounding of birth boosts.

Next, I turn to the productivity growth rate $g_A$. Proposition 3 implies $g_A = \varphi\mathcal{H}$, so fertility affects long-run productivity growth only through its impact on the aggregate high-growth share $\mathcal{H}$. Since childbearing shapes the worker growth-state composition along multiple margins, the effect of higher fertility on $g_A$ is ambiguous for both motherhood statuses. Specifically, the effect on $g_A$ of a local upward perturbation to mothers' fertility schedule $\lambda_M$ at age $a$ is

$$\begin{aligned}\frac{\delta g_A[\lambda_M]}{\delta \lambda_M(a)} = &\underbrace{\varphi\int_{\underline{a}^w}^{\bar{a}^w}[1-\Omega(a')]\wp^w(a')\frac{\delta h_M[\lambda_M]}{\delta\lambda_M(a)}da'}_{\text{growth-state reallocation holding the age structure fixed}} \\ &+\underbrace{g_A\left[\int_{\underline{a}^w}^{\bar{a}^w}a\wp^w(a)\,da - \int_{\underline{a}^w}^{\bar{a}^w}a\wp_H^w(a)\,da\right]\frac{\delta g_P[\lambda_M]}{\delta\lambda_M(a)}}_{\text{age-structure channel}},\end{aligned} \tag{53}$$

where $\wp_H^w(a)$ is the age profile of high-growth workers.[23] Expression (53) highlights two channels through which an increase in $\lambda_M(a)$ affects $g_A$. The first term captures growth-state reallocation holding the population age structure fixed: higher $\lambda_M(a)$ shifts mothers out of the high-growth state, lowering $g_A$. The second term captures an age-structure channel: by raising $g_P$, higher

[22] Explicitly, $T_b = \alpha\int_{\underline{a}^w}^{\bar{a}^r} a\{\lambda_N(a)\Omega(a) + \lambda_M(a)[1-\Omega(a)]\}e^{-\int_0^a[g_P+\xi(a')]da'}da$.

[23] Explicitly, $\wp_H^w(a) = \mathcal{H}^{-1}\{h_N(a)\Omega(a) + h_M(a)[1-\Omega(a)]\}\wp^w(a)$.

$\lambda_M(a)$ tilts the worker age profile toward younger ages. The sign of this channel is governed by the difference between the average age of all workers, $\int_{\underline{a}^w}^{\bar{a}^w} a\wp^w(a)\,da$, and the average age of high-growth workers, $\int_{\underline{a}^w}^{\bar{a}^w} a\wp_H^w(a)\,da$. If high-growth status is systematically more prevalent at younger ages so that $\int_{\underline{a}^w}^{\bar{a}^w} a\wp^w(a)\,da - \int_{\underline{a}^w}^{\bar{a}^w} a\wp_H^w(a)\,da > 0$, then a younger age structure mechanically raises the aggregate high-growth share $\mathcal{H}$, increasing $g_A$ and acting against the first channel.

Turning to fertility of non-mothers, the effect on $g_A$ of a local upward perturbation to the fertility schedule $\lambda_N$ at age $a$ is

$$\frac{\delta g_A[\lambda_N]}{\delta\lambda_N(a)} = \underbrace{\varphi\int_{\underline{a}^w}^{\bar{a}^w}\left[h_N(a') - h_M(a')\right]\wp^w(a')\frac{\delta\Omega[\lambda_N]}{\delta\lambda_N(a)}da'}_{\text{motherhood-status reallocation holding the age structure fixed}} + \underbrace{\varphi\int_{\underline{a}^w}^{\bar{a}^w}\sum_j \mathcal{P}_j(a')\wp^w(a')\frac{\delta h_j[\lambda_N]}{\delta\lambda_N(a)}da'}_{\text{growth-state reallocation holding the age structure fixed}}$$
$$+ \underbrace{g_A\left[\int_{\underline{a}^w}^{\bar{a}^w} a\wp^w(a)\,da - \int_{\underline{a}^w}^{\bar{a}^w} a\wp_H^w(a)\,da\right]\frac{\delta g_P[\lambda_N]}{\delta\lambda_N(a)}}_{\text{age-structure channel}}, \tag{54}$$

where the sign of the effect through $h_j$, for $j \in \{M, N\}$, can be read from Table 2. Relative to (53), an increase in $\lambda_N(a)$ introduces an additional channel: holding the age structure fixed, first births shift women permanently into motherhood, altering their subsequent growth-state transition dynamics. The sign of this motherhood-status reallocation effect depends on $h_N(a') - h_M(a')$ for $a' \in (a, \bar{a}^w]$, i.e., the high-growth share differential between non-mothers and mothers over the remaining working life. If this differential is positive on an age-weighted-average basis, then entering motherhood lowers the expected future prevalence of high-growth status, reducing the aggregate high-growth share $\mathcal{H}$ and hence $g_A$.[24]

Finally, the instrument that raises fertility matters for productivity growth. Changes in contraception effectiveness $\kappa_j(a)$ affect $g_A$ only through the induced fertility changes. By contrast, changes in the short- and long-term career impacts of motherhood, $\gamma$ and $\theta$, have an additional direct effect on $g_A$, because they shift the distribution of workers across growth states, holding fertility rates fixed. In particular, lower $\gamma$ and $\theta$ mechanically raise the aggregate high-growth share $\mathcal{H}$, so reductions in these parameters are directly growth-enhancing on top of any fertility response. Overall, the long-run growth effects of pro-birth policies are nuanced: they depend not only on *which* women are targeted (by age and motherhood status) but also on *how* the age-type-specific fertility rates are raised.

[24] In (54), $\frac{\delta\Omega[\lambda_N]}{\delta\lambda_N(a)} < 0$, since non-mother share $\Omega(a)$ is a survival probability with hazard rate $\lambda_N(a)$.

# 3 QUANTIFICATION

I now take the model to the data and quantify the implications of reproductive freedom for economic growth and welfare. Empirical discipline comes from the analytical relationships established in Section 2 between model primitives and equilibrium objects that can be mapped one-to-one onto observable data counterparts. In particular, key structural parameters such as contraception effectiveness $\kappa_j$, the career impacts of motherhood $\gamma$ and $\theta$, and the degree of intergenerational human capital spillovers $\varphi$ can be separately identified from a set of age-dependent demographic and economic observables. Online Appendix B provides details on data construction and numerical methods, along with additional results.

## 3.1 CALIBRATION

The model is calibrated to the United States over 1961–2019. Only female data is used. I map growth types $i \in \{H, L\}$ to the data as follows: high-growth types are women who are either enrolled in school or working full time; low-growth types include the remainder, namely those not enrolled in school, working part time, unemployed, or out of the labor force.[25] The model is discretized at a monthly age-time step. I allow the following primitives to be hit by exogenous shocks that are unanticipated by individuals: the Poisson death intensity $\xi(a,t)$, contraception effectiveness $\kappa_j(a,t)$ for $j \in \{M, N\}$, and the short- and long-term career impacts of motherhood $\gamma(t)$ and $\theta(t)$. I do *not* assume that the economy is on a BGP, either initially or during the studied period; the quantified dynamics are therefore transition dynamics in response to repeated, unanticipated shocks to the selected primitives. The first two columns of Table 4 summarize the primitives to be calibrated and their definitions.

**Externally calibrated parameters** The maximum age $\bar{a}$ is set to 100. I construct the age-specific monthly Poisson death intensity $\xi(a,t)$ from age-specific annual death rates expressed as shares of the population. Panel (a) of Figure 12 in Online Appendix B.1 plots $\xi(a,t)$ for 1961 and 2019: mortality declines since the 1960s are concentrated among individuals aged 70 and above. The female share of newborns $\alpha$ is set to 1/2.05, consistent with an average male-to-female sex ratio at birth of 1.05 over the 1961–2019 period. I calibrate the natural fertility rates $\beta(a)$ using evidence from the medical literature, separating the calibration into an age gradient and a level. The age gradient of $\beta(a)$ is intended to capture changes in female reproductive capacity driven purely by biological maturation and aging, unrelated to behavioral factors and medical conditions such as infertility. I then scale the level of $\beta(a)$ to match completed fertility in natural-fertility populations

[25] The high-growth state is intended to represent a regime of rapid human capital accumulation, through either formal schooling or sustained on-the-job learning. This classification is useful for disciplining the 16–24 age range, where schooling is prevalent and substantial historical changes in fertility occur.

TABLE 4: MODEL PRIMITIVES WITH DEFINITIONS AND CALIBRATION RESULTS

| Parameter | Definition | Value |
|---|---|---|
| *Demographics* | | |
| $\bar{a}$ | Maximum age | 100 |
| $\underline{a}^w$ | Minimum working age | 16 |
| $\bar{a}^w$ | Maximum working age | 65 |
| $\bar{a}^r$ | Reproductive horizon | 45 |
| $\xi(a,t)$ | Mortality rate | Figure 12 in Online Appendix B.1 |
| $\beta(a)$ | Natural fertility rate | Figure 12 in Online Appendix B.1 |
| $\alpha$ | Female share of newborns | 1/2.05 |
| *Preferences* | | |
| $\rho$ | Discount rate | 0.003 |
| $\zeta$ | Utility of a child | 0.01 |
| *Human capital dynamics* | | |
| $\phi(a)$ | Baseline high-to-low growth state transition intensity | Figure 13 in Online Appendix B.1 |
| $\psi(a)$ | Baseline low-to-high growth state transition intensity | Figure 13 in Online Appendix B.1 |
| $\gamma(t)$ | Short-term career impact of motherhood | Figure 2$^\dagger$ |
| $\theta(t)$ | Long-term career impact of motherhood | Figure 2$^\dagger$ |
| $\epsilon$ | Labor supply reduction in the low-growth state | 0.8 |
| $\mu_H$ | Human capital growth rate in the high-growth state | 0.0222$^\dagger$ |
| $\mu_L$ | Human capital growth rate in the low-growth state | 0.0204 |
| $\eta(a)$ | Age-specific reduction in the learning rate | Equation (55) |
| $\varphi$ | Degree of intergenerational human capital spillovers | 0.0016$^\dagger$ |
| *Contraception effectiveness* | | |
| $\kappa_M(a,t)$ | Contraception effectiveness for mothers | Figure 3$^\dagger$ |
| $\kappa_N(a,t)$ | Contraception effectiveness for non-mothers | Figure 3$^\dagger$ |

*Notes:* Calibration details, including targeted observables, are described in the text and Online Appendix B.1–B.2. Superscripts † in the "Value" column indicate internally inferred primitives.

documented in historical data. Panel (b) of Figure 12 in Online Appendix B.1 plots the calibrated $\beta(a)$. The monthly discount rate $\rho$ is set at 0.003, corresponding to an annual rate of 0.036. The utility of a child $\zeta$ is normalized to 0.01.

The baseline transition intensities $\phi(a)$ and $\psi(a)$ between the two growth states are intended to capture idiosyncratic labor market risks unrelated to fertility effort. I calibrate these intensities to match age-specific flows between the two states in matched adjacent-month Current Population Survey (CPS) data for single women without children. Figure 13 in Online Appendix B.1 plots the resulting $\phi(a)$ and $\psi(a)$ over the working life. While the baseline high-to-low transition intensity $\phi(a)$ exhibits no clear age pattern, the baseline low-to-high transition intensity $\psi(a)$ declines steadily with age.

The reduction in working hours in the low-growth state $\epsilon$ is set to 0.8, matching the difference in average weekly hours between individuals in the two growth states in the CPS. The human capital growth rate differential $\mu_H - \mu_L$ is set to 0.0018, matching the observed gap in mean monthly

wage growth between high- and low-growth types in the CPS. I parameterize the age-dependent reduction in the learning rate $\eta(a)$ as piecewise linear and nondecreasing:

$$\eta(a) = \begin{cases} \left(\frac{\mu_H - 0.0028}{25 - \underline{a}^w}\right)(a - \underline{a}^w) & \text{for } a \in \left[\underline{a}^w, 25\right), \\ \mu_H - 0.0028 & \text{for } a \in [25, 40], \\ \mu_H - \frac{0.0028}{\bar{a}^w - 40}(\bar{a}^w - a) & \text{for } a \in (40, \bar{a}^w]. \end{cases} \tag{55}$$

This parameterization implies that the human capital growth rate of high-growth individuals, $\mu_H - \eta(a)$, is 0.0028 for age $a \in [25, 40]$, matching the corresponding mean monthly wage growth in the CPS. For $a \in (40, \bar{a}^w]$, $\eta(a)$ rises with age so that $\mu_H - \eta(a)$ declines to zero at retirement.

**Identification strategy** For the internally inferred parameters, empirical discipline comes from a sequential and analytical mapping between a set of age-dependent empirical objects and the model primitives. Inference proceeds in two stages. The first stage recovers the short- and long-term career impacts of motherhood, $\gamma(t)$ and $\theta(t)$, in a self-contained block. In the second stage, given the inferred paths $\{\gamma(t), \theta(t)\}_t$, contraception effectiveness $\{\kappa_j(\cdot, t)\}_t$ can be identified separately from growth-related parameters, $\mu_H$ and $\varphi$. Each of these steps exploits different observable variations. Table 5 summarizes the identification strategy, which I describe in detail below.

In the first stage, $\gamma(t)$ and $\theta(t)$ are inferred, period by period, from the observed high-growth share by age $H(\cdot, t)$, whose model counterpart is $\widehat{H}(\cdot, t) = h_N(\cdot, t)\,\Omega(\cdot, t) + h_M(\cdot, t)\,[1 - \Omega(\cdot, t)]$. For a given $t$, I take the observed fertility rates $\lambda_j(\cdot, t)$ as input. By Lemma 1, $\lambda_N(\cdot, t)$ pins down the age-specific non-mother shares $\Omega(\cdot, t)$ given $\Omega(\cdot, t - \Delta)$, where $\Delta$ is the discretization time step. Given $\Omega(\cdot, t)$ and the observed $\lambda_j(\cdot, t)$, Lemma 2 maps any candidate pair $\gamma(t)$ and $\theta(t)$ into the age-specific high-growth shares by motherhood status $h_j(\cdot, t)$ given $h_j(\cdot, t - \Delta)$, and hence into the model-implied age profile of high-growth shares $\widehat{H}(\cdot, t)$.[26] The 1960 non-mother shares by age $\Omega^0$ and high-growth shares by age and motherhood status $h_j^0$ are used as initial conditions for the forward iterations on $\Omega$ and $h_j$. I then choose $\gamma(t)$ and $\theta(t)$ to minimize $\int_{\underline{a}^w}^{\bar{a}^w} \left[H(a, t) - \widehat{H}(a, t)\right]^2 da$.

Online Appendix B.2.1 shows that the first-order conditions of this distance-minimization problem project the residual age profile $H(\cdot, t) - \widehat{H}(\cdot, t)$ onto two derivative profiles $\partial\widehat{H}(\cdot, t)/\partial\gamma(t)$ and $\partial\widehat{H}(\cdot, t)/\partial\theta(t)$. Identification therefore comes from these two derivative profiles being sufficiently distinct over age. The short-term impact $\gamma(t)$ enters growth-state transition rates through the term $\gamma(t)\,\lambda_j(a, t)$, so it loads on current fertility effort for both mothers and non-mothers and is therefore most relevant over childbearing ages. By contrast, the long-term impact $\theta(t)$ enters only

[26] The observed fertility rates $\{\lambda_j(\cdot, t)\}_t$ are used to construct $\left\{\widehat{H}(\cdot, t)\right\}_t$ because contraception effectiveness $\{\kappa_j(\cdot, t)\}_t$ is later recovered in a way such that the model-generated fertility rates match the data exactly.

through the motherhood-status indicator $\mathbb{I}_{j=M}$, so it shifts growth-state dynamics only after entry into motherhood and therefore loads on ages and cohorts with larger mother shares $1-\Omega(a,t)$.

TABLE 5: IDENTIFICATION OF THE INTERNALLY INFERRED PARAMETERS

| Parameter | Target | Input from Data | Internally Inferred Input | Theory |
|---|---|---|---|---|
| | | FIRST STAGE | | |
| $\gamma(t), \theta(t)$ | $H(\cdot,t)$ | $\Omega^0, h_j^0, \{\lambda_j(\cdot,t')\}_{t'\leq t}$ | - | Lemmas 1–2 |
| | | SECOND STAGE | | |
| $\kappa_j(a,t)$ | - | $\lambda_M(\cdot,t), \lambda_N(\cdot,t)$ | $\gamma(t), \theta(t)$ | Proposition 1 |
| $\mu_H, \varphi$ | $y(\cdot,2019)$ | $p^0, \mathcal{Z}_{ij}^0, \{\lambda_j(\cdot,t)\}_t$ | $\{\gamma(t), \theta(t), \Omega(\cdot,t), h_j(\cdot,t)\}_t$ | Lemmas 3–4 |

*Notes:* The first column lists the parameters to be identified. The second column lists the observables targeted in the distance-minimization problems. The third and fourth columns list the input used to construct the model counterparts of the targeted observables. The last column references the theoretical results that support the identification strategy.

Once the paths $\{\gamma(t), \theta(t)\}_t$ are inferred, the remaining two sets of primitives, $\{\kappa_j(\cdot,t)\}_t$ and $\{\mu_H, \varphi\}$, can be disciplined separately in the second stage. For a given $t$, I recover contraception effectiveness $\kappa_j(\cdot,t)$ directly from the observed fertility rates $\lambda_j(\cdot,t)$, relying on the structure provided by Proposition 1. Online Appendix B.2.2 shows that, using the optimal fertility schedules (17), one can rewrite the ODE (20) that implicitly characterizes the motherhood-status value differential $\Phi$, so that $\Phi(\cdot,t)$ can be computed from the observed $\lambda_j(\cdot,t)$ and the inferred $\gamma(t)$ and $\theta(t)$, without requiring $\{\kappa_j(\cdot,t)\}_t$. Given the incentive term $\gamma(t)\widehat{\Psi}(a,t)+\Phi(a,t)\mathbb{I}_{j=N}-\zeta\Pi(a,t)$, I then back out $\kappa_j(a,t)$ as the reduced-form shifter that rationalizes the observed gap between the natural fertility rate $\beta(a)$ and the realized fertility rate $\lambda_j(a,t)$.

The intergenerational spillover parameter $\varphi$ governs the rightward-shifting speed of the entry human capital distribution, while $\mu_H$ shapes individual wage growth over the life cycle. I therefore choose $\mu_H$ and $\varphi$ jointly to minimize $\int_{25}^{\bar{a}^w}[y(a,2019)-\widehat{y}(a,2019)]^2\,da$, where $y(a,2019)$ is the observed 2019 mean income by age and $\widehat{y}(a,2019)$ is the model counterpart given by (46).[27] Separate identification of $\mu_H$ and $\varphi$ exploits the fact that the cross-sectional moment $y(a,2019)$ is the combined outcome of both within-cohort income growth and cross-cohort changes at the entry point: $\mu_H$ governs the slope of income within a cohort as workers age, while $\varphi$ governs the level shift across cohorts of different ages in the 2019 cross-section. For computation, Lemma 4 suggests that $\widehat{y}(a,2019)$ can be constructed by tracking the dynamics of $p$, $\Omega$, $h_j$, and $\mathcal{Z}_{ij}$.[28] The paths $\{\Omega(\cdot,t), h_j(\cdot,t)\}_t$ are obtained as by-products from the first stage. Given the observed fertility rates $\{\lambda_j(\cdot,t)\}_t$, the inferred non-mother shares $\{\Omega(\cdot,t)\}_t$, and the 1960 population age density $p^0$ as the initial condition, the path $\{p(\cdot,t)\}_t$ can be computed iteratively from (25) and (29), as

[27] I exclude individuals below age 25 from the distance-minimization problem because wages are a noisy proxy for human capital for the 16–24 age group, many of whom are still in school.

[28] Even though age density $p(a,t)$ does not directly appear in the expression of the income-by-age profile (46), it is a determinant of $\mathcal{Z}_{ij}(a,t)$ at the boundary $a=\underline{a}^w$ through the aggregate high-growth share $\mathcal{H}(t)$ given by (40).

described in Online Appendix B.2.3. Finally, given the observed $\{\lambda_j(\cdot,t)\}_t$ and the inferred paths $\{\gamma(t), \theta(t), \Omega(\cdot,t), h_j(\cdot,t), p(\cdot,t)\}_t$, Online Appendix B.2.4 leverages Lemma 3 and shows how any candidate pair $\mu_H$ and $\varphi$ can be mapped to a path $\{\mathcal{Z}_{ij}(\cdot,t)\}_t$—and hence a 2019 income-by-age profile $\widehat{y}(a, 2019)$—by forward iteration from the initial condition $\mathcal{Z}_{ij}^0$, constructed from the 1960 mean income by age, growth type, and motherhood status. Since the inference targets only a single cross-section $\widehat{y}(a, 2019)$, the income-by-age profiles across other years can serve as over-identification checks, which I report in Section 3.2.

**Internally inferred parameters** Figure 2 plots the inferred paths for $\gamma(t)$ and $\theta(t)$. The long-term career impact of motherhood $\theta(t)$ declines steadily, falling by 92.1% between 1961 and 2019. The short-term career impact $\gamma(t)$ is more volatile and declines by 47.2% over the same period.[29]

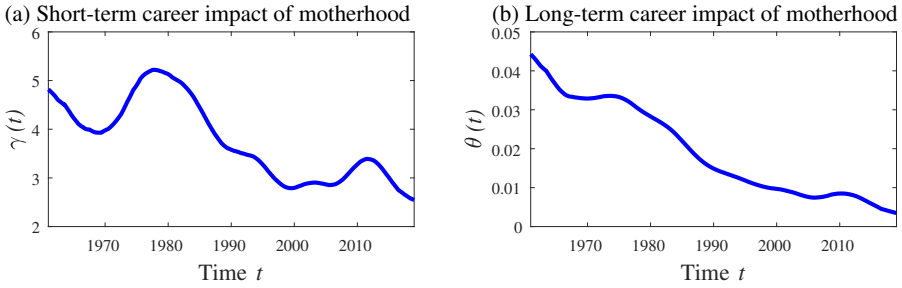



FIGURE 2: MODEL-IMPLIED CAREER IMPACTS OF MOTHERHOOD

Figure 3 plots the implied evolution of $\kappa_j(a,t)$ over time. Over 1961–2019, contraception effectiveness rises across the reproductive age spectrum. Averaged over reproductive ages, the implied improvement in contraception effectiveness is 323.3% for mothers and 292.4% for non-mothers.[30] In addition to this secular increase, the inferred $\kappa_j(a,t)$ typically exhibits a negative age slope at a given $t$. In the calibration, this life-cycle pattern of $\kappa_j(a,t)$ is mainly accounted for by the empirical age profile of the baseline low-to-high transition intensity $\psi(a)$ (see Panel (b) of Figure 13 in Online Appendix B.1): as $\psi(a)$ declines with age, low-growth episodes become more persistent, raising the continuation-value premium $\widehat{\Psi}(a)$ of being in the high-growth state and steepening the life-cycle opportunity-cost component of fertility incentives. As a result, matching the observed $\lambda_j(a,t)$ tends to require a negatively sloped age profile for $\kappa_j(a,t)$.

While $\kappa_j(a,t)$ is the model's reduced-form shifter governing the utility cost of pushing fertility below the biological benchmark, its welfare implications also depend on how far observed fertility $\lambda_j(a,t)$ lies below $\beta(a)$. Figure 4 therefore translates the inferred $\kappa_j(a,t)$ into the implied flow

[29] These downward trends are consistent with the reduced-form evidence in Kleven et al. (2025) showing attenuated child penalties, defined as the average post-first-birth decline in women's employment relative to men's, in the U.S. since the 1960s.

[30] The inferred upward trend in $\kappa_j(a,t)$ is consistent with the empirical literature documenting large post-1960 improvements in effective fertility control in the United States through multiple channels, including the diffusion of modern contraception methods, the relaxation of legal constraints on birth control access, and the expansion of publicly funded family planning programs (*e.g.,* Goldin and Katz 2002; Bailey 2010; Kearney and Levine 2009).

utility cost of birth control, $\chi_j(a,t) = \frac{1}{2\kappa_j(a,t)}\left[\beta(a) - \lambda_j(a,t)\right]^2$, which is plotted over reproductive ages for the beginning and the end of the studied period. Over 1961–2019, $\chi_j(a,t)$ falls for most ages, suggesting that improvements in contraception effectiveness $\kappa_j(a,t)$ typically translate into lower utility burden, given the observed fertility reduction $\beta(a) - \lambda_j(a,t)$. The main exception is young mothers, for whom the observed gap $\beta(a) - \lambda_j(a,t)$ widens sharply over 1961–2019 (see Panel (a) of Figure 1) and offsets the rise in $\kappa_j(a,t)$.

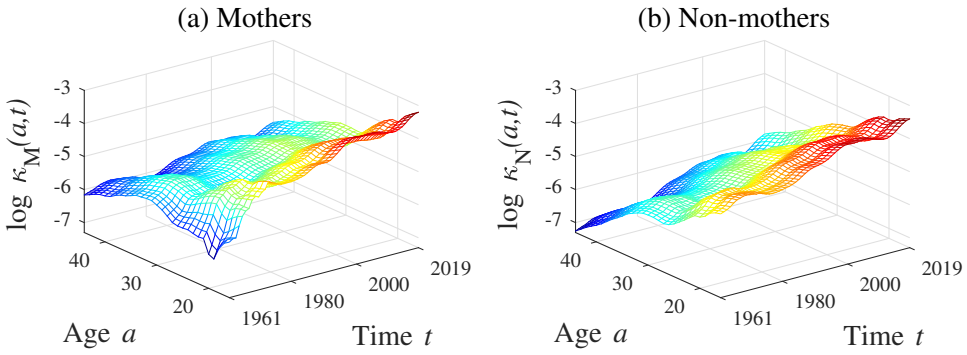



FIGURE 3: MODEL-IMPLIED CONTRACEPTION EFFECTIVENESS IN LOGS

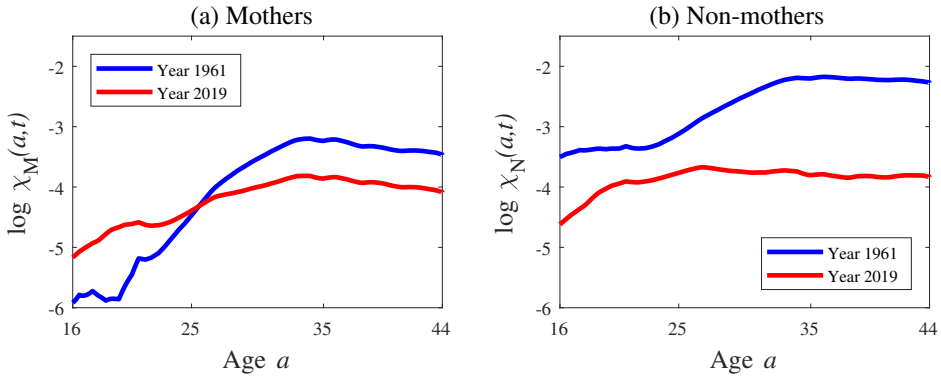



FIGURE 4: MODEL-IMPLIED UTILITY COST OF BIRTH CONTROL IN LOGS

## 3.2 MODEL VALIDATION

Before using the calibrated model for counterfactuals and projections, I assess model fit by comparing calibration outcomes with both targeted and untargeted observables. Figure 14 in Online Appendix B.3 compares the model-generated population age profile $\wp(a,t)$ to its empirical counterpart, untargeted in calibration. The model reproduces the evolution of the age distribution; the remaining discrepancies in later years reflect the assumption of no migration. Figure 15 in Online Appendix B.3 compares the model-generated age profile of high-growth share $H(a,t)$ to its empirical counterpart. The data show a steady rise in the high-growth share across the age spectrum over the past six decades. Panel (a) confirms that the calibrated model replicates the age profile of these shares, which are targeted period by period. Despite $\gamma(t)$ and $\theta(t)$ being age-independent,

panel (b) shows that the calibrated model tracks the time series of the high-growth share across the age spectrum. Finally, Figure 16 in Online Appendix B.3 compares the model-generated income dynamics to the data. Panel (a) shows that the model matches the time series of output per worker, while panels (b) and (c) show that it reproduces the dynamics of average income by age. This fit is noteworthy because (i) income-by-age profiles outside 2019 are *untargeted* in calibration, serving as over-identification checks, and (ii) the inferred parameters $\mu_H$ and $\varphi$ are neither age-specific nor time-varying. Overall, the calibrated model fits the age-structured dynamics of population, growth types, and labor income well.

## 3.3 COUNTERFACTUALS

Armed with the calibrated model, I now conduct counterfactual exercises to quantify the role of improvements in contraception effectiveness in accounting for aggregate changes in population structure, labor force participation, and labor productivity between 1961 and 2019.

In Scenario 1, I fix contraception effectiveness $\kappa_j(a,t)$ for all reproductive ages $a \in \left[\underline{a}^w, \bar{a}^r\right)$ and motherhood status $j \in \{M, N\}$, as well as the short- and long-term career impacts of motherhood $\gamma(t)$ and $\theta(t)$, at their 1961 levels. This scenario attributes the decline in the career impacts of motherhood entirely to rising contraception effectiveness, or more broadly to the same underlying forces.[31] In Scenario 2, contraception effectiveness is held at its 1961 level, while $\gamma(t)$ and $\theta(t)$ follow their calibrated paths over 1961–2019, implicitly treating the forces behind the declining career impacts of motherhood as orthogonal to changes in contraception effectiveness.

Figure 5 compares the counterfactual population dynamics to the calibrated baseline. Panels (a) and (b) report the 2019 age-specific fertility rates for mothers and non-mothers. In Scenario 1, the only time-varying primitives are mortality rates $\xi(a,t)$. With all other forces held fixed, declining mortality by itself reduces fertility, with a larger effect for non-mothers than for mothers. In Scenario 2, fertility rates rise above their 1961 levels across ages and motherhood status because the opportunity cost of motherhood—captured by $\gamma(t)$ and $\theta(t)$—falls over time, strengthening incentives to have children. Panels (c) and (d) plot the evolution of the total period fertility rate, $\int_{\underline{a}^w}^{\bar{a}^r} \{\lambda_N(a,t)\,\Omega(a,t) + \lambda_M(a,t)\,[1-\Omega(a,t)]\}\,da$, and the working-age share $P^w(t)/P(t)$. Relative to the baseline, both scenarios imply higher total period fertility and a lower working-age share over 1961–2019. The decline in the working-age share is driven mainly by faster population growth under higher fertility, which shifts the age distribution toward younger ages.

Turning to economic outcomes, Figure 6 compares the counterfactual scenarios to the baseline

[31] Improvements in contraception effectiveness may reduce the career impact of motherhood through both direct and indirect channels. For example, a direct channel may be the reduction of closely spaced pregnancies, which can harm women's health and hinder postpartum recovery; an indirect channel may be the effect of expanded fertility control on social norms around gender roles.

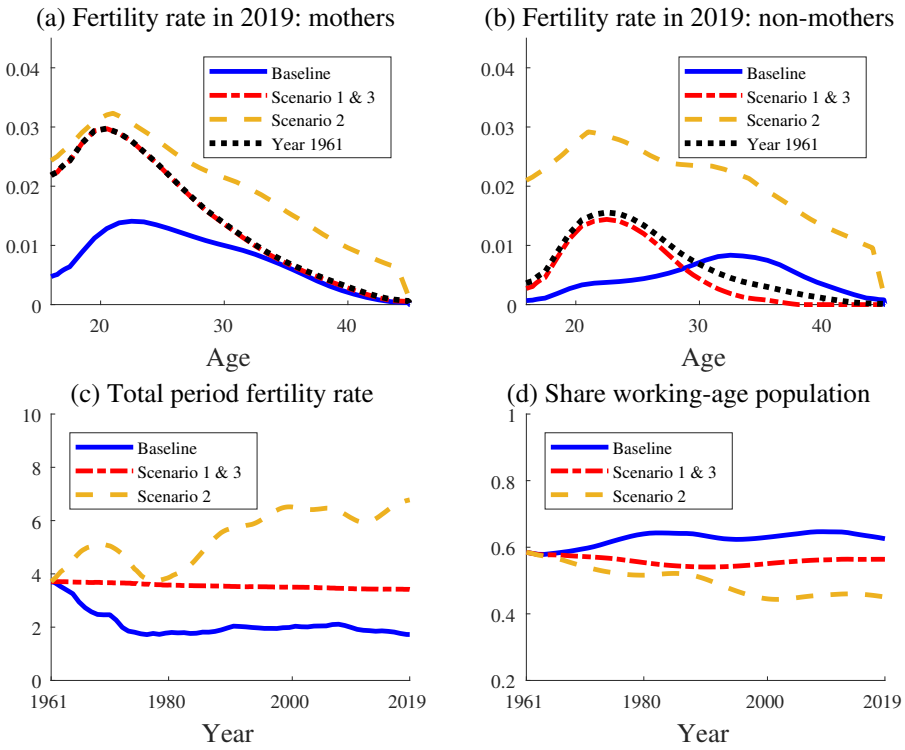



Figure 5: COUNTERFACTUAL OUTCOMES OF FERTILITY AND POPULATION

*Notes:* The baseline case maintains the calibrated parameter values given by Table 4. The counterfactual Scenarios 1 & 3 and Scenario 2 are defined in the text. In Panels (a) and (b), the 1961 fertility rates are also plotted as reference.

in terms of labor supply and aggregate productivity. Panel (a) shows that, in the baseline, average hours supplied per working-age individual, $\mathcal{H}(t) + (1-\epsilon)[1-\mathcal{H}(t)]$, rises by 48.7% between 1961 and 2019, whereas the corresponding increase is 9.9% in Scenario 1 and 39.0% in Scenario 2. Panel (b) reports that output per hour $A(t)$ rises by 181.5% in the baseline, compared with 111.4% in Scenario 1 and 120.4% in Scenario 2 over the same period.

A natural concern is that Scenario 2 generates fertility increases that imply total period fertility rates rarely observed in modern economies, making it an extreme counterfactual. I therefore introduce Scenario 3, in which individuals are oblivious to changes in $\gamma(t)$ and $\theta(t)$ when choosing fertility over the life cycle. In this case, the fallen career impacts of motherhood affect aggregate outcomes only through the transition intensities between human-capital-growth states, not through fertility behavior. By construction, demographic outcomes in Scenario 3 coincide with those in Scenario 1. Muting fertility responses allows Scenario 3 to close the gap in labor-supply growth, as shown in panel (a). However, panel (b) shows that Scenario 3 still implies a smaller increase in output per hour—152.1% between 1961 and 2019—than in the baseline.

Overall, taking the mean of Scenarios 2 and 3 as the conservative counterfactual and averaging it with the upper bound provided by Scenario 1, I conclude that the improvements in contraception

effectiveness contribute to 44% of the increase in female labor force participation, in terms of average hours supplied, and 32% of the rise in female labor productivity, in terms of output per hour, between 1961 and 2019.

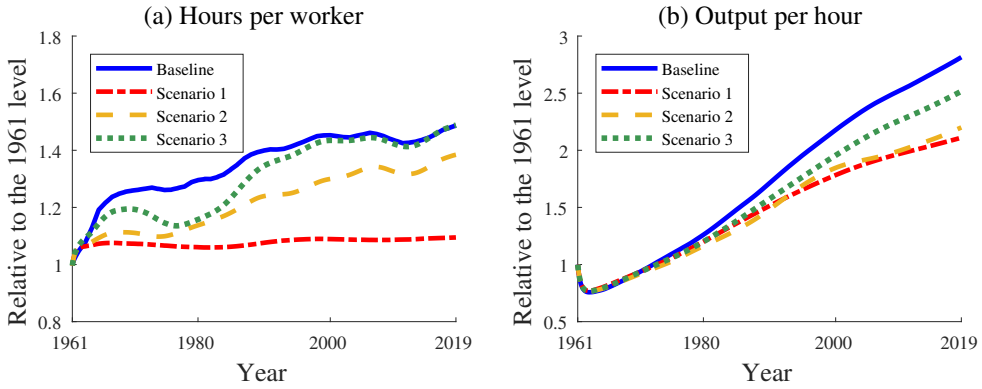



Figure 6: COUNTERFACTUAL OUTCOMES OF HOURS AND PRODUCTIVITY

*Notes:* The baseline case maintains the calibrated parameter values given by Table 4. The counterfactual Scenarios 1–3 are defined in the text.

Finally, to further interpret the sources of aggregate growth, Figure 17 in Online Appendix B.4 reports the growth-accounting decomposition (47) of the 1961–2019 change in output per worker $Y(t)/P^w(t)$ for the baseline and the three counterfactual scenarios. In all cases, the dominant contribution comes from within-cohort changes, which summarize how age-specific output per worker $y(a,t)$ evolves over time for incumbent cohorts as compositional shares $\Omega(a,t)$ and $h_j(a,t)$ and conditional mean human capital $\mathcal{Z}_{ij}(a,t)$ change. The entry margin contributes negatively because the average output of entrants $y(\underline{a}^w, t)$ remains below $Y(t)/P^w(t)$ throughout the transition, even as intergenerational spillovers raise entrant human capital over time. The retirement margin contributes positively because the average output of retirees $y(\bar{a}^w, t)$ is less than $Y(t)/P^w(t)$. The mortality margin is quantitatively negligible since mortality is low over working ages. Across counterfactuals, differences in output per worker growth are therefore primarily accounted for by differences in the within-cohort component, consistent with the model's emphasis on life-cycle human-capital and composition dynamics.

## 3.4 PROJECTIONS

In this section, I use the calibrated model to project future demographic and economic trajectories. I begin with a laissez-faire path in which all model primitives remain fixed at their 2019 values.[32] Figure 7 shows the transition to the long-run equilibrium. Panel (a) plots total population $P(t)$

[32]To minimize forecast error due to the no-migration assumption, the projection exercises use the observed 2019 population, instead of the model-simulated value, as the population initial condition.

and aggregate productivity $A(t)$. Population peaks around 2030 and then declines, with the long-run annual population growth rate converging to $-0.69\%$. This negative BGP growth rate results from a laissez-faire total period fertility rate of 1.72, below the replacement level of 2.05. Aggregate productivity, in contrast, continues to rise, registering an annual growth rate at 1.17% on the BGP. Panel (b) shows how population composition evolves along the transition. The working-age population share $P^w(t)/P(t)$ falls steadily and stabilizes at 0.57 by 2100, reflecting a shrunken workforce driven by population aging. The aggregate high-growth share $\mathcal{H}(t)$, in contrast, exhibits more pronounced oscillations during transition and converges to 0.63 on the BGP.

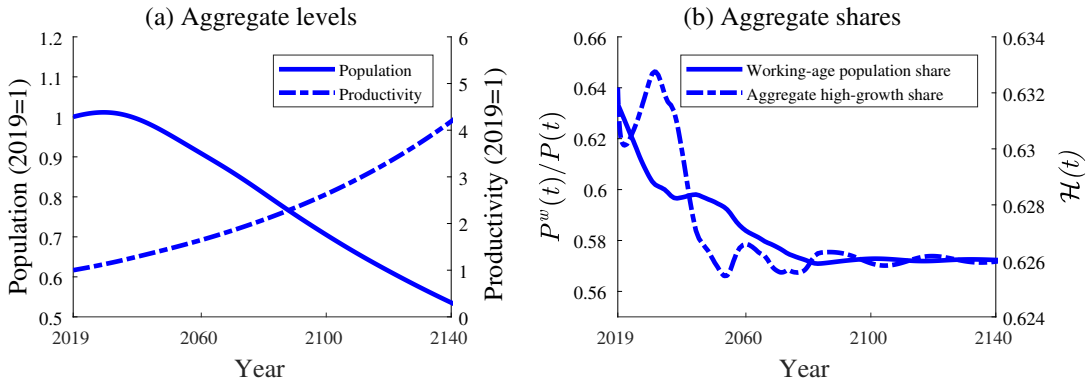



Figure 7: PROJECTIONS OF THE LAISSEZ-FAIRE ECONOMY

*Notes:* In Panel (a), the left axis corresponds to total population and the right axis aggregate productivity, both relative to the 2019 level. In Panel (b), the left axis corresponds to the share of population in the working age and the right axis the share of workers in the high-growth state.

Next, I investigate future demographic and economic trajectories when the economy is hit by a one-time exogenous shock to selected parameters. I consider three interventions that can, in principle, avert long-run population decline: (i) a permanent reduction in contraception effectiveness $\kappa_j(a)$ for all women; (ii) a permanent reduction in the short-term career impact of motherhood $\gamma$ for women aged 20 and above; and (iii) a permanent reduction in the long-term career impact of motherhood $\theta$ for women aged 20 and above.[33] In all cases, the shock is unanticipated and occurs in 2025. The first intervention can be interpreted as restricted reproductive freedom, while the latter two capture greater workplace family-friendliness.[34]

Figure 8 summarizes the long-run implications by plotting the BGP population and productivity growth rates, $g_P$ and $g_A$, as functions of the shock magnitude. Panel (a) shows that all three

[33]For projections, I allow the career-impact parameters to be age-dependent to model costless, age-targeted interventions. Reductions in the short- and long-term career impacts of motherhood are applied only to women aged 20 and above, so as not to directly encourage teen pregnancies. Even so, teenage non-mothers may still increase fertility effort in anticipation of lower motherhood costs later in life, reflecting the forward-looking nature of fertility planning.

[34]Pronatalist policies that restrict women's reproductive freedom are not merely hypothetical. The U.S. Supreme Court's 2022 decision overturning *Roe v. Wade* removed federal constitutional protection for abortion. Since abortion access and contraception are observationally equivalent with respect to fertility outcomes in this model, one interpretation of the reductions in $\kappa_j(a)$ is an expansion of abortion bans.

interventions can raise $g_P$ above zero. Population growth is least responsive to reductions in $\theta$, which affect fertility incentives only for non-mothers, whereas changes in $\kappa_j(a)$ and $\gamma$ influence incentives more broadly across motherhood status. Panel (b) shows that lowering $\gamma$ or $\theta$ unambiguously raises $g_A$ above the laissez-faire rate, while reducing contraception effectiveness can depress $g_A$ relative to laissez-faire. Thus, improving workplace family-friendliness can avoid a population-productivity trade-off, whereas restricting reproductive freedom may raise population growth at the cost of slower productivity growth.

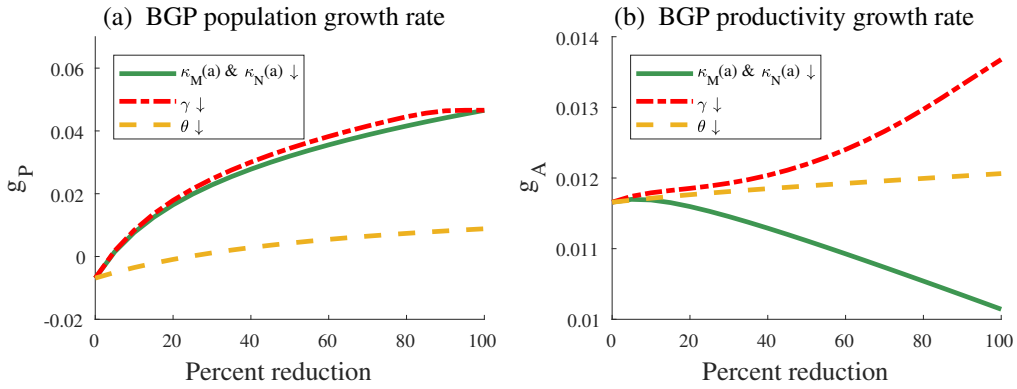



Figure 8: PROJECTIONS OF THE ECONOMY UNDER ONE-TIME SHOCK, BGP GROWTH RATES

*Notes:* This figure plots the BGP population and productivity growth rates for economies hit by a one-time exogenous shock to selected parameters, as described in the text. The horizontal axis corresponds to the permanent percent (proportional) reduction in the shocked parameter, with zero corresponding to the laissez-faire economy.

I then choose shock magnitudes for each intervention that generate the same BGP population growth rate and study the economy's transition after the shock occurs. Specifically, I consider: (i) an 11.1% reduction in contraception effectiveness $\kappa_j(a)$ for all women; (ii) a 10.4% reduction in the short-term career impact of motherhood $\gamma$ for women aged 20 and above; and (iii) the complete elimination of the long-term career impact of motherhood $\theta$ for women aged 20 and above.[35]

Figure 9 illustrates how the economy transitions to the BGP under each intervention. Panel (a) confirms that all three cases converge to the same long-run population growth rate of 0.88% per year, close to the average U.S. annual population growth rate since 2000. Panel (b) shows that each intervention implies a stationary working-age share of about 0.58, slightly above the laissez-faire projection because higher fertility mitigates population aging. Despite these similar demographic paths, the interventions differ in their economic implications. Panel (c) shows that eliminating the long-term career impact of motherhood $\theta$ yields the highest aggregate high-growth share $\mathcal{H}(t)$ and therefore the highest productivity growth both during the transition and on the BGP. While reductions in $\gamma$ and $\theta$ both enhance the likelihood of being in the high-growth state, the effect of a lower $\gamma$ is modulated by fertility effort $\lambda_j(a)$, whereas a lower $\theta$ applies uniformly to all mothers,

[35] Again, in all cases, the shock is unanticipated by individuals and hits the economy in 2025. Thus, the interventions should be read as surprise and immediate reforms rather than credible pre-announced transitions.

including those beyond reproductive age. It is worth noting that all three shocks lead to a BGP with a higher aggregate high-type share of workers, and hence a higher BGP productivity growth rate, than in the laissez-faire economy.[36] In the short to medium run, however, each shock generates losses in output per hour relative to the laissez-faire path, as shown in panel (d). These transitional productivity losses, reaching 4–6% by the 2080s, are larger under the shock that reduces contraception effectiveness than under shocks that alleviate the career penalty of motherhood.

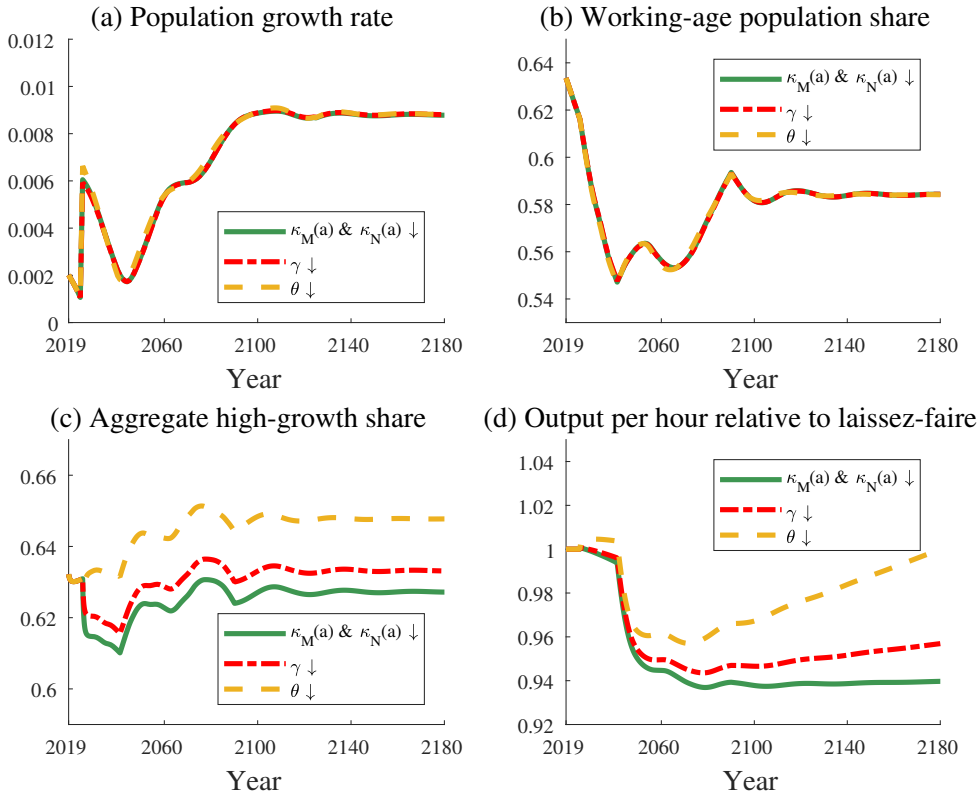



Figure 9: PROJECTIONS OF THE ECONOMY UNDER ONE-TIME SHOCK, TRANSITION PATHS

*Notes:* This figure plots the transition paths following three one-time, permanent exogenous shocks described in the text, each calibrated to generate a long-run population growth rate of 0.88% per year.

I conclude this section with the following policy implications. Although reducing the long-term career impact of motherhood $\theta$ has limited power to raise the long-run population growth rate $g_P$, it delivers the most favorable productivity-growth outcome among the costless interventions considered, conditional on achieving the same increase in $g_P$. Therefore, if the economy needs only a modest increase in $g_P$, policy should prioritize eliminating the long-term career impact of motherhood, through measures such as helping mothers who have completed childbearing return to full-time work. If instead the economy requires a considerable boost in $g_P$, policy should then

[36]The BGP aggregate high-growth share $\mathcal{H}$ equals 0.627 under the shock to $\kappa_j(a)$, 0.633 under the shock to $\gamma$, and 0.648 under the shock to $\theta$, all above the laissez-faire value of 0.626. Although reductions in $\kappa_j(a)$ do not directly affect transition intensities between growth states, they can still raise $\mathcal{H}$ by reshaping the population age structure, since younger workers are, on average, more likely to be in the high-growth state.

focus on reducing the short-term career impact of fertility effort, for instance by curbing workplace discrimination against pregnant and breastfeeding women and strengthening postpartum support. Finally, attempts to raise fertility by restricting women's reproductive freedom can entail long-lasting productivity losses.

## 3.5 WELFARE

As the final part of the quantitative analysis, I assess the welfare implications of changes in contraception effectiveness $\kappa_j(a,t)$ and in the short- and long-term career impacts of motherhood $\gamma(t)$ and $\theta(t)$. I conduct two exercises. First, I evaluate welfare along the historical 1961–2019 path by comparing the factual economy with the three counterfactual scenarios described in Section 3.3. Second, I assess the welfare effects of the alternative future parameter trajectories behind Figure 9 relative to the laissez-faire projection.

**Welfare measurement** Welfare gains or losses are measured by consumption equivalent variation (CEV): the permanent percentage change in consumption that makes an individual indifferent between being born to the factual/laissez-faire economy and the counterfactual/intervened economy. Since individuals have finite lifespans and cohorts differ due to secular trends, CEV is cohort-specific. The CEV for cohort $t$, $\mathcal{E}(t)$, is defined implicitly by $\mathcal{V}(t) + \Pi(0,t)\log(1+\mathcal{E}(t)) = \mathcal{V}^*(t)$, where $\mathcal{V}(t)$ and $\mathcal{V}^*(t)$ denote average realized lifetime utility in the factual/laissez-faire and counterfactual/intervened economies, respectively. Using Proposition 1 and Lemma 3, cohort-specific CEV admits the decomposition

$$\begin{aligned}\Pi(0,t)\log(1+\mathcal{E}(t)) = &\underbrace{\int_0^{\underline{a}^w} e^{-\int_0^{a'}[\rho+\xi(a'',t+a'')]da''}\log\frac{s^*(t+a')}{s(t+a')}da'}_{\text{intergenerational transfer via the government}}\\ &+\underbrace{e^{-\int_0^{\underline{a}^w}[\rho+\xi(a',t+a')]da'}\Pi\left(\underline{a}^w,t+\underline{a}^w\right)\log\frac{\mathcal{Z}^*_{\underline{a}^w}\left(t+\underline{a}^w\right)}{\mathcal{Z}_{\underline{a}^w}\left(t+\underline{a}^w\right)}}_{\text{intergenerational human capital spillover}}\\ &+\underbrace{e^{-\int_0^{\underline{a}^w}[\rho+\xi(a',t+a')]da'}\left[\check{\Phi}\left(\underline{a}^w,t+\underline{a}^w\right)+\check{\Psi}_H\left(\underline{a}^w,t+\underline{a}^w\right)\right]}_{\text{changes during the individual's working life}}\end{aligned} \tag{56}$$

where variables with an asterisk refer to the counterfactual/intervened paths.[37] The right-hand side of (56) highlights three distinct channels through which changes in the paths $\left\{\kappa_j(\cdot,t),\gamma(t),\theta(t)\right\}_t$

[37] In (56), I define $\check{\Phi} = \Phi^* - \Phi$ and $\check{\Psi}_H = \Psi_H^* - \Psi_H$, where $\Phi$ is the motherhood-status value differential characterized in Proposition 1. The term $\Psi_H$ denotes the remaining value of a working-age, high-type non-mother that is not accounted for by her current human capital level or motherhood status, i.e., $\Psi_H(a,t+a) = V_{HN}(x,a,t+a) - \Pi(a,t+a)\,x - \Phi(a,t+a)$. Derivation details of (56) are provided in Online Appendix B.5.1.

affect the welfare of a representative member of cohort $t$.[38] First, consumption prior to the working life depends on government transfers, which adjust each period to satisfy the balanced-budget condition (44). Since these transfers are financed by income taxes on the contemporaneous working-age population, this channel can be interpreted as inter-vivo transfers from earlier cohorts to later ones. Second, the cohort-$t$ individual draws initial human capital at age $\underline{a}^w$ from a distribution $f(x,t)$ that shifts over time with the economy's trajectory. Alternative paths $\{\kappa_j(\cdot,t),\gamma(t),\theta(t)\}_t$ generate different paths of the aggregate high-growth share $\mathcal{H}(t)$, which governs the traveling speed of $f(x,t)$; this channel captures intergenerational linkage through human capital spillovers. Third, once the individual enters working life, the altered primitive paths reshape her optimal fertility schedule and, through it, her life-cycle profiles of human capital and income.[39]

For aggregate welfare comparison across allocations, I adopt the *$\mathcal{A}$-Efficiency* criterion of Golosov et al. (2007), which is designed for normative analysis with endogenous populations. *$\mathcal{A}$-Efficiency* takes into account only individuals who are alive in both allocations being compared. In the present context, social welfare in the counterfactual/intervened economy is therefore $\mathcal{W}^* = \int_0^\infty e^{-\rho^s t}\mathcal{V}^*(t)\,p(0,t)\,dt$, where $p(0,t)$ is the cohort size in the factual/laissez-faire economy and $\rho^s$ is the social discount rate.[40] The aggregate welfare change $\mathcal{E}$, in terms of CEV, is defined by $\mathcal{W} + \int_0^\infty e^{-\rho^s t}\Pi(0,t)\,p(0,t)\,dt\log(1+\mathcal{E}) = \mathcal{W}^*$, where $\mathcal{W}$ denotes social welfare in the factual/laissez-faire economy.

**Historical counterfactuals** To quantify the welfare outcomes, two additional parameters need calibration: pension replacement rate $\upsilon$ and income tax rate $\tau$. I set $\upsilon = 0.4$ and $\tau = 0.15$, in line with the observed average rates in the US. Figure 10 reports welfare changes under the three counterfactual scenarios from Section 3.3.[41] As in the counterfactual analysis, I treat Scenario 1 as an upper bound on the quantitative importance of improvements in contraception effectiveness since 1961 and the mean of Scenarios 2 and 3 as a lower bound; I take the average of the upper and lower bounds as a single summary measure.

Panel (a) shows substantial heterogeneity across cohorts. Cohorts born around 2000 benefit the

[38] Because it governs the disutility of birth control, contraception effectiveness $\kappa_j$ can be viewed as a preference primitive. Welfare analysis with time-varying preferences can be difficult to interpret. In the current framework, however, conditional on the chosen fertility schedules $\lambda_j$, the relevant components of the value functions—$\Phi$ and $\Psi_H$—no longer depend on $\kappa_j$. As a result, $\kappa_j$ affects the right-hand side of (56) only through $\lambda_j$. Welfare comparisons across alternative paths $\{\kappa_j(\cdot,t)\}_t$ can therefore be interpreted as comparisons across the corresponding paths $\{\lambda_j(\cdot,t)\}_t$.

[39] For welfare assessment, I maintain the assumption used in the previous quantitative sections that, when choosing fertility effort $\lambda_j(a,t+a)$ over the working life, a cohort-$t$ individual forms myopic expectations about the future paths $\{\kappa_j(a,t+a),\gamma(t+a),\theta(t+a)\}_{a=\underline{a}^w}^{\bar{a}^w}$.

[40] *$\mathcal{A}$-Efficiency* circumvents the philosophical difficulty of assigning welfare weights to the unborn and has been used to evaluate fertility-related policies, for example in Kim et al. (2024). Since the counterfactual/intervened economy features weakly higher fertility than the factual/laissez-faire economy—i.e., $p^*(0,t) \geq p(0,t)$ for all $t$—I assume that every individual born in the factual/laissez-faire economy is also born in the counterfactual/intervened economy.

[41] After 2019, the factual and the three counterfactual paths $\{\kappa_j(\cdot,t),\gamma(t),\theta(t)\}_t$ are held constant.

most from the 1961–2019 expansion in reproductive freedom, with CEVs below −50%, meaning they would forgo more than half of lifetime consumption to remain in a world with rising contraception effectiveness. Welfare gains then decline for cohorts born after the early 2000s because the three channels in (56) increasingly offset one another. In particular, as the factual economy ages, these later cohorts receive less pre-working-age consumption support: the retirement of the Baby Boom generation raises the share of GDP devoted to pension payments, tightening resources available for the young. Panel (b) shows that aggregate welfare depends on the social discount rate $\rho^s$. When all cohorts are weighted equally ($\rho^s = 0$), the welfare gains from improvements in contraception effectiveness since 1961 are equivalent to a 37% increase in lifetime consumption. As $\rho^s$ rises to the private discount rate, the implied gain declines to 28%.

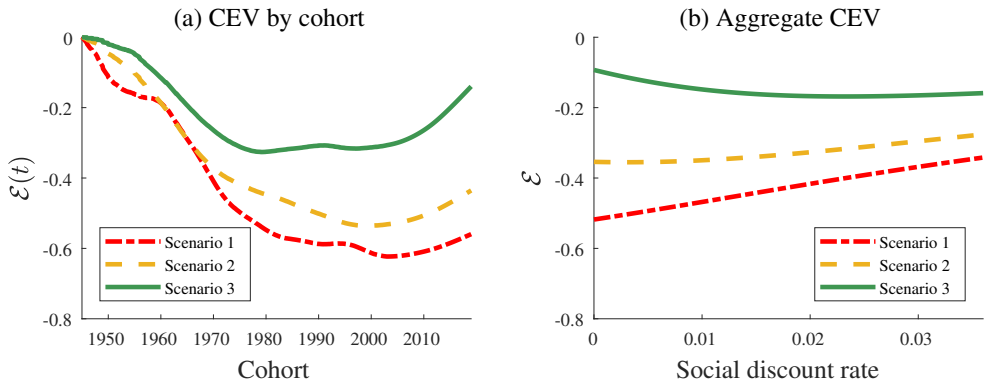



Figure 10: WELFARE ASSESSMENT OF HISTORICAL COUNTERFACTUALS

*Notes:* Panel (a) plots cohort-specific CEV for cohorts born between 1945 and 2019. Panel (b) plots aggregate CEV for various annual social discount rates, ranging from zero to the private discount rate. Counterfactual Scenarios 1–3 are defined in Section 3.3.

Figure 18 in Online Appendix B.5.3 decomposes the aggregate welfare gains into the three channels highlighted by (56). Pre-working-age transfer is the quantitatively dominant channel. The historical improvements in fertility control thus raise welfare largely because the counterfactual higher-fertility paths would have created more near-term dependents and crowded out resources for the cohorts growing up during the transition.

**Future projections** Figure 11 reports the welfare implications of the three costless population-boosting interventions from Section 3.4. Panel (a) shows that earlier cohorts are harmed by these interventions. Because births rise permanently from 2025 onward, the age-dependency ratio increases in the short to medium run, reducing per capita consumption for the pre-working-age population below the laissez-faire level. Cohorts born in the mid-2030s experience the largest welfare losses, with CEVs as low as −18%, meaning they would forgo up to 18% of lifetime consumption to avoid the intervened paths. Welfare effects turn positive for cohorts born around 2060 and later, once the higher birth rates translate into a sufficiently larger workforce that lowers the dependency

ratio and raises pre-working-age consumption above the laissez-faire level. Across cohorts, reducing contraception effectiveness $\kappa_j(a)$ generates the largest welfare losses (or smallest gains), whereas eliminating the long-term career impact of motherhood $\theta$ yields the smallest losses (or largest gains). Panel (b) shows that the same ranking holds for aggregate welfare. Relative to eliminating $\theta$, reducing $\kappa_j(a)$ delivers a smaller aggregate welfare gain (or a larger aggregate welfare loss) equivalent to 4.3% of lifetime consumption when averaged over $\rho^s \in [0, \rho]$. The aggregate welfare implications of the pro-natal interventions depend crucially on the social discount rate: as $\rho^s$ increases from zero to $\rho$, the implied aggregate welfare effect ranges from positive to negative.

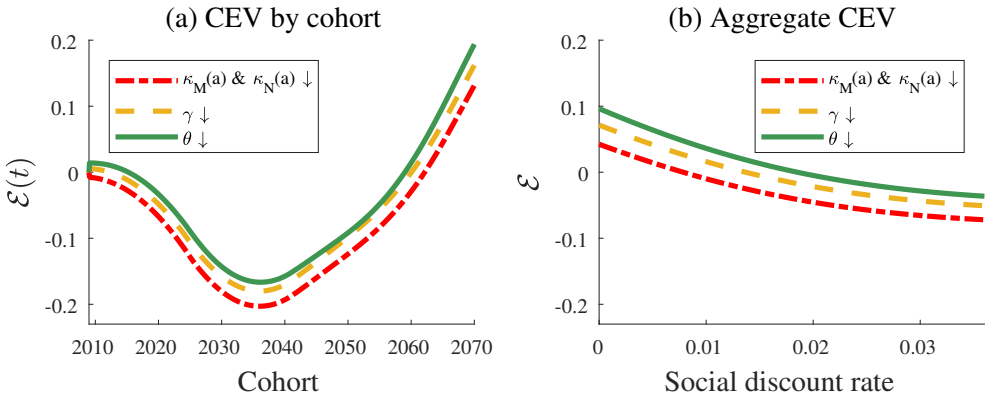



Figure 11: WELFARE ASSESSMENT OF INTERVENED FUTURE TRAJECTORIES

*Notes:* Panel (a) plots cohort-specific CEV for cohorts born between 2009 and 2070. Panel (b) plots aggregate CEV for various annual social discount rates, ranging from zero to the private discount rate. The interventions correspond to the three one-time, permanent exogenous shocks described in Section 3.4, each calibrated to generate a long-run population growth rate of 0.88% per year.

Figure 19 in Online Appendix B.5.3 decomposes the aggregate welfare changes according to (56). Again, pre-working-age transfer quantitatively dominates the other two channels: early cohorts lose because of baby-boom crowding; later cohorts may recover as the larger workforce arrives. Crucially, the decomposition highlights a qualitative difference between pro-natal interventions that restrict reproductive freedom versus improve workplace family friendliness. Under reduced career impacts of motherhood $\gamma$ and $\theta$, the spillover channel and the working-life channel both contribute positively to aggregate welfare, partially offsetting the transfer drag; by contrast, the welfare contribution from these two channels turns negative under reduced contraception effectiveness $\kappa_j(a)$.

To summarize, the welfare exercises in this section deliver three policy lessons. First, policies that appear age-neutral from a period perspective can generate heterogeneous welfare effects across cohorts, making the choice of a social discount rate consequential. Second, pro-natal interventions can impose welfare losses on near-term cohorts: baby booms raise the age-dependency ratio in the short to medium run, while the resulting workforce expansion arrives only with a lag. Third,

holding demographic outcomes fixed, restricting reproductive freedom entails additional welfare costs relative to policies that alleviate the career impact of motherhood for every affected cohort.

# 4 Conclusion

In modern high-income economies, where completed fertility is low and working lives are long, the key question at the fertility-growth nexus is not whether births occur, but when they occur and at what career costs. Embedding realistic life-cycle fertility choices into a non-stationary growth framework, this paper shows that fertility timing is a first-order determinant of aggregate productivity and welfare. By expanding women's ability to time births during prime years for human capital accumulation, reproductive freedom therefore has important implications for economic growth.

This paper yields three policy-relevant insights for advanced economies seeking to avert population decline. First, because entry into motherhood is irreversible and permanently alters women's human capital growth prospects, first births are qualitatively different from subsequent births, both in their responses to policy incentives and in their implications for aggregate productivity. Second, for economic growth, how fertility is increased matters as much as how much it is increased. Holding fixed the demographic target, policies that reduce the long-term career impact of motherhood deliver the most favorable productivity and welfare outcomes, whereas policies that restrict reproductive control deliver the least favorable outcomes. These differences arise not from preferences but from the interaction between fertility timing, human capital dynamics, and age-structured aggregation. Third, since demographic changes unfold slowly, their welfare consequences are inherently cohort-dependent. Even pro-natal policies that are beneficial in the long run can impose sizable transitional burdens through higher dependency ratios. As a result, aggregate welfare rankings of population policies depend critically on how societies weigh intergenerational inequalities.

The framework abstracts from several dimensions that could be incorporated in future work. Introducing savings and explicit financial costs of child rearing would allow a richer treatment of life-cycle fertility choices. Extending the model to couple formation could shed light on how reproductive freedom interacts with marital sorting. Finally, applying the framework across countries would help quantify how cross-country differences in reproductive freedom, labor market environment, and family policies shape the fertility-growth nexus in modern high-income economies.

# References

Abad, Nicolas, Johanna Etner, Natacha Raffin, and Thomas Seegmuller. 2025. New Fertility Patterns: The Role of Human versus Physical Capital. *Journal of Economic Theory* 228: 106037.

Adda, Jérôme, Christian Dustmann, and Katrien Stevens. 2017. "The Career Costs of Children." *Journal of Political Economy* 125 (2): 293-337.

Bailey, Martha J. 2006. "More Power to the Pill: The Impact of Contraceptive Freedom on Women's Lifecycle Labor Supply." *Quarterly Journal of Economics* 121 (1): 289-320.

Bailey, Martha J. 2010. ""Momma's Got the Pill": How Anthony Comstock and *Griswold v. Connecticut* Shaped US Childbearing." *American Economic Review* 100 (1): 98-129.

Bailey, Martha J., Brad Hershbein, and Amalia R. Miller. 2012. "The Opt-In Revolution? Contraception and the Gender Gap in Wages." *American Economic Journal: Applied Economics* 4 (3): 225-254.

Barro, Robert J., and Gary S. Becker. 1989. "Fertility Choice in a Model of Economic Growth." *Econometrica* 57 (2): 481-501.

Becker, Gary S., and Robert J. Barro. 1988. "A Reformulation of the Economic Theory of Fertility." *Quarterly Journal of Economics* 103 (1): 1-25.

Broekmans, Frank J., Erik A.H. Knauff, Egbert R. te Velde, Nick S. Macklon, and Bart C. Fauser. 2007. "Female Reproductive Aging: Current Knowledge and Future Trends". *Trends in Endocrinology and Metabolism* 18 (2): 58-65.

Choi, Sekyu. 2017. "Fertility Risk in the Life Cycle." *International Economic Review* 58 (1): 237-259.

Cortés, Patricia, and Jessica Pan. 2023. "Children and the Remaining Gaps in the Labor Market." *Journal of Economic Literature* 61 (4): 1359–1409.

d'Albis, Hippolyte, Emmanuelle Augeraud-Véron, and Katheline Schubert. 2010. "Demographic-economic Equilibria When the Age at Motherhood is Endogenous." *Journal of Mathematical Economics* 46 (6): 1211-1221.

d'Albis, Hippolyte, Angela Greulich, and Gregory Ponthiere. 2018. "Development, Fertility and Childbearing Age: A Unified Growth Theory." *Journal of Economic Theory* 177: 461-494.

de la Croix, David, and Matthias Doepke. 2003. "Inequality and Growth: Why Differential Fertility Matters." *American Economic Review* 93 (4): 1091-1113.

de la Croix, David, and Omar Licandro. 2013. "The Child is Father of the Man: Implications for the Demographic Transition." *Economic Journal* 123 (567): 236-261.

Eckstein, Zvi, Michael Keane, and Osnat Lifshitz. 2019. "Career and Family Decisions: Cohorts Born 1935-1975." *Econometrica* 87 (1): 217-253.

Gallen, Yana, Juanna Schrøter Joensen, Eva Rye Johansen, and Gregory F. Veramendi. 2025. "The Labor Market Returns to Delaying Pregnancy." *Working Paper.*

Galor, Oded, and David N. Weil. 1996. "The Gender Gap, Fertility, and Growth." *American Economic Review* 86 (3): 374-387.

Greenwood, Jeremy, Ananth Seshadri, and Guillaume Vandenbroucke. 2005. "The Baby Boom and Baby Bust." *American Economic Review* 95 (1): 183-207.

Goldin, Claudia. 2024. "Nobel Lecture: An Evolving Economic Force." *American Economic Review* 114 (6): 1515-1539.

Goldin, Claudia, and Lawrence Katz. 2002. "The Power of the Pill: Oral Contraceptives and Women's Career and Marriage Decisions." *Journal of Political Economy* 110 (4): 730-770.

Golosov, Mikhail, Larry E. Jones, and Michèle Tertilt. 2007. "Efficiency with Endogenous Population Growth." *Econometrica* 75 (4): 1039-1071.

Iannelli, Mimmo, and Fabio Milner. 2017. *The Basic Approach to Age-Structured Population Dynamics: Models, Methods, and Numerics*. Dordrecht: Springer Nature.

Iyigun, Murat F. 2000. "Timing of Childbearing and Economic Growth." *Journal of Development Economics* 61 (1): 255-269.

Jones, Charles I. 2022. "The End of Economic Growth? Unintended Consequences of a Declining Population." *American Economic Review* 112 (11): 3489–3527.

Kearney, Melissa S., and Phillip B. Levine. 2009. "Subsidized Contraception, Fertility, and Sexual Behavior." *Review of Economics and Statistics* 91 (1): 137-151.

Kim, Seongeun, Michèle Tertilt, and Minchul Yum. 2024. "Status Externalities in Education and Low Birth Rates in Korea." *American Economic Review* 114 (6): 1576-1611.

Kleven, Henrik, Camille Landais, and Gabriel Leite-Mariante. 2025. "The Child Penalty Atlas." *Review of Economic Studies* 92 (5): 3174–3207.

Myers, Caitlin Knowles. 2017. "The Power of Abortion Policy: Reexamining the Effects of Young Women's Access to Reproductive Control." *Journal of Political Economy* 125 (6): 2178-2224.

Seshadri, Ananth, and Anson Zhou. 2022. "Intergenerational Mobility Begins before Birth." *Journal of Monetary Economics* 129: 1-20.

Sommer, Kamila. 2016. "Fertility Choice in a Life Cycle Model with Idiosyncratic Uninsurable Earnings Risk." *Journal of Monetary Economics* 83: 27-38.

# Online Appendix

## A. Theory

### A.1 Proof of Proposition 1

For $a \in (\bar{a}^w, \bar{a}]$, solving (12) with the terminal condition $V^O(c, n, \bar{a}) = 0$ yields

$$V^O(c, n, a) = (\log c + \zeta n) \int_a^{\bar{a}} e^{-\int_a^{a'} [\rho + \xi(a'')] da''} da', \tag{57}$$

For $a \in \left[\underline{a}^w, \bar{a}^w\right]$, we conjecture that value functions for growth types $i \in \{H, L\}$ take the form:

$$V_{iM}(x, n, a) = \Pi(a)(x + \zeta n) + \Psi_i(a), \tag{58}$$

$$V_{iN}(x, a) = \Pi(a) x + \Psi_i(a) + \Phi(a), \tag{59}$$

where $\Pi(a)$, $\Phi(a)$, and $\Psi_i(a)$ are functions of $a$ yet to be determined. Substituting the conjectures (58)–(59) as well as the first-order conditions (9) and (11) into the HJB equations (8) and (10), we can see that the following equalities must hold

$$[\rho + \xi(a)] \Pi(a) = \Pi'(a) + 1, \tag{60}$$

$$\begin{aligned}[\rho + \xi(a)] \Psi_H(a) = &\left\{ \frac{\kappa_M(a)}{2} \left[ \gamma \widehat{\Psi}(a) - \zeta \Pi(a) \right] - \beta(a) \right\} \left[ \gamma \widehat{\Psi}(a) - \zeta \Pi(a) \right] \mathbb{I}_{a < \bar{a}^r} \\ &+ \Psi_H'(a) + \log(1 - \tau) + [\mu_H - \eta(a)] \Pi(a) - [\phi(a) + \theta] \widehat{\Psi}(a),\end{aligned} \tag{61}$$

$$\begin{aligned}[\rho + \xi(a)] \Psi_L(a) = &\left\{ \frac{\kappa_M(a)}{2} \left[ \gamma \widehat{\Psi}(a) - \zeta \Pi(a) \right] - \beta(a) \right\} \left[ \gamma \widehat{\Psi}(a) - \zeta \Pi(a) \right] \mathbb{I}_{a < \bar{a}^r} \\ &+ \Psi_L'(a) + \log[(1 - \epsilon)(1 - \tau)] + [\mu_L - \eta(a)] \Pi(a) + [\psi(a) - \theta] \widehat{\Psi}(a),\end{aligned} \tag{62}$$

$$\begin{aligned}[\rho + \xi(a)] [\Psi_H(a) + \Phi(a)] = &\left\{ \frac{\kappa_N(a)}{2} \left[ \gamma \widehat{\Psi}(a) + \Phi(a) - \zeta \Pi(a) \right] - \beta(a) \right\} \left[ \gamma \widehat{\Psi}(a) + \Phi(a) - \zeta \Pi(a) \right] \mathbb{I}_{a < \bar{a}^r} \\ &+ \Psi_H'(a) + \Phi'(a) + \log(1 - \tau) + [\mu_H - \eta(a)] \Pi(a) - \phi(a) \widehat{\Psi}(a),\end{aligned} \tag{63}$$

$$\begin{aligned}[\rho + \xi(a)] [\Psi_L(a) + \Phi(a)] = &\left\{ \frac{\kappa_N(a)}{2} \left[ \gamma \widehat{\Psi}(a) + \Phi(a) - \zeta \Pi(a) \right] - \beta(a) \right\} \left[ \gamma \widehat{\Psi}(a) + \Phi(a) - \zeta \Pi(a) \right] \mathbb{I}_{a < \bar{a}^r} \\ &+ \Psi_L'(a) + \Phi'(a) + \log[(1 - \epsilon)(1 - \tau)] + [\mu_L - \eta(a)] \Pi(a) + \psi(a) \widehat{\Psi}(a),\end{aligned} \tag{64}$$

where we define $\widehat{\Psi}(a) \equiv \Psi_H(a) - \Psi_L(a)$. Subtracting (62) from (61) and (64) from (63) both yield

$$\widehat{\Psi}'(a) = [\rho + \xi(a) + \phi(a) + \psi(a)] \widehat{\Psi}(a) + \log(1 - \epsilon) - (\mu_H - \mu_L) \Pi(a). \tag{65}$$

Subtracting (63) from (61) and (64) from (62) both yield

$$\Phi'(a) = \left\{ \frac{\kappa_M(a)}{2} \left[ \gamma \widehat{\Psi}(a) - \zeta \Pi(a) \right]^2 - \frac{\kappa_N(a)}{2} \left[ \gamma \widehat{\Psi}(a) + \Phi(a) - \zeta \Pi(a) \right]^2 + \beta(a) \Phi(a) \right\} \mathbb{I}_{a<\bar{a}^r} + [\rho + \xi(a)] \Phi(a) - \theta \widehat{\Psi}(a), \tag{66}$$

The value matching conditions (13)–(14) and the retirement value function (57) jointly imply

$$\Pi(\bar{a}^w) = \int_{\bar{a}^w}^{\bar{a}} e^{-\int_{\bar{a}^w}^{a'} [\rho + \xi(a'')] da''} da', \tag{67}$$

$$\Psi_i(\bar{a}^w) = [\log \upsilon + \log(1 - \mathbb{I}_{i=L} \epsilon)] \Pi(\bar{a}^w), \tag{68}$$

$$\Phi(\bar{a}^w) = 0. \tag{69}$$

Solving (60) with the terminal condition (67) yields (18). Solving (65) with the terminal condition $\widehat{\Psi}(\bar{a}^w) = \Psi_H(\bar{a}^w) - \Psi_L(\bar{a}^w) = -\log(1 - \epsilon) \Pi(\bar{a}^w)$ yields (19). For $a \in [\bar{a}^r, \bar{a}^w]$, solving (66) with terminal condition (69) yields

$$\Phi(a) = \int_a^{\bar{a}^w} e^{-\int_a^{a'} [\rho + \xi(a'')] da''} \theta \widehat{\Psi}(a') da'. \tag{70}$$

For $a \in \left[\underline{a}^w, \bar{a}^r\right)$, (66) reduces to (20). Value matching at $a = \bar{a}^r$ and (70) jointly imply that (20) has terminal condition (21). Solving (61) with the terminal condition (68) for $i = H$ yields

$$\begin{aligned} \Psi_H(a) = & \int_a^{\bar{a}^w} e^{-\int_a^{a'} [\rho + \xi(a'')] da''} \left\{ \frac{\kappa_M(a')}{2} \left[ \gamma \widehat{\Psi}(a') - \zeta \Pi(a') \right] - \beta(a') \right\} \left[ \gamma \widehat{\Psi}(a') - \zeta \Pi(a') \right] \mathbb{I}_{a'<\bar{a}^r} da' \\ & + \int_a^{\bar{a}^w} e^{-\int_a^{a'} [\rho + \xi(a'')] da''} \left\{ \log(1 - \tau) + [\mu_H - \eta(a')] \Pi(a') - [\phi(a') + \theta] \widehat{\Psi}(a') \right\} da' \\ & + e^{-\int_a^{\bar{a}^w} [\rho + \xi(a'')] da''} \log \upsilon \Pi(\bar{a}^w). \end{aligned} \tag{71}$$

Thus, we have verified that value functions for $a \in \left[\underline{a}^w, \bar{a}^w\right]$ indeed take the form of (58)–(59), where $\Pi(a)$ is given by (18), $\Psi_H(a)$ is given by (71), $\Psi_L(a) = \Psi_H(a) - \widehat{\Psi}(a)$ with $\widehat{\Psi}(a)$ given by (19), $\Phi(a)$ for $a \in [\bar{a}^r, \bar{a}^w]$ is given by (70), and $\Phi(a)$ for $a \in \left[\underline{a}^w, \bar{a}^r\right)$ is implicitly by the solution to the terminal value problem (20)–(21). Finally, substituting value functions (58) and (59) into the first-order conditions (9) and (11) and rearranging yields (17). □

## A.2 Assumption OA1 and proof of Corollary 1

Assumption OA1. *(i) For all* $a \in \left[\underline{a}^w, \bar{a}^r\right)$*, the following holds:*

$$0 < \gamma\widehat{\Psi}(a) - \zeta\Pi(a) < \frac{\beta(a)}{\max\{\kappa_M(a), \kappa_N(a)\}}, \tag{72}$$

$$\int_a^{\bar{a}^r} e^{-\int_a^{a'}[\rho+\xi(a'')]da''} \frac{\beta(a')^2}{2\kappa_N(a')} da' < \int_a^{\bar{a}^w} e^{-\int_a^{a'}[\rho+\xi(a'')]da''} \theta\widehat{\Psi}(a')\, da' + \Theta(a) < \frac{\beta(a)}{\kappa_N(a)}, \tag{73}$$

$$\frac{\beta(a)}{\kappa_N(a)} > \max\left\{\int_a^{\bar{a}^r} e^{-\int_a^{a'}[\rho+\xi(a'')]da''} \frac{\beta(a')^2}{2\kappa_N(a')} da', \Theta(a)\right\}, \tag{74}$$

*where* $\Pi(a)$ *and* $\widehat{\Psi}(a)$ *are given by (18) and (19), and* $\Theta(a)$ *is defined as*

$$\begin{aligned}\Theta(a) \equiv{}& \gamma\widehat{\Psi}(a) - \zeta\Pi(a) \\ &- \int_a^{\bar{a}^r} e^{-\int_a^{a'}[\rho+\xi(a'')]da''} \left\{\frac{\kappa_M(a')}{2}\left[\gamma\widehat{\Psi}(a') - \zeta\Pi(a')\right] - \beta(a')\right\}\left[\gamma\widehat{\Psi}(a') - \zeta\Pi(a')\right] da';\end{aligned}$$

*(ii) for all* $a \in [\bar{a}^r, \bar{a}^w]$*,* $\psi(a) > \theta$*; for all* $a \in \left[\underline{a}^w, \bar{a}^r\right)$*,* $\psi(a) > \theta + \gamma \max\{\lambda_M(a), \lambda_N(a)\}$*, where* $\lambda_j(a)$ *for* $j \in \{M, N\}$ *is given by (17)–(21).*

In part (i), conditions (72) and (73) respectively bound the flow utility of a child $\zeta$ and the long-term career impact of motherhood $\theta$; condition (74) ensures that the restriction imposed on $\theta$, namely (73), does not imply an empty set. Part (ii) ensures that the low-to-high transition intensities $\omega_{LH,j}(a)$, for $j \in \{M, N\}$, remain positive throughout the working life.

### Proof of Corollary 1

Assumption 2 ensures that the integrals in (18), (19), and (21) are well-defined. Applying (72) to (17) with $j = M$ yields $0 < \lambda_M(a) < \beta(a)$ for all $a \in \left[\underline{a}^w, \bar{a}^r\right)$. To show that $\lambda_N(a)$ given by (17)–(21) with $j = N$ exists and satisfies $0 < \lambda_N(a) < \beta(a)$ for all $a \in \left[\underline{a}^w, \bar{a}^r\right)$, it suffices to prove that the terminal value problem (20)–(21) admits a unique solution $\Phi(a)$ satisfying $\zeta\Pi(a) - \gamma\widehat{\Psi}(a) < \Phi(a) < \zeta\Pi(a) - \gamma\widehat{\Psi}(a) + \frac{\beta(a)}{\kappa_N(a)}$ for all $a \in \left[\underline{a}^w, \bar{a}^r\right)$. Rewrite (20) as

$$\Phi'(a) = \mathcal{A}_2(a)\Phi(a)^2 + \mathcal{A}_1(a)\Phi(a) + \mathcal{A}_0(a) + [\rho + \xi(a)]\Phi(a) - \theta\widehat{\Psi}(a), \tag{75}$$

where
$$\mathcal{A}_0(a) = \frac{\kappa_M(a) - \kappa_N(a)}{2}\left[\zeta\Pi(a) - \gamma\widehat{\Psi}(a)\right]^2,$$
$$\mathcal{A}_1(a) = \kappa_N(a)\left[\zeta\Pi(a) - \gamma\widehat{\Psi}(a)\right] + \beta(a),$$
$$\mathcal{A}_2(a) = -\frac{\kappa_N(a)}{2}.$$

Thus, the terminal value problem (20)–(21) can be recast as the integral equation

$$\Phi(a) = -\int_a^{\bar{a}^r} e^{-\int_a^{a'}[\rho+\xi(a'')]da''}\left[\mathcal{A}_2(a')\Phi(a')^2 + \mathcal{A}_1(a')\Phi(a') + \mathcal{A}_0(a')\right]da' + \int_a^{\bar{a}^w} e^{-\int_a^{a'}[\rho+\xi(a'')]da''}\theta\widehat{\Psi}(a')\,da'. \tag{76}$$

We proceed with a fixed-point argument regarding (76). Instead of working with the usual sup-norm, we use the *Bielecki norm* (exponentially weighted sup-norm) defined as

$$\|\Phi\|_\nu = \sup\left\{e^{-\nu(\bar{a}^r-a)}|\Phi(a)| : a \in \left[\underline{a}^w, \bar{a}^r\right]\right\}, \tag{77}$$

where $\nu \geq 0$ is fixed (Edwards, 1995).[42] Define $X = \left\{\Phi \in C\left[\underline{a}^w, \bar{a}^r\right] : \underline{\Phi} \leq \Phi \leq \bar{\Phi}\right\}$ where

$$\underline{\Phi}(a) \equiv \zeta\Pi(a) - \gamma\widehat{\Psi}(a) \qquad \text{and} \qquad \bar{\Phi}(a) \equiv \underline{\Phi}(a) + \frac{\beta(a)}{\kappa_N(a)}.$$

The set $X$ equipped with the norm (77) is a complete metric space since it is a closed subset of a Banach space, i.e., $C\left[\underline{a}^w, \bar{a}^r\right]$ with norm (77). Define an operator $\mathcal{T}$ on $X$ as

$$(\mathcal{T}\Phi)(a) = -\int_a^{\bar{a}^r} e^{-\int_a^{a'}[\rho+\xi(a'')]da''}\left(\mathcal{A}_2\Phi^2 + \mathcal{A}_1\Phi + \mathcal{A}_0\right)(a')\,da' + \int_a^{\bar{a}^w} e^{-\int_a^{a'}[\rho+\xi(a'')]da''}\theta\widehat{\Psi}(a')\,da'.$$

First, we show that $\mathcal{T}$ maps $X$ into itself. Since $\mathcal{A}_2 < 0$, we have $\partial\left(\mathcal{A}_2\Phi^2 + \mathcal{A}_1\Phi + \mathcal{A}_0\right)/\partial\Phi = 2\mathcal{A}_2\Phi + \mathcal{A}_1 > 2\mathcal{A}_2\bar{\Phi} + \mathcal{A}_1 = 0$. Thus, $\mathcal{A}_2\Phi^2 + \mathcal{A}_1\Phi + \mathcal{A}_0$ is nondecreasing in $\Phi$ everywhere over $\underline{\Phi} \leq \Phi \leq \bar{\Phi}$. For any $\Phi \in X$, condition (73) implies that

$$\begin{aligned}(\mathcal{T}\Phi)(a) &\geq -\int_a^{\bar{a}^r} e^{-\int_a^{a'}[\rho+\xi(a'')]da''}\left(\mathcal{A}_2\bar{\Phi}^2 + \mathcal{A}_1\bar{\Phi} + \mathcal{A}_0\right)(a')\,da' + \int_a^{\bar{a}^w} e^{-\int_a^{a'}[\rho+\xi(a'')]da''}\theta\widehat{\Psi}(a')\,da' \\ &= \underline{\Phi}(a) + \Theta(a) - \int_a^{\bar{a}^r} e^{-\int_a^{a'}[\rho+\xi(a'')]da''}\frac{\beta(a')^2}{2\kappa_N(a')}da' + \int_a^{\bar{a}^w} e^{-\int_a^{a'}[\rho+\xi(a'')]da''}\theta\widehat{\Psi}(a')\,da' \\ &> \underline{\Phi}(a),\end{aligned} \tag{78}$$

and

$$\begin{aligned}(\mathcal{T}\Phi)(a) &\leq -\int_a^{\bar{a}^r} e^{-\int_a^{a'}[\rho+\xi(a'')]da''}\left(\mathcal{A}_2\underline{\Phi}^2 + \mathcal{A}_1\underline{\Phi} + \mathcal{A}_0\right)(a')\,da' + \int_a^{\bar{a}^w} e^{-\int_a^{a'}[\rho+\xi(a'')]da''}\theta\widehat{\Psi}(a')\,da' \\ &= \bar{\Phi}(a) + \Theta(a) - \frac{\beta(a)}{\kappa_N(a)} + \int_a^{\bar{a}^w} e^{-\int_a^{a'}[\rho+\xi(a'')]da''}\theta\widehat{\Psi}(a')\,da' \\ &< \bar{\Phi}(a).\end{aligned} \tag{79}$$

[42] When $\nu = 0$, the Bielecki norm is identical to the usual sup-norm. By discounting future dates, the Bielecki norm—with a suitably chosen constant $\nu$—allows us to establish a contraction mapping without the unnecessarily strict restrictions on the model primitives that would be required if we were to use the usual sup-norm.

Therefore, $\mathcal{T}$ is a self-map. Next, we show that $\mathcal{T}$ is a contraction. For any $\Phi_1, \Phi_2 \in X$, we have

$$\begin{aligned} e^{-\nu(\bar{a}^r-a)} \left|\left(\mathcal{T}\Phi_1 - \mathcal{T}\Phi_2\right)(a)\right| &\leq \int_a^{\bar{a}^r} e^{-\int_a^{a'}[\nu+\rho+\xi(a'')]da''} \left|\mathcal{A}_2(a')\left[\Phi_1(a') + \Phi_2(a')\right] + \mathcal{A}_1(a')\right| da' \left\|\Phi_1 - \Phi_2\right\|_\nu \\ &\leq \int_a^{\bar{a}^r} e^{-\int_a^{a'}[\nu+\rho+\xi(a'')]da''} da' 2\bar{\beta} \left\|\Phi_1 - \Phi_2\right\|_\nu, \end{aligned} \tag{80}$$

where we use the fact that, for $a \in \left[\underline{a}^w, \bar{a}^r\right]$, condition (72) implies that $\bar{\Phi}(a) > 0$ and $\mathcal{A}_1(a) > 0$, which in turn implies that

$$\begin{aligned} \left|\mathcal{A}_2(a)\left[\Phi_1(a) + \Phi_2(a)\right] + \mathcal{A}_1(a)\right| &\leq 2\left|\mathcal{A}_2(a)\right| \max\left\{-\underline{\Phi}(a), \bar{\Phi}(a)\right\} + \left|\mathcal{A}_1(a)\right| \\ &= \max\left\{\beta(a), 2\kappa_N(a)\underline{\Phi}(a) + 2\beta(a)\right\} \\ &\leq 2\bar{\beta}, \end{aligned}$$

where we used the fact that condition (72) implies that $\underline{\Phi}(a) < 0$ for $a \in \left[\underline{a}^w, \bar{a}^r\right]$; Assumption 1 implies that there exists $\bar{\beta} < \infty$ as the maximum of $\beta$ over $\left[\underline{a}^w, \bar{a}^r\right]$. Therefore, (80) implies that

$$\left\|\mathcal{T}\Phi_1 - \mathcal{T}\Phi_2\right\|_\nu < \frac{2\bar{\beta}}{\nu}\left\|\Phi_1 - \Phi_2\right\|_\nu.$$

Choosing the constant $\nu$ such that $\nu \geq 2\bar{\beta} > 0$, we establish that $\mathcal{T}$ is a contraction and hence admits a unique $\Phi \in X$ such that $\mathcal{T}\Phi = \Phi$ by the Contraction Mapping Theorem. Furthermore, (78) and (79) jointly imply that the unique fixed point $\Phi(a)$ lies strictly between $\underline{\Phi}(a) = \zeta\Pi(a) - \gamma\widehat{\Psi}(a)$ and $\bar{\Phi}(a) = \zeta\Pi(a) - \gamma\widehat{\Psi}(a) + \frac{\beta(a)}{\kappa_N(a)}$ for all $a \in \left[\underline{a}^w, \bar{a}^r\right)$. □

## A.3 Proof of comparative statics in Table 1

For primitives that are functions, comparative statics use functional derivatives. Formally, the functional derivative of a functional $F$ with respect to a function $\varsigma$ at point $a'$ is defined as

$$\frac{\delta F[\varsigma]}{\delta\varsigma(a')} = \lim_{\varepsilon\to 0}\frac{F[\varsigma(a) + \varepsilon\delta(a-a')] - F[\varsigma(a)]}{\varepsilon} = \frac{d}{d\varepsilon}F[\varsigma(a) + \varepsilon\delta(a-a')]\,|_{\varepsilon=0},$$

where $\delta(\cdot)$ denotes the Dirac delta function.

### Optimal fertility schedule for mothers

The expression of $\lambda_M(a)$ is given by (17) with $j = M$. Partially differentiating $\lambda_M(a)$ with respect to the parameters of interest yields $\frac{\partial\lambda_M(a)}{\partial\gamma} \propto -\widehat{\Psi}(a) < 0$, $\frac{\partial\lambda_M(a)}{\partial\theta} = 0$, $\frac{\partial\lambda_M(a)}{\partial\iota} \propto -\frac{\partial\widehat{\Psi}(a)}{\partial\iota}$ for $\iota \in$

$\{\widehat{\mu}, \epsilon, \bar{a}^w\}$, and $\frac{\partial \lambda_M(a)}{\partial \bar{a}} \propto \left[\zeta \frac{\partial \Pi(a)}{\partial \bar{a}} - \gamma \frac{\partial \widehat{\Psi}(a)}{\partial \bar{a}}\right]$, where

$$\begin{aligned}
\frac{\partial \widehat{\Psi}(a)}{\partial \widehat{\mu}} &= \int_a^{\bar{a}^w} e^{-\int_a^{a'} [\rho + \xi(a'') + \phi(a'') + \psi(a'')] da''} \Pi(a')\, da', \\
\frac{\partial \widehat{\Psi}(a)}{\partial \epsilon} &= \frac{1}{1-\epsilon} \left\{ \int_a^{\bar{a}^w} e^{-\int_a^{a'} [\rho + \xi(a'') + \phi(a'') + \psi(a'')] da''} da' + e^{-\int_a^{\bar{a}^w} [\rho + \xi(a') + \phi(a') + \psi(a')] da'} \Pi(\bar{a}^w) \right\}, \\
\frac{\partial \widehat{\Psi}(a)}{\partial \bar{a}^w} &= e^{-\int_a^{\bar{a}^w} [\rho + \xi(a') + \phi(a') + \psi(a')] da'} \Pi(\bar{a}^w) \left\{ \widehat{\mu} + [\phi(\bar{a}^w) + \psi(\bar{a}^w)] \log(1-\epsilon) \right\}, \\
\frac{\partial \widehat{\Psi}(a)}{\partial \bar{a}} &= e^{-\int_a^{\bar{a}} [\rho + \xi(a')] da'} \left\{ \widehat{\mu} \int_a^{\bar{a}^w} e^{-\int_a^{a'} [\phi(a'') + \psi(a'')] da''} da' - e^{-\int_a^{\bar{a}^w} [\phi(a') + \psi(a')] da'} \log(1-\epsilon) \right\}, \\
\frac{\partial \Pi(a)}{\partial \bar{a}} &= e^{-\int_a^{\bar{a}} [\rho + \xi(a')] da'}.
\end{aligned}$$

It is straightforward to check that $\frac{\partial \widehat{\Psi}(a)}{\partial \widehat{\mu}} > 0$, $\frac{\partial \widehat{\Psi}(a)}{\partial \epsilon} > 0$, $\frac{\partial \widehat{\Psi}(a)}{\partial \bar{a}} > 0$, and $\frac{\partial \Pi(a)}{\partial \bar{a}} > 0$, since $\widehat{\mu} > 0$, $\epsilon \in (0,1)$, and $\Pi(a) > 0$ for $a \in \left[\underline{a}^w, \bar{a}^w\right]$; the sign of $\frac{\partial \widehat{\Psi}(a)}{\partial \bar{a}^w}$ is ambiguous, depending on the value of $\widehat{\mu}$, $\epsilon$, $\phi(\bar{a}^w)$, and $\psi(\bar{a}^w)$. Therefore, $\frac{\partial \lambda_M(a)}{\partial \widehat{\mu}} < 0$, $\frac{\partial \lambda_M(a)}{\partial \epsilon} < 0$, whereas $\frac{\partial \lambda_M(a)}{\partial \bar{a}^w}$ and $\frac{\partial \lambda_M(a)}{\partial \bar{a}}$ have ambiguous signs. For the primitives of interest that are functions, the functional derivatives of $\lambda_M$ with respect to $\kappa_j$ for $j \in \{M, N\}$ are trivial, since the expression of $\lambda_M(a)$ does not depend on $\kappa_N$ and depends on $\kappa_M$ only at age $a$. The comparative static of $\lambda_M(a)$ with respect to $\kappa_M$ at age $a' = a$ is simply given by the partial derivative $\frac{\partial \lambda_M(a)}{\partial \kappa_M(a)}$. We are left with the functional derivative of $\lambda_M$ with respect to $\xi$ at age $a'$, which is given by $\frac{\delta \lambda_M[\xi]}{\delta \xi(a')} = \kappa_M(a) \left\{ \zeta \frac{\delta \Pi[\xi]}{\delta \xi(a')} - \gamma \frac{\delta \widehat{\Psi}[\xi]}{\delta \xi(a')} \right\}$, where

$$\begin{aligned}
\frac{\delta \Pi[\xi]}{\delta \xi(a')} &= -\int_{a'}^{\bar{a}} e^{-\int_a^{a''} [\rho + \xi(a''')] da'''} da'', \\
\frac{\delta \widehat{\Psi}[\xi]}{\delta \xi(a')} &= -\int_{a'}^{\bar{a}^w} e^{-\int_a^{a''} [\rho + \xi(a''') + \phi(a''') + \psi(a''')] da'''} \left[\hat{\mu} \Pi(a'') - \log(1-\epsilon)\right] da'' \\
&\quad + \int_a^{\bar{a}^w} e^{-\int_a^{a''} [\rho + \xi(a''') + \phi(a''') + \psi(a''')] da'''} \hat{\mu} \frac{\delta \Pi[\xi]}{\delta \xi(a')}(a'')\, da'' \\
&\quad + e^{-\int_a^{\bar{a}^w} [\rho + \xi(a'') + \phi(a'') + \psi(a'')] da''} \left[ \Pi(\bar{a}^w) + \int_{a'}^{\bar{a}} e^{-\int_{\bar{a}^w}^{a''} [\rho + \xi(a''')] da'''} da'' \right] \log(1-\epsilon).
\end{aligned}$$

It is straightforward to check that $\frac{\delta \Pi[\xi]}{\delta \xi(a')} < 0$ and $\frac{\delta \widehat{\Psi}[\xi]}{\delta \xi(a')} < 0$ for all $a' \in [a, \bar{a})$; thus, $\frac{\delta \lambda_M[\xi]}{\delta \xi(a')}$ has ambiguous sign.

### MOTHERHOOD-STATUS VALUE DIFFERENTIAL

In order to conduct comparative statics of the optimal fertility schedule for non-mothers $\lambda_N(a)$, we need to determine how the motherhood-status value differential $\Phi(a)$ responds to changes in the primitives of interest. Since $\Phi(a)$ does not have a closed-form expression, we study the

variational equation of the nonlinear ODE (75). For parameters $\iota \in \{\gamma, \theta, \widehat{\mu}, \epsilon, \bar{a}^w, \bar{a}\}$, let $S_\iota(a)$ denote the partial derivative of the solution $\Phi(a)$ with respect to that parameter: $S_\iota(a) \equiv \frac{\partial \Phi(a)}{\partial \iota}$. Differentiating both sides of (75) with respect to $\iota$ and using the definition of $S_\iota(a)$ yields

$$S_\iota'(a) = \left[2\mathcal{A}_2(a)\Phi(a) + \mathcal{A}_1(a) + \rho + \xi(a)\right] S_\iota(a) - \widehat{\mathcal{A}}_\iota(a),$$

$$\text{with} \quad \widehat{\mathcal{A}}_\iota(a) = -\frac{\partial \mathcal{A}_2(a)}{\partial \iota}\Phi(a)^2 - \frac{\partial \mathcal{A}_1(a)}{\partial \iota}\Phi(a) - \frac{\partial \mathcal{A}_0(a)}{\partial \iota} + \frac{\partial\left[\theta\widehat{\Psi}(a)\right]}{\partial \iota},$$

which is a linear ODE whose solution with terminal condition $S_\iota(\bar{a}^r) = \frac{\partial \Phi(\bar{a}^r)}{\partial \iota}$ is given by

$$S_\iota(a) = \int_a^{\bar{a}^r} e^{-\int_a^{a'}\left[2\mathcal{A}_2(a'')\Phi(a'') + \mathcal{A}_1(a'') + \rho + \xi(a'')\right]da''} \widehat{\mathcal{A}}_\iota(a')\, da'$$
$$+ e^{-\int_a^{\bar{a}^r}\left[2\mathcal{A}_2(a')\Phi(a') + \mathcal{A}_1(a') + \rho + \xi(a')\right]da'} \frac{\partial \Phi(\bar{a}^r)}{\partial \iota}.$$

Thus, the sign of $S_\iota(a)$ depends on the sign of $\widehat{\mathcal{A}}_\iota(a')$ for $a' \in [a, \bar{a}^r]$ as well as the sign of $\frac{\partial \Phi(\bar{a}^r)}{\partial \iota}$, where $\Phi(\bar{a}^r)$ is given by (21). It is straightforward to check that $S_\iota(a)$ has ambiguous signs for all parameters $\iota \in \{\gamma, \theta, \widehat{\mu}, \epsilon, \bar{a}^w, \bar{a}\}$ except $\theta$, for which $\widehat{\mathcal{A}}_\theta(a') = \widehat{\Psi}(a') > 0$ for all $a' \in [a, \bar{a}^r]$ and $\frac{\partial \Phi(\bar{a}^r)}{\partial \theta} = \int_{\bar{a}^r}^{\bar{a}^w} e^{-\int_{\bar{a}^r}^{a'}[\rho + \xi(a'')]da''} \widehat{\Psi}(a')\, da' > 0$; hence, $S_\theta(a) > 0$.

We then consider how $\Phi(a)$ changes with respect to perturbations to the primitive functions $\xi$ and $\kappa_j$ for $j \in \{M, N\}$. We have already established that a perturbation to the mortality function $\xi$ at point $a' \in [a, \bar{a})$ has an ambiguous effect on $\zeta\Pi(a) - \gamma\widehat{\Psi}(a)$; therefore, its impact on $\Phi(a)$ is also ambiguous, since $\Phi(a)$ implicitly depends on $\zeta\Pi(a) - \gamma\widehat{\Psi}(a)$ via (75). Consider the perturbation from $\kappa_N(a)$ to $\kappa_N(a) + \varepsilon\delta(a - a')$, where $\delta(\cdot)$ is the Dirac delta function. Let $\Phi^\varepsilon(a) = \Phi(\kappa_N(a) + \varepsilon\delta(a - a'))$ be the solution to the following differential equation:

$$(\Phi^\varepsilon)'(a) = \mathcal{A}_2^\varepsilon(a)\Phi^\varepsilon(a)^2 + \mathcal{A}^\varepsilon{}_1(a)\Phi^\varepsilon(a) + \mathcal{A}_0^\varepsilon(a) + \left[\rho + \xi(a)\right]\Phi^\varepsilon(a) - \theta\widehat{\Psi}(a), \quad (81)$$

$$\text{with} \quad \mathcal{A}_0^\varepsilon(a) = \frac{\left[\kappa_M(a) - \kappa_N(a) - \varepsilon\delta(a - a')\right]}{2}\left[\zeta\Pi(a) - \gamma\widehat{\Psi}(a)\right]^2,$$
$$\mathcal{A}_1^\varepsilon(a) = \left[\kappa_N(a) + \varepsilon\delta(a - a')\right]\left[\zeta\Pi(a) - \gamma\widehat{\Psi}(a)\right] + \beta(a),$$
$$\mathcal{A}_2^\varepsilon(a) = -\frac{\left[\kappa_N(a) + \varepsilon\delta(a - a')\right]}{2}.$$

Define $S_\varepsilon(a) \equiv \frac{\Phi^\varepsilon(a) - \Phi(a)}{\varepsilon}$. Subtracting (75) from (81) yields

$$S_\varepsilon'(a) = \left\{\mathcal{A}_2^\varepsilon(a)\left[2\Phi(a) + \varepsilon S_\varepsilon(a)\right] + \mathcal{A}^\varepsilon{}_1(a) + \rho + \xi(a)\right\} S_\varepsilon(a)$$
$$- \frac{\delta(a - a')}{2}\left[\gamma\widehat{\Psi}(a) + \Phi(a) - \zeta\Pi(a)\right]^2, \quad (82)$$

with $S_\varepsilon(\bar{a}^r) = 0$. Taking the limit as $\varepsilon \to 0$ of both sides of (82), we have

$$\frac{d}{da}\left(\frac{\delta\Phi[\kappa_N]}{\delta\kappa_N(a')}\right) = [2\mathcal{A}_2(a)\Phi(a) + \mathcal{A}_1(a) + \rho + \xi(a)]\frac{\delta\Phi[\kappa_N]}{\delta\kappa_N(a')} - \frac{\delta(a-a')}{2}\left[\gamma\widehat{\Psi}(a) + \Phi(a) - \zeta\Pi(a)\right]^2, \tag{83}$$

where $\frac{\delta\Phi[\kappa_N]}{\delta\kappa_N(a')} = \lim_{\varepsilon\to 0} S_\varepsilon(a)$ is the functional derivative of $\Phi$ with respect to $\kappa_N$ at point $a'$. Solving for $\frac{\delta\Phi[\kappa_N]}{\delta\kappa_N(a')}$ from (83) with terminal condition $\frac{\delta\Phi[\kappa_N]}{\delta\kappa_N(a')}(\bar{a}^r) = 0$, we have

$$\frac{\delta\Phi[\kappa_N]}{\delta\kappa_N(a')} = e^{-\int_a^{a'}[2\mathcal{A}_2(a'')\Phi(a'')+\mathcal{A}_1(a'')+\rho+\xi(a'')]da''}\frac{1}{2}\left[\zeta\Pi(a') - \gamma\widehat{\Psi}(a') - \Phi(a')\right]^2 > 0.$$

Analogously, we can show that the functional derivative of $\Phi$ with respect to $\kappa_M$ at point $a'$ is

$$\frac{\delta\Phi[\kappa_M]}{\delta\kappa_M(a')} = -e^{-\int_a^{a'}[2\mathcal{A}_2(a'')\Phi(a'')+\mathcal{A}_1(a'')+\rho+\xi(a'')]da''}\frac{1}{2}\left[\zeta\Pi(a') - \gamma\widehat{\Psi}(a')\right]^2 < 0.$$

### Optimal fertility schedule for non-mothers

The expression of $\lambda_N(a)$ is given by (17) with $j = N$. Partially differentiating $\lambda_N(a)$ with respect to the parameters of interest yields $\frac{\partial\lambda_N(a)}{\partial\gamma} = -\kappa_N(a)\left[\widehat{\Psi}(a) + \frac{\partial\Phi(a)}{\partial\gamma}\right]$, $\frac{\partial\lambda_N(a)}{\partial\theta} = -\kappa_N(a)\frac{\partial\Phi(a)}{\partial\theta}$, $\frac{\partial\lambda_N(a)}{\partial\iota} = -\kappa_N(a)\left[\gamma\frac{\partial\widehat{\Psi}(a)}{\partial\iota} + \frac{\partial\Phi(a)}{\partial\iota}\right]$ for $\iota \in \{\widehat{\mu}, \epsilon, \bar{a}^w\}$, and $\frac{\partial\lambda_N(a)}{\partial\bar{a}} = -\kappa_N(a)\left[\gamma\frac{\partial\widehat{\Psi}(a)}{\partial\bar{a}} + \frac{\partial\Phi(a)}{\partial\bar{a}} - \zeta\frac{\partial\Pi(a)}{\partial\bar{a}}\right]$. Since $\frac{\partial\Phi(a)}{\partial\theta} > 0$, we have $\frac{\partial\lambda_N(a)}{\partial\theta} < 0$. It is straightforward to check that all the other partial derivatives of $\lambda_N(a)$ have ambiguous signs. Taking the functional derivatives of $\lambda_N$ with respect to $\xi$ and $\kappa_j$ for $j \in \{M, N\}$ at point $a'$ yields respectively

$$\begin{aligned}
\frac{\delta\lambda_N[\xi]}{\delta\xi(a')} &= -\kappa_N(a)\left\{\gamma\frac{\delta\widehat{\Psi}[\xi]}{\delta\xi(a')} + \frac{\delta\Phi[\xi]}{\delta\xi(a')} - \zeta\frac{\delta\Pi[\xi]}{\delta\xi(a')}\right\},\\
\frac{\delta\lambda_N[\kappa_N]}{\delta\kappa_N(a')} &= -\left[\gamma\widehat{\Psi}(a) + \Phi(a) - \zeta\Pi(a)\right]\delta(a-a') - \kappa_N(a)\frac{\delta\Phi[\kappa_N]}{\delta\kappa_N(a')},\\
\frac{\delta\lambda_N[\kappa_M]}{\delta\kappa_M(a')} &= -\kappa_N(a)\frac{\delta\Phi[\kappa_M]}{\delta\kappa_M(a')}.
\end{aligned}$$

The sign of $\frac{\delta\lambda_N[\xi]}{\delta\xi(a')}$ is ambiguous, because both $\zeta\frac{\delta\Pi[\xi]}{\delta\xi(a')} - \gamma\frac{\delta\widehat{\Psi}[\xi]}{\delta\xi(a')}$ and $\frac{\delta\Phi[\xi]}{\delta\xi(a')}$ have ambiguous signs. Since $\frac{\delta\Phi[\kappa_N]}{\delta\kappa_N(a')} > 0$ and $\gamma\widehat{\Psi}(a) + \Phi(a) - \zeta\Pi(a) > 0$ by Assumption OA1, we have $\frac{\delta\lambda_N[\kappa_N]}{\delta\kappa_N(a')} < 0$. Since $\frac{\delta\Phi[\kappa_M]}{\delta\kappa_M(a')} < 0$, we have $\frac{\delta\lambda_N[\kappa_M(a)]}{\delta\kappa_M(a')} > 0$. □

## A.4 Proof of Lemma 1

Partially differentiating both sides of (28), we have

$$\frac{\partial \Omega(a,t)}{\partial t}+\frac{\partial \Omega(a,t)}{\partial a}=\int_{-\infty}^{\infty}\sum_{i}\left[\frac{\partial l_{iN}(x,a,t)}{\partial t}+\frac{\partial l_{iN}(x,a,t)}{\partial a}\right]dx\frac{\Omega(a,t)}{\int_{-\infty}^{\infty}\sum_{i}l_{iN}(x,a,t)\,dx}$$
$$-\left[\frac{\partial p(a,t)}{\partial t}+\frac{\partial p(a,t)}{\partial a}\right]\frac{\Omega(a,t)}{p(a,t)}. \tag{84}$$

Substituting (22) for $i\in\{H,L\}$ and (25) into (84) yields the following PDE of $\Omega(a,t)$:

$$\frac{\partial \Omega(a,t)}{\partial t}+\frac{\partial \Omega(a,t)}{\partial a}=-\lambda_{N}(a)\,\Omega(a,t), \tag{85}$$

where we have used the following conjecture for $i\in\{H,L\}$ and $a\in\left(\underline{a}^{w},\bar{a}^{w}\right]\times[0,T)$:

$$\int_{-\infty}^{\infty}\frac{\partial l_{iN}(x,a,t)}{\partial x}dx=\lim_{x\to\infty}l_{iN}(x,a,t)-\lim_{x\to-\infty}l_{iN}(x,a,t)=0. \tag{86}$$

In a later proof, we will establish (86) formally, essentially as the consequence of Assumptions 3 and OA2. The boundary conditions for $l_{iN}(x,a,t)$ at $a=\underline{a}^{w}$ imply $\Omega\left(\underline{a}^{w},t\right)=1$. Solving PDE (85) with boundary condition $\Omega\left(\underline{a}^{w},t\right)=1$ and initial condition $\Omega(a,0)=\Omega^{0}(a)$ yields the expression of $\Omega(a,t)$ in Lemma 1. □

## A.5 Proof of Lemma 2

Partially differentiating both sides of (30), we have

$$\frac{\partial h_{j}(a,t)}{\partial t}+\frac{\partial h_{j}(a,t)}{\partial a}=\int_{-\infty}^{\infty}\left[\frac{\partial l_{Hj}(x,a,t)}{\partial t}+\frac{\partial l_{Hj}(x,a,t)}{\partial a}\right]dx\frac{h_{j}(a,t)}{\int_{-\infty}^{\infty}l_{Hj}(x,a,t)\,dx}$$
$$-\int_{-\infty}^{\infty}\sum_{i}\left[\frac{\partial l_{ij}(x,a,t)}{\partial t}+\frac{\partial l_{ij}(x,a,t)}{\partial a}\right]dx\frac{h_{j}(a,t)}{\int_{-\infty}^{\infty}\sum_{i}l_{ij}(x,a,t)\,dx}. \tag{87}$$

Substituting (22) for $i\in\{H,L\}$ into (87) yields the following PDE of $h_{N}(a,t)$:

$$\frac{\partial h_{N}(a,t)}{\partial t}+\frac{\partial h_{N}(a,t)}{\partial a}=-\omega_{HL,N}(a)\,h_{N}(a,t)+\omega_{LH,N}(a)\left[1-h_{N}(a,t)\right], \tag{88}$$

where we have used again the later verified conjecture (86). Substituting (24) for $i\in\{H,L\}$ into (87) and using (28) yields the following PDE of $h_{M}(a,t)$:

$$\frac{\partial h_{M}(a,t)}{\partial t}+\frac{\partial h_{M}(a,t)}{\partial a}=-\omega_{HL,M}(a)\,h_{M}(a,t)+\omega_{LH,M}(a)\left[1-h_{M}(a,t)\right]$$
$$+\left[h_{N}(a,t)-h_{M}(a,t)\right]\frac{\lambda_{N}(a)\,\Omega(a,t)}{1-\Omega(a,t)}, \tag{89}$$

where we have used a later verified conjecture that for $i \in \{H, L\}$ and $(a,t) \in \left(\underline{a}^w, \bar{a}^w\right] \times [0,T)$:

$$\int_{-\infty}^{\infty} \frac{\partial l_{iM}(x,a,t)}{\partial x} dx = \lim_{x\to\infty} l_{iM}(x,a,t) - \lim_{x\to-\infty} l_{iM}(x,a,t) = 0. \tag{90}$$

The boundary conditions for $l_{HN}(x,a,t)$ and $l_{LN}(x,a,t)$ at $a = \underline{a}^w$ imply $h_N\left(\underline{a}^w, t\right) = \sigma$. Since $h_M(a,t)$ is not well-defined at $a = \underline{a}^w$, we instead impose a limit boundary condition $\lim_{a\downarrow\underline{a}^w} h_M(a,t) = h_N\left(\underline{a}^w, t\right) = \sigma$.[43] Solving (88) with boundary condition $h_N\left(\underline{a}^w, t\right) = \sigma$ and initial condition $h_N(a,0) = h_N^0(a)$ yields the expression of $h_N(a,t)$ in Lemma 2. Solving (89) with limit boundary condition $\lim_{a\downarrow\underline{a}^w} h_M(a,t) = \sigma$ and initial condition $h_M(a,0) = h_M^0(a)$ yields

$$\begin{aligned} h_M(a,t) = {} & \left[\sigma \mathbb{I}_{a-t\leq\underline{a}^w} + h_M^0(a-t)\,\mathbb{I}_{a-t>\underline{a}^w}\right] e^{-\int_{\max\{\underline{a}^w, a-t\}}^{a}\left[\phi(a')+\psi(a')+\frac{\lambda_N(a')\Omega(a',t-a+a')}{1-\Omega(a',t-a+a')}\right]da'} \\ & + \int_{\max\{\underline{a}^w, a-t\}}^{a} e^{-\int_{a'}^{a}\left[\phi(a'')+\psi(a'')+\frac{\lambda_N(a'')\Omega(a'',t-a+a'')}{1-\Omega(a'',t-a+a'')}\right]da''} \omega_{LH,M}(a')\,da' \\ & + \int_{\max\{\underline{a}^w, a-t\}}^{a} e^{-\int_{a'}^{a}\left[\phi(a'')+\psi(a'')+\frac{\lambda_N(a'')\Omega(a'',t-a+a'')}{1-\Omega(a'',t-a+a'')}\right]da''} \frac{\lambda_N(a')\,\Omega(a',t-a+a')}{1-\Omega(a',t-a+a')} h_N(a',t-a+a')\,da' \end{aligned}$$

Applying integration by parts to the integral in the last line of the above equation using (88), we obtain the expression of $h_M(a,t)$ in Lemma 2. □

## A.6 Proof of comparative statics in Table 2

We save notation by defining the following objects:

$$\Upsilon(a) \equiv e^{-\int_{\underline{a}^w}^{a}[\phi(a')+\psi(a')]da'},$$

$$\Gamma(a,t-a) \equiv \Upsilon(a)\, e^{-\int_{\underline{a}^w}^{a}\frac{\lambda_N(a')\Omega(a',t-a+a')}{1-\Omega(a',t-a+a')}da'}.$$

By Lemma 2, the independence of $h_N(a,t)$ on $\lambda_M$ is obvious from inspecting the expression of $h_N(a,t)$. Taking the functional derivative of $h_N(a,t)$ with respect to $\lambda_N$ at point $a' \leq a$ yields:

$$\frac{\delta h_N[\lambda_N]}{\delta \lambda_N(a')} = -\gamma \frac{\Upsilon(a)}{\Upsilon(a')} < 0.$$

Taking the functional derivative of $h_M(a,t)$ with respect to $\lambda_M$ at point $a' \leq a$ yields:

$$\frac{\delta h_M[\lambda_M]}{\delta \lambda_M(a')} = -\gamma \frac{\Gamma(a,t-a)}{\Gamma(a',t-a)} < 0.$$

From the expression of $h_M(a,t)$, we can see that it depends on $\lambda_N$ directly, as well as indirectly through $h_N(a,t)$ and $\Omega$. Taking the functional derivative of $h_M(a,t)$ with respect to $\lambda_N$ at point

[43] Mothers of age just above $\underline{a}^w$ are newly transitioned from the non-mother status, so their growth-type composition inherits $h_N\left(\underline{a}^w, t\right)$.

$a' \leq a$ yields:

$$\begin{aligned}\frac{\delta h_M[\lambda_N]}{\delta \lambda_N(a')} &= \frac{\delta h_N[\lambda_N]}{\delta \lambda_N(a')} + \gamma \frac{\Gamma(a, t-a)}{\Gamma(a', t-a)} \\ &- \frac{\Omega(a', t-a+a')}{1-\Omega(a', t-a+a')} \int_{\max\{\underline{a}^w, a-t\}}^{a'} \frac{\Gamma(a, t-a)}{\Gamma(a'', t-a)} \left[\omega_{LH,M}(a'') - \omega_{LH,N}(a'')\right] da'' \\ &+ \int_{\max\{\underline{a}^w, a-t\}}^{a} \int_{a''}^{a} \frac{\lambda_N(a''') \Omega(a''', t-a+a''')}{[1-\Omega(a''', t-a+a''')]^2} da''' \frac{\Gamma(a, t-a)}{\Gamma(a'', t-a)} \left[\omega_{LH,M}(a'') - \omega_{LH,N}(a'')\right] da'',\end{aligned}$$

whose sign is ambiguous in general. □

## A.7 Proof of Lemma 3

We can check that (35) is the solution to the given initial value problem by substituting it back to the PDE (5). Differentiating both sides of (31) and using (5), we have

$$\frac{\mathcal{Z}'_{\underline{a}^w}(t)}{\mathcal{Z}_{\underline{a}^w}(t)} = \int_{-\infty}^{\infty} x \frac{\partial f(x,t)}{\partial t} dx = -\varphi \mathcal{H}(t) \int_{-\infty}^{\infty} x \frac{\partial f(x,t)}{\partial x} dx = \varphi \mathcal{H}(t), \tag{91}$$

where integration by parts implies

$$\int_{-\infty}^{\infty} x \frac{\partial f(x,t)}{\partial x} dx = \lim_{x\to\infty} x f(x,t) - \lim_{x\to-\infty} x f(x,t) - \int_{-\infty}^{\infty} f(x,t)\, dx = -1,$$

since (35) and Assumption 3 jointly imply that $\lim_{x\to\infty} x f(x,t) = \lim_{x\to\infty} x f^0\left(x - \varphi \int_0^t \mathcal{H}(t')\, dt'\right) = 0$ and $\lim_{x\to-\infty} x f(x,t) = \lim_{x\to-\infty} x f^0\left(x - \varphi \int_0^t \mathcal{H}(t')\, dt'\right) = 0$. Equality (91) gives an ODE of $\mathcal{Z}_{\underline{a}^w}(t)$ with initial condition $\mathcal{Z}_{\underline{a}^w}(0) = e^{\int_{-\infty}^{\infty} x f^0(x) dx}$; the solution to this initial value problem satisfies (34). Finally, the normalized entry distribution $\tilde{f}(\tilde{x}, t)$ satisfies

$$\begin{aligned}\tilde{f}(\tilde{x}, t) &= f\left(\tilde{x} + \log \mathcal{Z}_{\underline{a}^w}(t), t\right) \\ &= f^0\left(\tilde{x} + \log \mathcal{Z}_{\underline{a}^w}(t) - \varphi \int_0^t \mathcal{H}(t')\, dt'\right) \qquad \text{by (35)} \\ &= f^0\left(\tilde{x} + \int_{-\infty}^{\infty} x f^0(x)\, dx\right) \qquad \text{by (34)}\end{aligned}$$

which is independent of the calendar time. □

## A.8 Derivation of the normalized KFE (37)

By the definitions (27)–(28) and (30), as well as the normalization (33), we have

$$l_{HN}(x,a,t) = \tilde{\ell}_{HN}(\tilde{x},a,t)\, h_N(a,t)\, \Omega(a,t)\, p(a,t), \tag{92}$$

$$l_{LN}(x,a,t) = \tilde{\ell}_{LN}(\tilde{x},a,t)\, [1-h_N(a,t)]\, \Omega(a,t)\, p(a,t), \tag{93}$$

$$l_{HM}(x,a,t) = \tilde{\ell}_{HM}(\tilde{x},a,t)\, h_M(a,t)\, [1-\Omega(a,t)]\, p(a,t), \tag{94}$$

$$l_{LM}(x,a,t) = \tilde{\ell}_{LM}(\tilde{x},a,t)\, [1-h_M(a,t)]\, [1-\Omega(a,t)]\, p(a,t). \tag{95}$$

Partially differentiating both sides of (92) with respect to $t$ and $a$ yields:

$$\begin{aligned}\frac{\partial l_{HN}(x,a,t)}{\partial t} + \frac{\partial l_{HN}(x,a,t)}{\partial a} = &\left[\frac{\partial \tilde{\ell}_{HN}(\tilde{x},a,t)}{\partial t} + \frac{\partial \tilde{\ell}_{HN}(\tilde{x},a,t)}{\partial \tilde{x}}\frac{d\tilde{x}}{dt} + \frac{\partial \tilde{\ell}_{HN}(\tilde{x},a,t)}{\partial a}\right]\frac{l_{HN}(x,a,t)}{\tilde{\ell}_{HN}(\tilde{x},a,t)} \\ &+ \left[\frac{\partial h_N(a,t)}{\partial t} + \frac{\partial h_N(a,t)}{\partial a}\right]\frac{l_{HN}(x,a,t)}{h_N(a,t)} \\ &+ \left[\frac{\partial \Omega(a,t)}{\partial t} + \frac{\partial \Omega(a,t)}{\partial a}\right]\frac{l_{HN}(x,a,t)}{\Omega(a,t)} \\ &+ \left[\frac{\partial p(a,t)}{\partial t} + \frac{\partial p(a,t)}{\partial a}\right]\frac{l_{HN}(x,a,t)}{p(a,t)}.\end{aligned} \tag{96}$$

Partially differentiating both sides of (92) with respect to $x$ yields:

$$\frac{\partial l_{HN}(x,a,t)}{\partial x} = \frac{\partial \tilde{\ell}_{HN}(\tilde{x},a,t)}{\partial \tilde{x}}\frac{d\tilde{x}}{dx} h_N(a,t)\,\Omega(a,t)\,p(a,t) = \frac{\partial \tilde{\ell}_{HN}(\tilde{x},a,t)}{\partial \tilde{x}}\frac{l_{HN}(x,a,t)}{\tilde{\ell}_{HN}(\tilde{x},a,t)}, \tag{97}$$

where we used the fact that the normalization (32) implies $d\tilde{x}/dx = 1$. By the normalization (32) and Lemma 3, we have

$$\frac{d\tilde{x}}{dt} = -\frac{\mathcal{Z}'_{\underline{a}^w}(t)}{\mathcal{Z}_{\underline{a}^w}(t)} = -\varphi\mathcal{H}(t). \tag{98}$$

Substituting (22) with $i = H$, (25), (85), (88), (97), and (98) into (96) and rearranging, we arrive at (37) for $i = H$ and $j = N$, where we have used the fact that

$$\frac{l_{LN}(x,a,t)}{l_{HN}(x,a,t)}\tilde{\ell}_{HN}(\tilde{x},a,t) = \frac{\int_{-\infty}^{\infty} l_{LN}(x,a,t)\,dx}{\int_{-\infty}^{\infty} l_{HN}(x,a,t)\,dx}\frac{l_{LN}(x,a,t)}{\int_{-\infty}^{\infty} l_{LN}(x,a,t)\,dx} = \frac{1-h_N(a,t)}{h_N(a,t)}\tilde{\ell}_{LN}(\tilde{x},a,t).$$

The KFEs for $\tilde{\ell}_{LN}(\tilde{x},a,t)$, $\tilde{\ell}_{HM}(\tilde{x},a,t)$ and $\tilde{\ell}_{LM}(\tilde{x},a,t)$ can be derived respectively from the identities (93), (94), and (95) in an entirely analogous fashion as the derivation for the KFE of $\tilde{\ell}_{HN}(\tilde{x},a,t)$ illustrated above. I omit the repetition to save space.

## A.9 Assumption OA2 and proof of Proposition 2

Assumption OA2. *The initial distributions* $p^0 : [0, \bar{a}] \to [0, \infty)$, $l^0_{iM} : \mathbb{R} \times \left(\underline{a}^w, \bar{a}^w\right] \to [0, \infty)$ *for* $i \in \{H, L\}$, *and* $l^0_{iN} : \mathbb{R} \times \left[\underline{a}^w, \bar{a}^w\right] \to [0, \infty)$ *for* $i \in \{H, L\}$ *satisfy (i)* $p^0$ *is continuously differentiable on* $[0, \bar{a})$ *with* $\lim_{a \uparrow \bar{a}} p^0(a) = 0$*; (ii) for* $i \in \{H, L\}$ *and* $j \in \{M, N\}$, $l^0_{ij}$ *is continuously differentiable in* $(\tilde{x}, a)$, *with* $\lim_{|x| \to \infty} |x| \, l^0_{ij}(x, a) = 0$, $\int_{-\infty}^{\infty} \left| \partial l^0_{ij}(x, a) / \partial x \right| dx < \infty$, $0 < \int_{-\infty}^{\infty} l^0_{ij}(x, a) \, dx < \infty$, $\int_{-\infty}^{\infty} x l^0_{ij}(x, a) \, dx < \infty$, *and* $\int_{-\infty}^{\infty} e^x l^0_{ij}(x, a) \, dx < \infty$ *over their respective age domain; (iii)* $\sum_j \sum_i \int_{-\infty}^{\infty} l^0_{ij}(x, a) \, dx = p^0(a)$ *for all* $a \in \left[\underline{a}^w, \bar{a}^w\right]$.

Part (i) ensures that $p^0$ is sufficiently smooth and consistent with $\lim_{a \uparrow \bar{a}} \xi(a) = \infty$. Part (ii) is analogous to Assumption 3, ensuring finite average log human capital, finite aggregate output, and vanishing boundary terms in integration-by-parts arguments; in addition, $0 < \int_{-\infty}^{\infty} l^0_{ij}(x, a) \, dx < \infty$ ensures that the initial high-growth shares $h^0_j(a) = \int_{-\infty}^{\infty} l^0_{Hj}(x, a) \, dx / \int_{-\infty}^{\infty} \sum_i l^0_{ij}(x, a) \, dx$ and the initial conditional human capital distribution $\ell^0_{ij}(x, a) = l^0_{ij}(x, a) / \int_{-\infty}^{\infty} l^0_{ij}(x, a) \, dx$ are well-defined. Part (iii) ensures consistency between the initial population age density $p^0$ and the initial worker density $l^0_{ij}$. Lemma OA1 establishes some results useful for the proof of Proposition 2.

Lemma OA1. *Under Assumptions 1–2 and OA1, the following holds: (i)* $\lambda_j$ *for* $j \in \{M, N\}$ *is bounded and piecewise continuous on* $[0, \bar{a}]$ *with one jump at* $a = \underline{a}^w$*; (ii)* $\Omega$ *and* $\partial\Omega/\partial t$ *are continuous in* $(a, t)$ *on* $\left(\underline{a}^w, \bar{a}^r\right) \times [0, T]$ *for arbitrary* $T > 0$*; (iii) for* $j \in \{M, N\}$, $\omega_{HL,j}$ *and* $\omega_{LH,j}$ *are uniformly positive, bounded and continuous on* $\left[\underline{a}^w, \bar{a}^w\right]$*; (iv) for* $j \in \{M, N\}$, $h_j$ *is bounded away from* 0 *and* 1 *on* $\left(\underline{a}^w, \bar{a}^w\right] \times [0, T]$ *for arbitrary* $T > 0$.

Proof: (i) The feasibility constraint implies that $\lambda_j(a) = 0$ for all $a \in [0, \bar{a}] \setminus \left[\underline{a}^w, \bar{a}^r\right)$. Assumptions 1–2, Proposition 1, and Corollary 1 jointly imply that $\lambda_j$ is continuous on $\left[\underline{a}^w, \bar{a}^r\right)$, $0 < \lambda_j(a) < \beta(a) < \infty$ for all $a \in \left[\underline{a}^w, \bar{a}^r\right)$, and $\lim_{a \uparrow \bar{a}^r} \lambda_j(a) = 0$. (ii) The proof follows directly from Lemmas 1, OA1 part (i), and Assumption OA2 ($p^0$ and $l^0_{iN}$ being continuously differentiable). (iii) The proof follows directly from the definition (7), Assumptions 2 and OA1 part (ii), and Lemma OA1 part (i). (iv) The right-hand side of (88) goes to $\omega_{LH,N}$ as $h_N \to 0$ and to $-\omega_{HL,N}$ as $h_N \to 1$. Lemma OA1 part (iii) , $h_N\left(\underline{a}^w, t\right) = \sigma \in (0, 1)$, and $h^0_N(a) \in (0, 1)$ then jointly imply that $h_N$ is bounded away from 0 and 1 on $\left(\underline{a}^w, \bar{a}^w\right] \times [0, T]$. The right-hand side of (89) goes to $\omega_{LH,M} + h_N \frac{\lambda_N \Omega}{1-\Omega}$ as $h_M \to 0$ and to $-\left[\omega_{HL,M} + (1 - h_N) \frac{\lambda_N \Omega}{1-\Omega}\right]$ as $h_M \to 1$. For all $a \in \left(\underline{a}^w, \bar{a}^w\right]$, $0 < \Omega(a, t) < 1$ since it is the survival probability with a positive and finite hazard rate; this, together with Lemma OA1 part (iii), imply that $0 < \omega_{LH,M} + h_N \frac{\lambda_N \Omega}{1-\Omega} < \infty$ and $-\infty < -\left[\omega_{HL,M} + (1 - h_N) \frac{\lambda_N \Omega}{1-\Omega}\right] < 0$ on $\left(\underline{a}^w, \bar{a}^w\right] \times [0, T]$. $\lim_{a \downarrow \underline{a}^w} h_M(a, t) = \sigma \in (0, 1)$ and $h^0_M(a) \in (0, 1)$ then jointly imply that $h_M$ is bounded away from 0 and 1 on $\left(\underline{a}^w, \bar{a}^w\right] \times [0, T]$. □

## Proof of Proposition 2

First, we show that there exists a unique solution $p : [0, \bar{a}] \times [0, \infty) \to [0, \infty)$ to (25) with boundary condition (29) and initial condition $p(a, 0) = p^0(a)$. Integrating (25) along characteristics yields

$$p(a,t) = \begin{cases} b(t-a)\, e^{-\int_0^a \xi(a')da'} & \text{if } a \leq t, \\ p^0(a-t)\, e^{-\int_{a-t}^a \xi(a')da'} & \text{if } a > t. \end{cases} \tag{99}$$

Substituting (99) into (29) yields a Volterra integral equation of the second kind for $b(t)$:

$$b(t) = F(t) + \int_0^t K(t,t')\, b(t')\, dt', \tag{100}$$

$$\text{with} \qquad F(t) = \alpha \int_t^\infty \{\lambda_N(a)\, \Omega(a,t) + \lambda_M(a)\, [1 - \Omega(a,t)]\}\, e^{-\int_{a-t}^a \xi(a')da'} p^0(a-t)\, da, \tag{101}$$

$$K(t,t') = \alpha \{\lambda_N(t-t')\, \Omega(t-t',t) + \lambda_M(t-t')\, [1 - \Omega(t-t',t)]\}\, e^{-\int_0^{t-t'} \xi(a)da}, \tag{102}$$

where the functions $\lambda_j$, $p^0$, and $e^{-\int_0^a \xi(a')da'}$ are extended by zero outside the interval $[0, \bar{a}]$ while $\Omega(a,t)$ is extended by one for $a \in \left[0, \underline{a}^w\right)$ and by $\Omega(\bar{a}^r, t)$ for $a \geq \bar{a}^r$. Let $T > 0$ be arbitrary. By Assumptions OA1–2 and Lemma OA1, $F$ and $K$ are continuous respectively on $[0,T]$ and $[0,T]^2$, and hence bounded there. Existence and uniqueness of a continuous solution $b$ to (100)–(102) on $[0,T]$ then follow from the standard Picard-iteration argument for Volterra integral equations with continuous kernels.[44] To recover $p$ from the solution $b$, we have to consider the jump of $\lambda_j$ at $a = \underline{a}^w$. Assumptions 2, OA2 and Lemma OA1 ensure that $F$ is continuously differentiable on $(0,T) \setminus \left\{\underline{a}^w\right\}$,while $K$ and $\partial K/\partial t$ are continuous on the triangle $\{(t,t') : 0 \leq t' \leq t \leq T\}$ away from the lines $t - t' = \underline{a}^w$. Therefore, $b$ is continuously differentiable on $(0,T) \setminus \left\{\underline{a}^w\right\}$. Substituting $b$ into (99) yields a unique solution $p$ to (25) with boundary condition (29) and initial condition $p(a,0) = p^0(a)$; furthermore, $p$ is continuously differentiable in $(a,t)$ on each of the regions separated by the characteristic lines $t = a$ and $t - a = \underline{a}^w$, i.e., a unique piecewise classical solution on $[0, \bar{a}] \times [0,T]$. Since $T$ is arbitrary, such a unique solution $p$ exists on $[0, \bar{a}] \times [0, \infty)$ .

Given the unique solution $p$, the aggregate high-growth share $\mathcal{H}$ is determined by (40). We next show that there exists a unique solution $\tilde{\ell}_{ij} : \mathbb{R} \times \left(\underline{a}^w, \bar{a}^w\right] \times [0, \infty) \to [0, \infty)$ for $i \in \{H, L\}$ and $j \in \{M, N\}$ to (37) with boundary condition (39) and initial conditions $\tilde{\ell}_{ij}(\tilde{x}, a, 0) = \tilde{\ell}^0_{ij}(\tilde{x}, a)$. To save notation when integrating (37) along characteristics, we define the following 3-tuple

$$\Lambda_i(\tilde{x}, a', a, t) \equiv \left(\tilde{x} - \int_{a'}^a [\mu_i - \eta(a'') - \varphi \mathcal{H}(t - a + a'')]\, da'', a', t - a + a'\right).$$

[44] See, for example, Kolmogorov and Fomin (1975) Section 8.3.

Integrating (37) along characteristics using Duhamel's principle, we obtain

$$
\begin{aligned}
&\tilde{\ell}_{ij}\left(\tilde{x},a,t\right)\\
&=\mathbb{I}_{a-t\leq\underline{a}^{w}}E_{i'i,j}\left(a,t-a\right)f^{0}\left(\tilde{x}+\int_{-\infty}^{\infty}xf^{0}\left(x\right)dx-\int_{\underline{a}^{w}}^{a}\left[\mu_{i}-\eta\left(a'\right)-\varphi\mathcal{H}\left(t-a+a'\right)\right]da'\right)\\
&+\mathbb{I}_{a-t>\underline{a}^{w}}E_{i'i,j}\left(a,t-a\right)\tilde{\ell}_{ij}^{0}\left(\tilde{x}-\int_{a-t}^{a}\left[\mu_{i}-\eta\left(a'\right)-\varphi\mathcal{H}\left(t-a+a'\right)\right]da',a-t\right)\\
&+\int_{\max\left\{\underline{a}^{w},a-t\right\}}^{a}\frac{E_{i'i,j}\left(a,t-a\right)}{E_{i'i,j}\left(a',t-a\right)}\omega_{i'i,j}\left(a'\right)\frac{Q_{i'j}\left(a',t-a+a'\right)}{Q_{ij}\left(a',t-a+a'\right)}\tilde{\ell}_{i'j}\left(\Lambda_{i}\left(\tilde{x},a',a,t\right)\right)da'\\
&+\mathbb{I}_{j=M}\int_{\max\left\{\underline{a}^{w},a-t\right\}}^{a}\frac{E_{i'i,j}\left(a,t-a\right)}{E_{i'i,j}\left(a',t-a\right)}\frac{\lambda_{N}\left(a'\right)\Omega\left(a',t-a+a'\right)}{1-\Omega\left(a',t-a+a'\right)}\frac{Q_{iN}\left(a',t-a+a'\right)}{Q_{iM}\left(a',t-a+a'\right)}\tilde{\ell}_{ij'}\left(\Lambda_{i}\left(\tilde{x},a',a,t\right)\right)da',
\end{aligned}
\tag{103}
$$

where $i'\neq i$, $i'\in\{H,L\}$, $j'\neq j$, $j'\in\{M,N\}$, and we save notation by defining

$$
E_{i'i,j}\left(a,t-a\right)\equiv e^{-\int_{\max\left\{\underline{a}^{w},a-t\right\}}^{a}\left[\omega_{i'i,j}\left(a'\right)\frac{Q_{i'j}\left(a',t-a+a'\right)}{Q_{ij}\left(a',t-a+a'\right)}+\frac{\lambda_{N}\left(a'\right)\Omega\left(a',t-a+a'\right)}{1-\Omega\left(a',t-a+a'\right)}\frac{Q_{iN}\left(a',t-a+a'\right)}{Q_{iM}\left(a',t-a+a'\right)}\mathbb{I}_{j=M}\right]da'}. \tag{104}
$$

We focus on the case of $a-t\leq\underline{a}^{w}$; the proof for the case of $a-t>\underline{a}^{w}$ is entirely analogous. Since $\Omega\left(\underline{a}^{w},t\right)=1$, $\frac{\Omega(a,t)}{1-\Omega(a,t)}$ is unbounded at $a=\underline{a}^{w}$, which complicates a direct fixed-point argument using (103). We thus rewrite (103) for $j=M$ by applying integration by parts to the last integral, so that integral kernels become uniformly bounded:

$$
\begin{aligned}
&\tilde{\ell}_{iM}\left(\tilde{x},a,t\right)\\
&=E_{i'i,N}\left(a,t-a\right)f^{0}\left(\tilde{x}+\int_{-\infty}^{\infty}xf^{0}\left(x\right)dx-\int_{\underline{a}^{w}}^{a}\left[\mu_{i}-\eta\left(a'\right)-\varphi\mathcal{H}\left(t-a+a'\right)\right]da'\right)\\
&+\int_{\underline{a}^{w}}^{a}\frac{E_{i'i,M}\left(a,t-a\right)}{E_{i'i,M}\left(a',t-a\right)}\omega_{i'i,M}\left(a'\right)\frac{Q_{i'M}\left(a',t-a+a'\right)}{Q_{iM}\left(a',t-a+a'\right)}\tilde{\ell}_{i'M}\left(\Lambda_{i}\left(\tilde{x},a',a,t\right)\right)da'\\
&+\int_{\underline{a}^{w}}^{a}\left[\frac{E_{i'i,N}\left(a,t-a\right)}{E_{i'i,N}\left(a',t-a\right)}-\frac{E_{i'i,M}\left(a,t-a\right)}{E_{i'i,M}\left(a',t-a\right)}\right]\omega_{i'i,N}\left(a'\right)\frac{Q_{i'N}\left(a',t-a+a'\right)}{Q_{iN}\left(a',t-a+a'\right)}\tilde{\ell}_{i'N}\left(\Lambda_{i}\left(\tilde{x},a',a,t\right)\right)da'\\
&+\int_{\underline{a}^{w}}^{a}\frac{E_{i'i,M}\left(a,t-a\right)}{E_{i'i,M}\left(a',t-a\right)}\left[\omega_{i'i,N}\left(a'\right)\frac{Q_{i'N}\left(a',t-a+a'\right)}{Q_{iN}\left(a',t-a+a'\right)}-\omega_{i'i,M}\left(a'\right)\frac{Q_{i'M}\left(a',t-a+a'\right)}{Q_{iM}\left(a',t-a+a'\right)}\right]\tilde{\ell}_{iN}\left(\Lambda_{i}\left(\tilde{x},a',a,t\right)\right)da'.
\end{aligned}
\tag{105}
$$

Define $\mathcal{M}=\mathbb{R}\times\left[\underline{a}^{w},\bar{a}^{w}\right]\times\left[a-\underline{a}^{w},T\right]$ and define the unknown vector $\mathbf{L}=\left(\tilde{\ell}_{HM},\tilde{\ell}_{LM},\tilde{\ell}_{HN},\tilde{\ell}_{LN}\right)$. Let $X$ be the space of bounded continuous vector fields $\mathbf{L}:\mathcal{M}\rightarrow[0,\infty)^{4}$ that vanish uniformly in $\tilde{x}$ as $|\tilde{x}|\rightarrow\infty$, with norm

$$
\left\|\mathbf{L}\right\|_{\nu}=\max_{k\in\{HM,LM,HN,LN\}}\sup\left\{e^{-\nu\left(a-\underline{a}^{w}\right)}\left|\tilde{\ell}_{k}\left(\tilde{x},a,t\right)\right|:\left(\tilde{x},a,t\right)\in\mathcal{M}\right\}. \tag{106}
$$

Then $X$ with the norm (106) is a Banach space.[45] Define an operator $\mathcal{T}$ on $X$ component-wise by the right-hand side of (103) or (105). Concretely, for $i \in \{H, L\}$, $(\mathcal{T}\mathbf{L})_{iM}(\tilde{x}, a, t)$ is given by the right-hand side of (105) and $(\mathcal{T}\mathbf{L})_{iN}(\tilde{x}, a, t)$ is given by the right-hand side of (103), with $a - t \leq \underline{a}^w$ and $j = N$. Assumptions 2–3 and Lemma OA1 imply that each component of $\mathcal{T}\mathbf{L}$ is bounded and continuous on $\mathcal{M}$, vanishing uniformly in $\tilde{x}$ as $|\tilde{x}| \to \infty$. It is straightforward to check from (103) that $(\mathcal{T}\mathbf{L})_{iN}$ are non-negative. For $(\mathcal{T}\mathbf{L})_{iM}$, we can reverse the integration by parts and check from (103) that they are non-negative. Therefore, $\mathcal{T} : X \to X$. To show that $\mathcal{T}$ is a contraction, note that $\mathcal{T}$ is affine: $\mathcal{T}\mathbf{L} = \mathbf{G} + \mathcal{K}\mathbf{L}$, where $\mathbf{G}$ is a vector of the boundary terms involving $f^0$ and $\mathcal{K}$ is a linear integral operator. For each component $k \in \{HM, LM, HN, LN\}$,

$$(\mathcal{K}\mathbf{L})_k(\tilde{x}, a, t) = \int_{\underline{a}^w}^{a} \sum_{k' \{HM,LM,HN,LN\}} K_{kk'}(a', a, t)\, \tilde{\ell}_{k'}\left(\Lambda_{i(k)}(\tilde{x}, a', a, t)\right) da',$$

where $i(k) = H$ for $k \in \{HM, HN\}$, $i(k) = L$ for $k \in \{LM, LN\}$, and each $K_{kk'}$ maps to the kernel coefficient in front of the corresponding $\tilde{\ell}_{k'}$ inside the integrals of (103) and (105). Lemma OA1 implies that $K_{kk'}$ is bounded for all $k, k' \in \{HM, LM, HN, LN\}$. Define a single constant that uniformly bounds all the kernels:

$$C_K = \max_{k,k'} \sup \left\{ |K_{kk'}(a', a, t)| : (a', a, t) \in \left[\underline{a}^w, \bar{a}^w\right]^2 \times \left[a - \underline{a}^w, T\right] \right\} < \infty.$$

Consider any $\mathbf{L}_1, \mathbf{L}_2 \in X$. Since $\mathbf{G}$ cancels, $\|\mathcal{T}\mathbf{L}_1 - \mathcal{T}\mathbf{L}_2\|_\nu = \|\mathcal{K}\mathbf{L}_1 - \mathcal{K}\mathbf{L}_2\|_\nu$. Fixing a component $k$, we have

$$|\mathcal{K}(\mathbf{L}_1 - \mathbf{L}_2)_k(\tilde{x}, a, t)| \leq \int_{\underline{a}^w}^{a} \sum_{k'} e^{\nu\left(a' - \underline{a}^w\right)} |K_{kk'}(a', a, t)|\, \|\mathbf{L}_1 - \mathbf{L}_2\|_\nu\, da', \tag{107}$$

where we have used triangle inequality and the fact that the shift in $\tilde{x}$ does not change sup bounds. By (106) and (107), we have

$$\begin{aligned}
\|\mathcal{K}\mathbf{L}_1 - \mathcal{K}\mathbf{L}_2\|_\nu &\leq \max_k \sup \left\{ \int_{\underline{a}^w}^{a} e^{-\nu(a-a')} \sum_{k'} |K_{kk'}(a', a, t)|\, da' : (a, t) \in \left[\underline{a}^w, \bar{a}^w\right] \times \left[a - \underline{a}^w, T\right] \right\} \|\mathbf{L}_1 - \mathbf{L}_2\|_\nu \\
&\leq \int_{\underline{a}^w}^{a} e^{-\nu(a-a')} \sum_{k'} C_K da' \, \|\mathbf{L}_1 - \mathbf{L}_2\|_\nu \\
&\leq \frac{3C_K}{\nu} \|\mathbf{L}_1 - \mathbf{L}_2\|_\nu,
\end{aligned}$$

where we have used the fact that, for all $k \in \{HM, LM, HN, LN\}$, $(\mathcal{K}\mathbf{L})_k(\tilde{x}, a, t)$ contains at most

[45] The norm (106) is the Bielecki norm (exponentially weighted sup-norm) used in the proof of Corollary 1. By properly choosing the age weights, this norm allows a contraction argument for the entire age domain $\left[\underline{a}^w, \bar{a}^w\right]$. Alternatively, one can use the usual sup-norm and establish contraction on a small age slab $\left[\underline{a}^w, \underline{a}^w + \Delta\right]$, and then iterate slab-by-slab to reach $\bar{a}^w$.

three integral couplings. Choose $\nu > 3C_K$, then $\mathcal{T}$ is a contraction on $X$ with norm (106). Thus, there exists a unique continuous solution $\tilde{\ell}_{ij}(\tilde{x}, a, t)$ to the integral equation system on $\mathcal{M}$. Furthermore, Assumptions 2–3 and OA2 and Lemma OA1 imply that $\tilde{\ell}_{ij}$ is continuously differentiable in $(\tilde{x}, a, t)$ on $\mathbb{R} \times \left(\underline{a}^w, \bar{a}^w\right] \times \left(a - \underline{a}^w, T\right]$. Thus, there exists a unique piecewise classical solution $\tilde{\ell}_{ij}$ to (37) with boundary condition (39) on $\mathbb{R} \times \left(\underline{a}^w, \bar{a}^w\right] \times \left[a - \underline{a}^w, T\right]$. Since $T > 0$ is arbitrary, such a unique solution $\tilde{\ell}_{ij}$ exists on $\mathbb{R} \times \left(\underline{a}^w, \bar{a}^w\right] \times \left[a - \underline{a}^w, \infty\right)$. An analogous proof goes through for the case of $a - t > \underline{a}^w$, relying on the regularity conditions on $l_{ij}^0$ in Assumption OA2 part (ii) instead of those on $f^0$.

Finally, since $\lim_{|\tilde{x}| \to \infty} \tilde{\ell}_{ij}(\tilde{x}, a, t) = 0$ for all $(a, t) \in \left(\underline{a}^w, \bar{a}^w\right] \times [0, \infty)$, we have verified the conjectures (86) and (90). □

## A.10 Proof of Proposition 3

From (49), define

$$\mathcal{F}(g_P) = \alpha \int_{\underline{a}^w}^{\bar{a}^r} \{\lambda_N(a)\,\Omega(a) + \lambda_M(a)\,[1 - \Omega(a)]\}\, e^{-\int_0^a [g_P + \xi(a')]da'} da - 1, \tag{108}$$

where $\Omega(a)$ is given by Lemma 1(the case of $a - t \leq \underline{a}^w$) and hence depends only on primitives. The function $\mathcal{F}$ satisfies $\lim_{g_P \to -\infty} \mathcal{F}(g_P) = \infty$, $\lim_{g_P \to \infty} \mathcal{F}(g_P) = -1 < 0$, and is strictly decreasing:

$$\mathcal{F}'(g_P) = -\alpha \int_{\underline{a}^w}^{\bar{a}^r} a\,\{\lambda_N(a)\,\Omega(a) + \lambda_M(a)\,[1 - \Omega(a)]\}\, e^{-\int_0^a [g_P + \xi(a')]da'} da < 0.$$

Therefore, $\mathcal{F}(g_P) = 0$ has a unique solution $g_P \in \mathbb{R}$. Given $g_P$, Lemma 2 (the case of $a - t \leq \underline{a}^w$) uniquely pins down the stationary shares $h_j(a)$ and hence $\mathcal{H}$ via (50). Lemma 3 then implies $\mathcal{Z}'_{\underline{a}^w}(t) / \mathcal{Z}_{\underline{a}^w}(t) = \varphi\mathcal{H}$, so the BGP aggregate productivity growth rate is uniquely $g_A = \varphi\mathcal{H}$. Finally, the existence and uniqueness of the stationary distribution $\tilde{\ell}_{ij}(\tilde{x}, a)$ follow from Proposition 2 applied in the stationary environment. □

## A.11 Proofs of comparative statics in Table 3

Taking functional derivative with respective to $\lambda_M$ at point $a$ of both sides of (49) yields

$$\begin{aligned} 0 = &\int_{\underline{a}^w}^{\bar{a}^r} \delta(a' - a)\,[1 - \Omega(a')]\,\frac{\wp(a')}{\wp(0)} da' \\ &+ \frac{\partial}{\partial g_P}\left(\int_{\underline{a}^w}^{\bar{a}^r} \{\lambda_N(a)\,\Omega(a) + \lambda_M(a)\,[1 - \Omega(a)]\}\, e^{-\int_0^a [g_P + \xi(a')]da'} da\right) \frac{\delta g_P[\lambda_M]}{\delta \lambda_M(a)}, \end{aligned} \tag{109}$$

where $\delta(\cdot)$ inside the integral is the Dirac delta function. Rearranging (109) yields (51). Taking functional derivative with respective to $\lambda_N$ at point $a$ of both sides of (49) yields

$$0 = \int_{\underline{a}^w}^{\bar{a}^r} \left\{ \delta(a'-a)\,\Omega(a') - [\lambda_N(a') - \lambda_M(a')] \int_{\underline{a}^w}^{a'} \delta(a''-a)\,da''\Omega(a') \right\} \frac{\wp(a')}{\wp(0)} da' + \frac{\partial}{\partial g_P} \left( \int_{\underline{a}^w}^{\bar{a}^r} \{\lambda_N(a)\,\Omega(a) + \lambda_M(a)\,[1-\Omega(a)]\}\, e^{-\int_0^a [g_P+\xi(a')]da'} da \right) \frac{\delta g_P[\lambda_N]}{\delta \lambda_N(a)}, \tag{110}$$

where $\delta(\cdot)$ inside the integrals are the Dirac delta function. Rearranging (110) yields (52).

Turning to $g_A$, the expressions (53)–(54) can be derived by taking functional derivative of $g_A$ with respect to $\lambda_j$, for $j \in \{M, N\}$, at point $a$ yields and using the fact that

$$\frac{\delta \wp^w[\lambda_j]}{\delta \lambda_j(a)} = \frac{\partial \wp^w(a')}{\partial g_P} \frac{\delta g_P[\lambda_j]}{\delta \lambda_j(a)} = \left[ \int_{\underline{a}^w}^{\bar{a}^w} a' \wp^w(a')\,da' - a' \right] \wp^w(a') \frac{\delta g_P[\lambda_j]}{\delta \lambda_j(a)}. \quad \square$$

# B. Quantification

## B.1 Data construction

The quantitative exercises use five data sources: the Human Fertility Database (HFD), the National Vital Statistics System (NVSS), the Human Mortality Database (HMD), the Current Population Survey (CPS), and the 1960 Census. Unless otherwise noted, all data are for the United States, female only, and cover 1961–2019. The 1960 Census is used to construct the initial condition.

**Population** From the HMD (HMD, 2025), I obtain annual population counts at one-year age intervals for ages 0–100 over 1960–2019, using the 1960 distribution to construct the initial population age density $p^0(a)$.[46] To convert the population from one-year to one-month age intervals, I assume the population within each one-year age bin is evenly distributed across the 12 months.

**Mortality rates** From the HMD, I retrieve annual age-specific death rates (deaths as a share of population) at a $1 \times 1$ age-by-year grid, discarding ages above 100.[47] Along the age dimension, I linearly interpolate the data from one-year to one-month age intervals to obtain annual death rates at monthly age resolution, $D(a,t)$. I then compute the monthly Poisson death probability as $\xi(a,t) = -\frac{1}{12}\log[1-D(a,t)]$, assuming that $\xi(a,t)$ is constant within each calendar year. Panel (a) of Figure 12 plots $\xi(a,t)$ against age for selected years.

[46] Link to the data: https://www.mortality.org/File/GetDocument/hmd.v6/USA/STATS/Population.txt
[47] Link to the data: https://www.mortality.org/File/GetDocument/hmd.v6/USA/STATS/Mx_1x1.txt

**Natural fertility rates** The age gradient of $\beta(a)$ is calibrated in the following steps. First, I set reproductive horizon $\bar{a}^r$ at 45 as a conservative bound, due to scarce medical research on natural conception probabilities beyond this age. Second, consistent with Assumption 1, I set $\beta(a) = 0$ for $a \notin [16, 45)$.[48] Third, $\beta(a)$ is set to reach its maximum at age 21, in line with the consensus that female fecundability peaks in the early 20s. Fourth, for $a \in (21, 45)$, I calibrate the ratio $\beta(a)/\beta(21)$ to match Wesselink et al. (2017), who estimate the rate of reproductive aging using data from a large preconception cohort study of pregnancy planners in the U.S. and Canada.[49] Finally, for $a \in [16, 21)$, I proxy reproductive maturation using the occurrence of ovulatory menstrual cycles reported by Carlson and Shaw (2019). Specifically, I set $\beta(16)/\beta(21)$ at 0.75, in line with the share of adolescent women with ovulatory cycles four years after menarche. The age at menarche is taken to be 12, the average of U.S. women born 1950–2005 reported by Wang et al. (2024). I then obtain $\beta(a)/\beta(21)$ for $a \in (16, 21)$ by linear interpolation. Given the calibrated age gradient of $\beta(a)$, I set the reference point $\beta(21)$ at 0.035, which implies an average of 8.9 births over the life cycle, consistent with Eijkemans et al. (2014) based on historical natural fertility populations. Panel (b) of Figure 12 plots $\beta(a)$ against age.

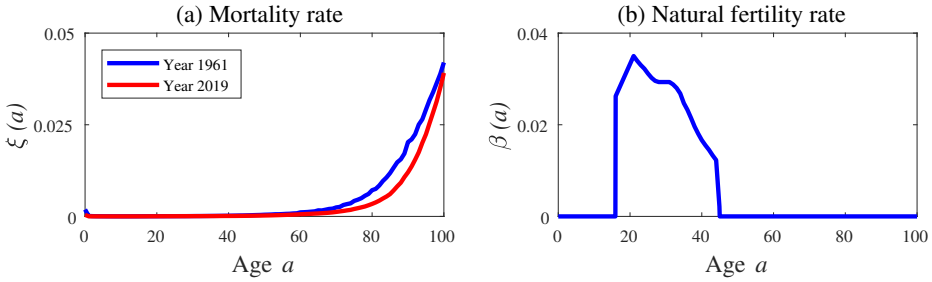



FIGURE 12: CALIBRATION OF AGE-DEPENDENT DEMOGRAPHIC PRIMITIVES

**Motherhood status distribution** From the HFD, I retrieve population counts by age and parity (i.e., the number of children previously borne). I group all women with positive parity into a single motherhood status $j = M$ and define $W_j(a, t)$ as the population of age $a$ and motherhood status $j \in \{M, N\}$ in year $t$.[50] HFD coverage of population by parity is incomplete along the age dimension for 1961–1972. To fill the missing ages, I use the NVSS Cohort Fertility Tables to obtain

[48] According to the HFD birth data, births to U.S. women younger than 16 as a share of annual total births range from 0.17% in 2019 to 1.5% in 1973, with a 1961–2019 period average of 0.83%. Births to women aged 45 and above account for about 0.1% of total annual births on average over 1961–2019. Although this share has risen steadily since the 1980s, it remains below 0.3% in 2019. Thus, by ignoring births outside the age range $[16, 45)$, the model empirically misses, in an average year, less than 1% of total annual births.

[49] Preconception cohort studies in contemporary populations, such as Pregnancy Study Online used by Wesselink et al. (2017), track time to pregnancy for couples without a history of fertility problems who attempt to conceive naturally. Wesselink et al. (2017) also collect background information to control for factors correlated with both age and fecundability, such as intercourse frequency.

[50] Link to the data: https://www.humanfertility.org/File/GetDocument/Files/USA/20250425/USAexposRRpa.txt

non-mother shares by age for 1961–1972.[51] I then combine these shares with the population-by-age series to recover $W_j(a,t)$ for 1961–1972. Finally, I use the 1960 Census to obtain the initial non-mother shares by age, $\Omega^0(a)$, which are smoothed across age via three-year centered moving averages and then converted to one-month age intervals via linear interpolation.[52]

**Fertility rates** From the HFD, I obtain annual birth counts by maternal age and birth order.[53] I aggregate second and higher-order births into a single category and define $B_j(a,t)$ as the number of births in year $t$ to women of age $a$ and motherhood status $j \in \{M, N\}$. To construct monthly fertility rates from annual data at one-year age resolution, I proceed as follows. I distribute the population count $W_j(a,t)$ evenly across the 12 monthly ages within each one-year age bin and linearly interpolate $W_j(a,t)$ from annual to monthly time resolution. I also assume that the birth count $B_j(a,t)$ is evenly distributed over the $12 \times 12$ month-by-month age-time grid within $[a, a+1) \times [t, t+1)$. Monthly fertility rates at one-month age resolution are then given by $\lambda_j(a',t') = \frac{B_j(a,t)}{12W_j(a,t')}$ for $j \in \{M, N\}$, $a' \in [a, a+1)$ and $t' \in [t, t+1)$. Finally, I smooth $\lambda_j(a,t)$ across ages using three-year centered moving averages.

**Growth-type distribution** I use CPS microdata (Flood et al., 2025) to construct the annual series of high-growth shares by age $H(a,t)$. Because of data availability, I split the time period into 1961–1975 and 1976–2019. For 1976–2019, I use the October Monthly Survey with the Educational Supplement, drawing employment status from *WKSTAT* and school enrollment from *EDATT*. For 1961–1975, I use *FULLPART* from the Annual Social and Economic Supplement (ASEC) for employment status. School enrollment is not consistently observed in the CPS microdata for this earlier period, so I instead use the CPS Historical Time Series Tables on School Enrollment.[54] Because employment and enrollment come from separate sources for 1961–1975, the implied high-growth shares could be inflated by double counting individuals who both work full time and are enrolled in school. To adjust for this overlap, I proceed as follows. First, using CPS microdata for 1976, I compute age-specific shares of individuals who are enrolled in school (either full time or part time) while working full time. I then compute the same overlap shares by age in 1960 and 1970 using Census data, where employment and enrollment are observed for the same individual. Next, I linearly interpolate the overlap shares by age over 1960–1970 and 1970–1976. The high-growth shares by age for 1961–1975 are then constructed as $H(a,t) = \min\{1, FT(a,t) + Enroll(a,t) - Overlap(a,t)\}$, where $FT$ denotes the full-time employment share, $Enroll$ the enrollment share, and $Overlap$ the share enrolled while working full

[51] Link to the data: https://ftp.cdc.gov/pub/Health_Statistics/NCHS/nvss/birth/cohort/Table03.csv

[52] The 1960 Census data are accessed via IPUMS (Ruggles et al., 2025).

[53] Link to the data: https://www.humanfertility.org/File/GetDocument/Files/USA/20250425/USAbirthsRRbo.txt

[54] Link to the data: https://www2.census.gov/programs-surveys/demo/tables/school-enrollment/time-series/cps-historical-time-series/tablea-2.xlsx

time. The merged series $H(a,t)$ are smoothed across ages via five-year centered moving averages and then interpolated along the age and time dimensions to monthly age-time intervals. Finally, I use the 1960 Census to construct the initial high-growth shares by age and motherhood status, $h_j^0(a)$ for $j \in \{M,N\}$, at one-year age intervals, smooth them across age using five-year centered moving averages, and convert them to one-month age intervals via linear interpolation.

**Labor market risks** To construct the age-specific monthly transition intensities between the two growth states, $\phi(a)$ and $\psi(a)$, I use matched adjacent-month CPS microdata. Using *WKSTAT* and *SCHLCOLL* for employment and enrollment status, I compute, by age, the share of individuals who switch growth type between two adjacent months and average these shares over 1989–2019.[55] I restrict the sample to single women without children, for whom labor market risks are most plausibly unrelated to fertility effort. I also restrict the base month to October to align with the construction of $H(a,t)$ for 1976–2019, which is based on the October Monthly Survey. The resulting age-specific switch shares, $\mathcal{S}_{HL}(a)$ and $\mathcal{S}_{LH}(a)$, are smoothed across age using five-year centered moving averages and then converted to one-month age intervals via linear interpolation. I then compute baseline transition rates as $\phi(a) = -\log[1-\mathcal{S}_{HL}(a)]$ and $\psi(a) = \max\{-\log[1-\mathcal{S}_{LH}(a)], 0.05\}$.[56] Figure 13 plots $\phi(a)$ and $\psi(a)$ against age.

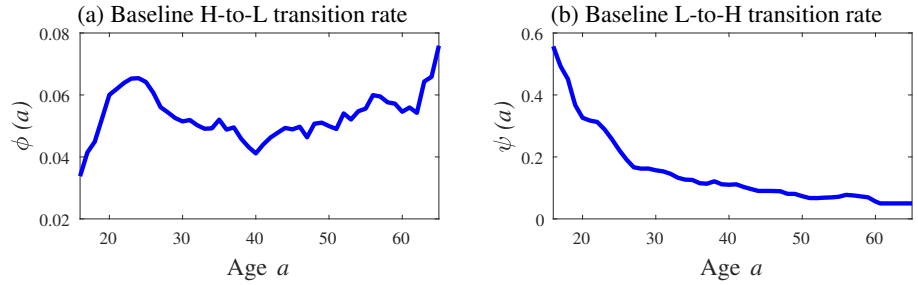



FIGURE 13: CALIBRATION OF THE AGE-SPECIFIC GROWTH TYPE TRANSITION RATES

**Hours and wage income** Full-time employment corresponds to usual weekly hours worked of 35 or more. To calibrate the fraction of hours reduced in the low-growth state, $\epsilon$, I use *UHRSWORK1* (usual hours worked per week) from the CPS ASEC. I restrict the sample to women aged 25–55, excluding those enrolled in school or self-employed. Averaging over 1985–2019 and over ages 25–55, mean weekly hours are 41.3 for high-growth types and 8.4 for low-growth types, implying $\epsilon = 0.8$.[57] To calibrate the human capital growth rate differential $\mu_H - \mu_L$ , I use the

[55] The calculation starts in 1989 because it is the first year in which school enrollment is available at monthly frequency in the CPS.

[56] The lower bound on $\psi(a)$ ensures that the overall low-to-high transition rate for mothers, $\psi(a) - \gamma(t)\lambda_M(a,t) - \theta(t)$, remains positive throughout the working life in the studied period, given the observed $\lambda_M(a,t)$ and calibrated $\gamma(t)$ and $\theta(t)$. This bound binds only for ages above 60: over $a \in (60,65]$, $-\log[1-\mathcal{S}_{LH}(a)]$ falls to about 0.03, although data for this age range are substantially noisier than earlier in the working life.

[57] The sample starts in 1985 because this is the first year in which usual hours and enrollment status are jointly available in the CPS ASEC.

CPS ASEC longitudinal sample for women aged 25–55 who are not in school and earn positive wages. I use *EARNWEEK* and *UHRSWORK* jointly to construct hourly wages, and adjust wages for inflation using *CPI99*. For individuals who remain in the same growth type in adjacent years, I compute the growth rate of hourly wages. I then average these growth rates by type over ages 25–55 and over 1989–2019, and convert annual growth rates to monthly rates by dividing by 12.[58] To construct the time-varying income-by-age profile $y(a,t)$ for $a \in [16,65]$ and $t \in [1961,2019]$, I use *INCWAGE* from the CPS ASEC to compute average annual wage earnings by age, adjusting for inflation with *CPI99*. I smooth the resulting series over age and time using five-year centered moving averages and then interpolate to one-month age and time intervals. Finally, I use the 1960 Census to construct the initial average human capital $\mathcal{Z}_{ij}^0(a)$ by age $a$, growth state $i \in \{H,L\}$, and motherhood status $j \in \{M,N\}$. I convert annual wage earnings (*INCWAGE* deflated by *CPI99*) to hourly wages using reported hours per week and weeks per year (*HRSWORK2* and *WKSWORK2*), replacing each response interval with its midpoint. I then smooth $\mathcal{Z}_{ij}^0(a)$ across age using five-year centered moving averages and convert it to one-month age intervals via linear interpolation.

## B.2 Numerical procedures

### B.2.1 Calibration of the career impacts of motherhood

The left-hand sides of (85) and (88)–(89) can be approximated as

$$\left(\frac{\partial}{\partial t}+\frac{\partial}{\partial a}\right)\Omega(a,t)=\frac{\Omega(a+\Delta,t+\Delta)-\Omega(a,t)}{\Delta},\quad \left(\frac{\partial}{\partial t}+\frac{\partial}{\partial a}\right)h_j(a,t)=\frac{h_j(a+\Delta,t+\Delta)-h_j(a,t)}{\Delta},$$

where $j \in \{M,N\}$ and $\Delta$ is the age-time step for discretization. By the backward finite-difference method, we can write the approximated PDEs (85) and (88)–(89) as

$$\Omega(a,t)=\frac{\Omega(a-\Delta,t-\Delta)}{1+\lambda_N(a,t)\Delta}, \tag{111}$$

$$h_j(a,t)=\overline{h}_j(a,t)+\gamma(t)\frac{\partial h_j(a,t)}{\partial\gamma(t)}+\mathbb{I}_{j=M}\theta(t)\frac{\partial h_M(a,t)}{\partial\theta(t)}, \tag{112}$$

$$\text{where}\quad \overline{h}_j(a,t)=\frac{h_j(a-\Delta,t-\Delta)+\left[\psi(a)+\mathbb{I}_{j=M}\frac{\lambda_N(a,t)\Omega(a,t)}{1-\Omega(a,t)}\overline{h}_N(a,t)\right]\Delta}{1+\left[\phi(a)+\psi(a)+\mathbb{I}_{j=M}\frac{\lambda_N(a,t)\Omega(a,t)}{1-\Omega(a,t)}\right]\Delta}, \tag{113}$$

$$\frac{\partial h_j(a,t)}{\partial\gamma(t)}=\frac{\left[-\lambda_j(a,t)+\mathbb{I}_{j=M}\frac{\lambda_N(a,t)\Omega(a,t)}{1-\Omega(a,t)}\frac{\partial h_N(a,t)}{\partial\gamma(t)}\right]\Delta}{1+\left[\phi(a)+\psi(a)+\mathbb{I}_{j=M}\frac{\lambda_N(a,t)\Omega(a,t)}{1-\Omega(a,t)}\right]\Delta}, \tag{114}$$

$$\frac{\partial h_M(a,t)}{\partial\theta(t)}=-\frac{\Delta}{1+\left[\phi(a)+\psi(a)+\frac{\lambda_N(a,t)\Omega(a,t)}{1-\Omega(a,t)}\right]\Delta}. \tag{115}$$

[58] The shorter time span reflects the availability of earnings information in the longitudinal sample.

The distance-minimizing problem for calibrating $\gamma(t)$ and $\theta(t)$ can then be written as

$$\min_{\gamma(t),\theta(t)} \int_{\underline{a}^w}^{\bar{a}^w} \left[ H(a,t) - \overline{H}(a,t) - \gamma(t) \frac{\partial \widehat{H}(a,t)}{\partial \gamma(t)} - \theta(t) \frac{\partial \widehat{H}(a,t)}{\partial \theta(t)} \right]^2 da, \tag{116}$$

where
$$\overline{H}(a,t) = \overline{h}_N(a,t)\,\Omega(a,t) + \overline{h}_M(a,t)\,[1-\Omega(a,t)],$$
$$\frac{\partial \widehat{H}(a,t)}{\partial \gamma(t)} = \frac{\partial h_N(a,t)}{\partial \gamma(t)}\Omega(a,t) + \frac{\partial h_M(a,t)}{\partial \gamma(t)}[1-\Omega(a,t)],$$
$$\frac{\partial \widehat{H}(a,t)}{\partial \theta(t)} = \frac{\partial h_M(a,t)}{\partial \theta(t)}[1-\Omega(a,t)].$$

The first-order conditions of (116) with respect to $\gamma(t)$ and $\theta(t)$ can be written in matrix form as

$$\begin{bmatrix} \int_{\underline{a}^w}^{\bar{a}^w} \left[\frac{\partial \widehat{H}(a,t)}{\partial \gamma(t)}\right]^2 da & \int_{\underline{a}^w}^{\bar{a}^w} \frac{\partial \widehat{H}(a,t)}{\partial \gamma(t)} \frac{\partial \widehat{H}(a,t)}{\partial \theta(t)} da \\ \int_{\underline{a}^w}^{\bar{a}^w} \frac{\partial \widehat{H}(a,t)}{\partial \gamma(t)} \frac{\partial \widehat{H}(a,t)}{\partial \theta(t)} da & \int_{\underline{a}^w}^{\bar{a}^w} \left[\frac{\partial \widehat{H}(a,t)}{\partial \theta(t)}\right]^2 da \end{bmatrix} \begin{bmatrix} \gamma(t) \\ \theta(t) \end{bmatrix} = \begin{bmatrix} \int_{\underline{a}^w}^{\bar{a}^w} \left[H(a,t) - \overline{H}(a,t)\right] \frac{\partial \widehat{H}(a,t)}{\partial \gamma(t)} da \\ \int_{\underline{a}^w}^{\bar{a}^w} \left[H(a,t) - \overline{H}(a,t)\right] \frac{\partial \widehat{H}(a,t)}{\partial \theta(t)} da \end{bmatrix},$$

Therefore, the distance-minimizing $\gamma(t)$ and $\theta(t)$ are given by

$$\begin{bmatrix} \gamma(t) \\ \theta(t) \end{bmatrix} = \begin{bmatrix} \int_{\underline{a}^w}^{\bar{a}^w} \left[\frac{\partial \widehat{H}(a,t)}{\partial \gamma(t)}\right]^2 da & \int_{\underline{a}^w}^{\bar{a}^w} \frac{\partial \widehat{H}(a,t)}{\partial \gamma(t)} \frac{\partial \widehat{H}(a,t)}{\partial \theta(t)} da \\ \int_{\underline{a}^w}^{\bar{a}^w} \frac{\partial \widehat{H}(a,t)}{\partial \gamma(t)} \frac{\partial \widehat{H}(a,t)}{\partial \theta(t)} da & \int_{\underline{a}^w}^{\bar{a}^w} \left[\frac{\partial \widehat{H}(a,t)}{\partial \theta(t)}\right]^2 da \end{bmatrix}^{-1} \begin{bmatrix} \int_{\underline{a}^w}^{\bar{a}^w} \left[H(a,t) - \overline{H}(a,t)\right] \frac{\partial \widehat{H}(a,t)}{\partial \gamma(t)} da \\ \int_{\underline{a}^w}^{\bar{a}^w} \left[H(a,t) - \overline{H}(a,t)\right] \frac{\partial \widehat{H}(a,t)}{\partial \theta(t)} da \end{bmatrix},$$

which can be computed by forward iterations on $\Omega(a,t)$ and $h_j(a,t)$, using (111)–(115) with initial conditions $\Omega^0(a)$ and $h_j^0(a)$. The high-growth share of entering workers, $\sigma$, is set to the average of one and the observed high-growth share of 16-year-old non-mothers in 1960, capturing the fact this share has risen since the 1960s. The inferred paths $\{\gamma(t), \theta(t)\}_t$ are smoothed using five-year centered moving averages.

### B.2.2 Computation of the optimal fertility schedule

To back out the path of contraception effectiveness $\kappa_j(a,t)$ and to conduct counterfactuals and projections, we need to compute the optimal fertility schedule given by Proposition 1. This is straightforward except for solving the nonlinear ODE (20) with boundary condition (21), to which we apply the finite difference method using the assumption that shocks to $\gamma(t)$, $\theta(t)$, and $\kappa_j(a,t)$ are unanticipated by the individual. In particular, when recovering $\kappa_j(a,t)$ from observed fertility rates, we can use Proposition 1 to write the approximation of (20) by a backward finite-difference scheme with age-step $\Delta$ as

$$\frac{\Phi(a,t) - \Phi(a-\Delta,t)}{\Delta} = \left\{\rho + \xi(a,t) + \beta(a) + \frac{1}{2}\left[\lambda_N(a,t) - \beta(a)\right]\right\}\Phi(a,t) - \theta(t)\,\widehat{\Psi}(a,t)$$
$$+ \frac{1}{2}\left[\zeta\Pi(a,t) - \gamma(t)\,\widehat{\Psi}(a,t)\right]\left[\lambda_M(a,t) - \lambda_N(a,t)\right],$$

which then allows one to compute $\Phi(a,t)$ for $a \in \left[\underline{a}^w, \bar{a}^w\right)$ by backward iteration from the terminal condition $\Phi(\bar{a}^w, t) = 0$, without requiring $\left\{\kappa_j(\cdot,t)\right\}_t$.

### B.2.3 Computation of the population dynamics

We approximate the PDE (25) with boundary condition (26) using the Implicit Euler-Riemann method with age-time step $\Delta$, which implies

$$p(a,t) = \frac{p(a-\Delta, t-\Delta)}{1+\xi(a,t)\Delta} \qquad \text{for } a > 0, \tag{117}$$

$$p(0,t) = \alpha \sum_{a_n=\Delta}^{\bar{a}^r} \left\{\lambda_N(a_n,t)\,\Omega(a_n,t) + \lambda_M(a_n,t)\left[1-\Omega(a_n,t)\right]\right\} p(a_n,t), \tag{118}$$

where $p(a_n,t)$ is the population mass in an age bin of width $\Delta$. Given initial condition $p^0$, the path $\{p(\cdot,t)\}_t$ can be computed iteratively using (117)–(118), where the path $\{\Omega(\cdot,t)\}_t$ is computed as described in Online Appendix B.2.1.

### B.2.4 Calibration of $\mu_H$ and $\varphi$

Partially differentiating both sides of (45) with respect to $t$ and $a$ and using (37), we have

$$\begin{aligned}\frac{\partial \mathcal{Z}_{ij}(a,t)}{\partial t} + \frac{\partial \mathcal{Z}_{ij}(a,t)}{\partial a} &= \left[\mu_i - \eta(a)\right]\mathcal{Z}_{ij}(a,t) + \omega_{i'i,j}(a)\frac{Q_{i'j}(a,t)}{Q_{ij}(a,t)}\left[\mathcal{Z}_{i'j}(a,t) - \mathcal{Z}_{ij}(a,t)\right] \\ &\quad + \mathbb{I}_{j=M}\frac{\lambda_N(a)\,\Omega(a,t)}{1-\Omega(a,t)}\frac{Q_{iN}(a,t)}{Q_{iM}(a,t)}\left[\mathcal{Z}_{iN}(a,t) - \mathcal{Z}_{iM}(a,t)\right], \end{aligned} \tag{119}$$

where $i, i' \in \{H,L\}$, $i' \neq i$, and $j \in \{M,N\}$. The derivation of (119) relies on the additional assumptions that $\lim_{x\to\infty} e^x f^0(x) = 0$ and $\lim_{x\to\infty} e^x l^0_{ij}(x,a) = 0$, which imply $\lim_{\tilde{x}\to\infty} e^{\tilde{x}}\tilde{\ell}_{ij}(\tilde{x},a,t) = 0$ and hence

$$\int_{-\infty}^{\infty} e^{\tilde{x}}\frac{\partial \tilde{\ell}_{ij}(\tilde{x},a,t)}{\partial \tilde{x}}d\tilde{x} = -\int_{-\infty}^{\infty} e^{\tilde{x}}\tilde{\ell}_{ij}(\tilde{x},a,t)\,d\tilde{x} = -\frac{\mathcal{Z}_{ij}(a,t)}{\mathcal{Z}_{\underline{a}^w}(t)}.$$

The left-hand side of (119) can be approximated as

$$\frac{\partial \mathcal{Z}_{ij}(a,t)}{\partial t} + \frac{\partial \mathcal{Z}_{ij}(a,t)}{\partial a} = \frac{\mathcal{Z}_{ij}(a,t) - \mathcal{Z}_{ij}(a-\Delta, t-\Delta)}{\Delta},$$

where $\Delta$ is the age-time step for discretization. By the backward finite-difference method, we can approximate the system of PDEs (119) with (limit) boundary conditions $\mathcal{Z}_{iN}\left(\underline{a}^w, t\right) = \lim_{a\downarrow\underline{a}^w}\mathcal{Z}_{iM}(a,t) = \mathcal{Z}_{\underline{a}^w}(t)\int_{-\infty}^{\infty} e^{\tilde{x}}\tilde{f}(\tilde{x})\,d\tilde{x}$ by the following system of difference equations in matrix form:

$$\underbrace{\begin{bmatrix} \mathcal{D}_{LH,M}(a,t) & \mathcal{C}_{LH,M}(a,t) & \mathcal{E}_H(a,t) & 0 \\ \mathcal{C}_{HL,M}(a,t) & \mathcal{D}_{HL,M}(a,t) & 0 & \mathcal{E}_L(a,t) \\ 0 & 0 & \mathcal{D}_{LH,N}(a,t) & \mathcal{C}_{LH,N}(a,t) \\ 0 & 0 & \mathcal{C}_{HL,N}(a,t) & \mathcal{D}_{HL,N}(a,t) \end{bmatrix}}_{\Xi(a,t)} \underbrace{\begin{bmatrix} \mathcal{Z}_{HM}(a,t) \\ \mathcal{Z}_{LM}(a,t) \\ \mathcal{Z}_{HN}(a,t) \\ \mathcal{Z}_{LN}(a,t) \end{bmatrix}}_{\mathrm{Z}(a,t)} = \underbrace{\begin{bmatrix} \mathcal{Z}_{HM}(a-\Delta,t-\Delta) \\ \mathcal{Z}_{LM}(a-\Delta,t-\Delta) \\ \mathcal{Z}_{HN}(a-\Delta,t-\Delta) \\ \mathcal{Z}_{LN}(a-\Delta,t-\Delta) \end{bmatrix}}_{\mathrm{Z}(a-\Delta,t-\Delta)}, \tag{120}$$

with, for $i, i' \in \{H, L\}$, $i' \neq i$, and $j \in \{M, N\}$,

$$\begin{aligned} \mathcal{C}_{i'i,j}(a,t) &= -\omega_{i'i,j}(a,t)\frac{\mathcal{Q}_{i'j}(a,t)}{\mathcal{Q}_{ij}(a,t)}\Delta, \\ \mathcal{E}_i(a,t) &= -\frac{\lambda_N(a,t)\,\Omega(a,t)}{1-\Omega(a,t)}\frac{\mathcal{Q}_{iN}(a,t)}{\mathcal{Q}_{iM}(a,t)}\Delta, \\ \mathcal{D}_{i'i,j}(a,t) &= 1-[\mu_i-\eta(a)]\Delta-\mathcal{C}_{i'i,j}(a,t)-\mathbb{I}_{j=M}\mathcal{E}_i(a,t), \end{aligned}$$

where the growth-state transition intensities $\omega_{HL,j}(a,t)$ and $\omega_{LH,j}(a,t)$ are time-dependent because of the time-varying career impacts of motherhood $\gamma(t)$ and $\theta(t)$. Since $\mathcal{Z}_{ij}\left(\underline{a}^w,t\right)$ and $\mathcal{Z}_{\underline{a}^w}(t)$ grow at the same rate, namely $\varphi\mathcal{H}(t)$ by Lemma 3, we can approximate the dynamics of $\mathcal{Z}_{ij}\left(\underline{a}^w,t\right)$ as $\frac{\mathcal{Z}_{ij}\left(\underline{a}^w,t\right)-\mathcal{Z}_{ij}\left(\underline{a}^w,t-\Delta\right)}{\Delta} = \varphi\mathcal{H}(t)\,\mathcal{Z}_{ij}\left(\underline{a}^w,t\right)$, which implies

$$\mathcal{Z}_{ij}\left(\underline{a}^w,t\right) = \frac{\mathcal{Z}_{ij}\left(\underline{a}^w,t-\Delta\right)}{1-\varphi\mathcal{H}(t)\Delta} = \frac{\mathcal{Z}_{\underline{a}^w}(t-\Delta)\int_{-\infty}^{\infty}e^{\tilde{x}}\tilde{f}(\tilde{x})\,d\tilde{x}}{1-\varphi\mathcal{H}(t)\Delta}, \tag{121}$$

where $\mathcal{H}(t)$ is given by (40). I calibrate the initial boundary value as

$$\begin{aligned} \mathcal{Z}^0_{\underline{a}^w}\int_{-\infty}^{\infty}e^{\tilde{x}}\tilde{f}(\tilde{x})\,d\tilde{x} = &\left\{\mathcal{Z}^0_{HN}\left(\underline{a}^w\right)h^0_N\left(\underline{a}^w\right)+\mathcal{Z}^0_{LN}\left(\underline{a}^w\right)\left[1-h^0_N\left(\underline{a}^w\right)\right]\right\}\Omega^0\left(\underline{a}^w\right) \\ &+\left\{\mathcal{Z}^0_{HM}\left(\underline{a}^w\right)h^0_M\left(\underline{a}^w\right)+\mathcal{Z}^0_{LM}\left(\underline{a}^w\right)\left[1-h^0_M\left(\underline{a}^w\right)\right]\right\}\left[1-\Omega^0\left(\underline{a}^w\right)\right]. \end{aligned}$$

For $i \in \{H, L\}$ and $j \in \{M, N\}$, given initial condition $\mathcal{Z}^0_{ij}$, the path $\left\{\mathcal{Z}_{ij}(\cdot,t)\right\}_t$ can be computed iteratively using $\mathrm{Z}(a,t) = \Xi(a,t)^{-1}\mathrm{Z}(a-\Delta,t-\Delta)$ and (121), where matrix $\Xi(a,t)$ is defined in (120), the paths $\left\{\gamma(t),\theta(t),\Omega(\cdot,t),h_j(\cdot,t)\right\}_t$ are computed as described in Online Appendix B.2.1, and the path $\{p(\cdot,t)\}_t$—used in the computation of $\{\mathcal{H}(t)\}_t$—is computed as described in Online Appendix B.2.3. The model-generated path of income by age $\{\widehat{y}(\cdot,t)\}_t$ can then be computed using (42). To solve the distance-minimization problem $\min_{\mu_H,\varphi}\int_{25}^{\tilde{a}^w}[y(a,2019)-\widehat{y}(a,2019)]^2\,da$, I conduct a grid search over $(\mu_H,\varphi)$ using 50 grid points for each parameter.

## B.3 MODEL VALIDATION RESULTS

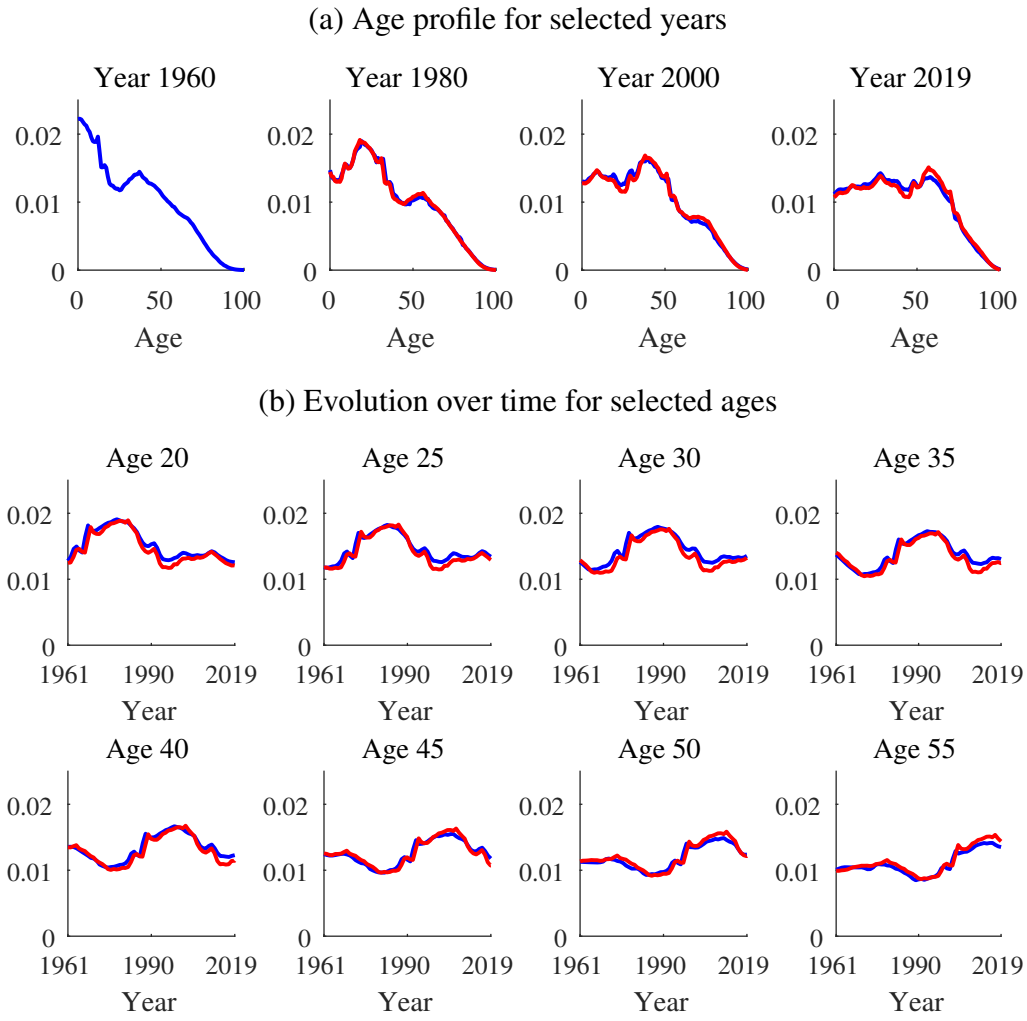



FIGURE 14: POPULATION AGE PROFILE $\wp(a,t)$, DATA VERSUS MODEL

*Notes:* Panel (a) shows the population age profile in 1960 and, for three additional years at roughly 20-year intervals, compares the data (blue lines) with the calibrated model (red lines). Panel (b) shows, for eight selected working ages, the evolution over 1961–2019 of each age group's population share in the data (blue lines) and in the calibrated model (red lines). The y-axes report percentage shares of total population for one-year age groups.

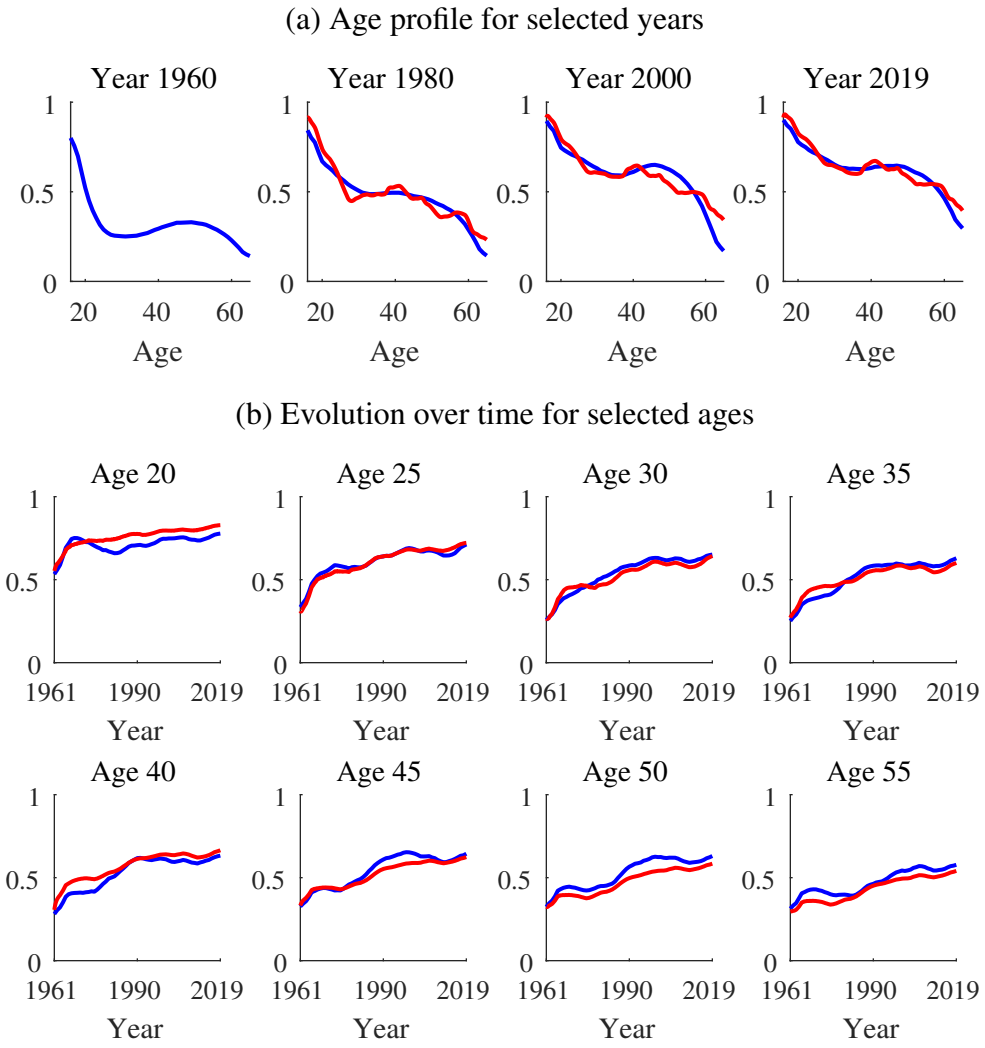



FIGURE 15: HIGH-GROWTH SHARES BY AGE $H(a,t)$, DATA VERSUS MODEL

*Notes:* Panel (a) shows the high-growth shares by age in 1960 and, for three additional years at roughly 20-year intervals, compares the data (blue lines) with the calibrated model (red lines). Panel (b) shows, for eight selected working ages, the evolution over 1961–2019 of the high-growth shares in the data (blue lines) and in the calibrated model (red lines).

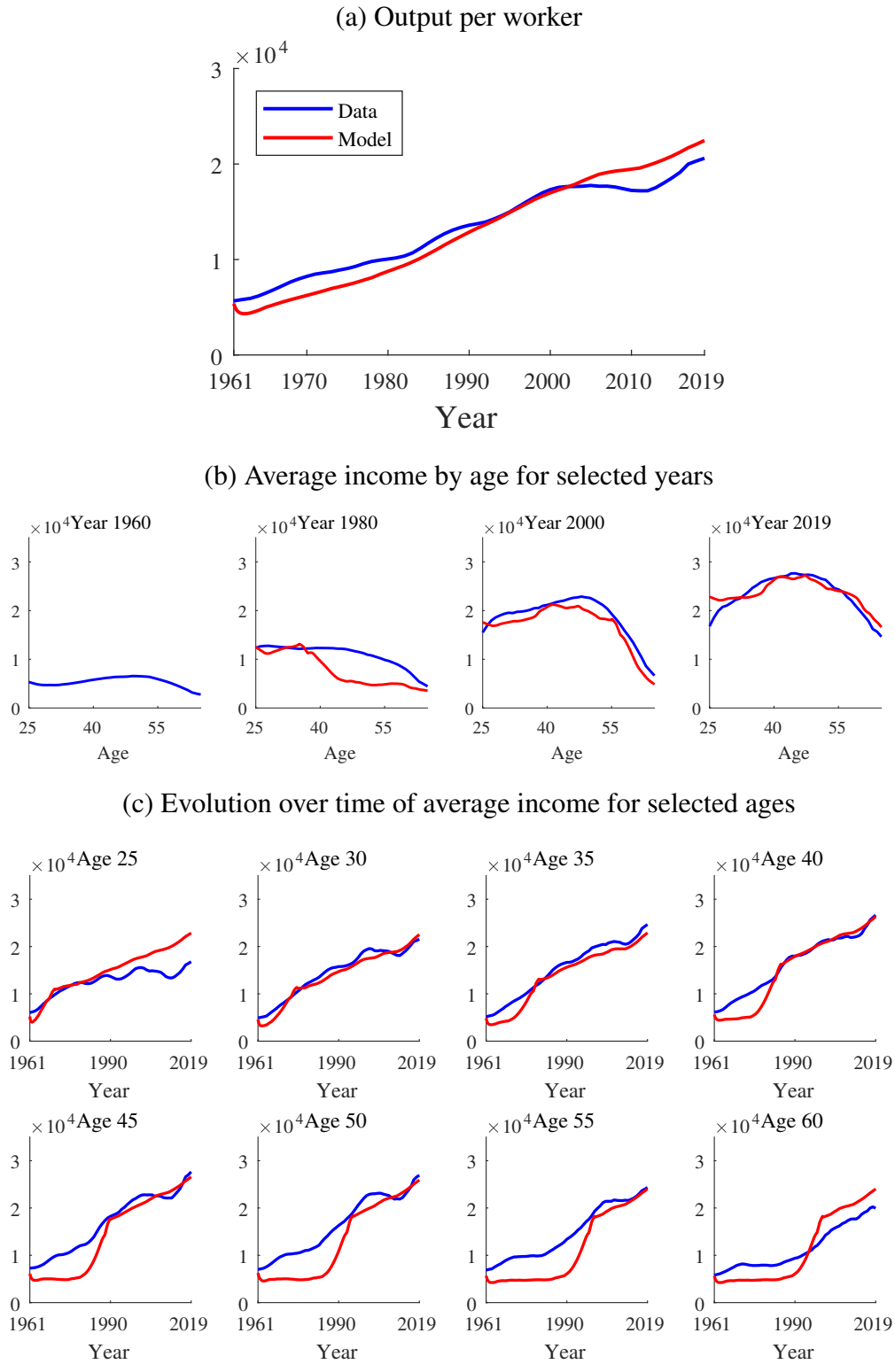



FIGURE 16: INCOME DYNAMICS, DATA VERSUS MODEL

*Notes:* Panel (a) plots output per worker $Y(t)/P^w(t)$, which corresponds empirically to mean annual wage earnings. Panel (b) shows the income-by-age profile $y(a,t)$ in 1960 and, for three additional years at roughly 20-year intervals, compares the data (blue lines) with the calibrated model (red lines). Panel (c) shows, for eight selected working ages, the evolution over 1961–2019 of average annual income in the data (blue lines) and in the calibrated model (red lines). Income is measured in constant 1999 dollars.

## B.4 Growth decomposition

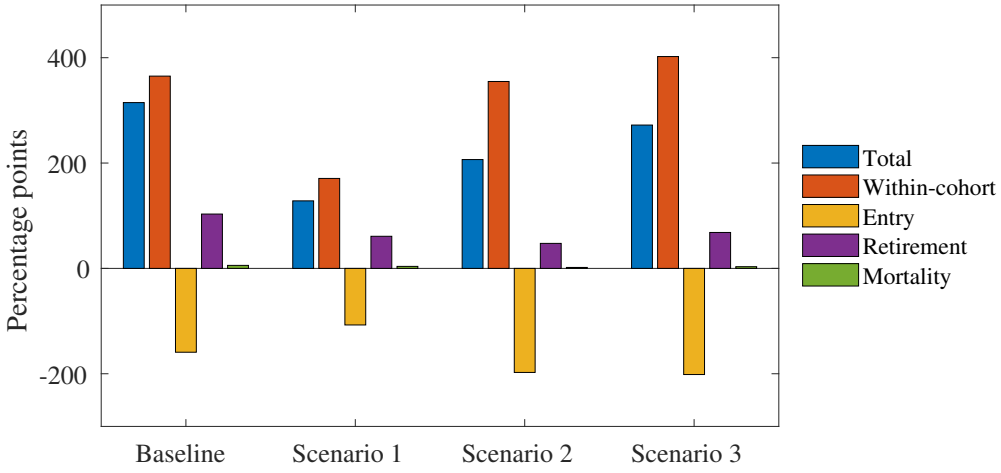



Figure 17: Decomposition of the 1961–2019 change in output per worker

*Notes:* This figure plots the decomposition (47) of the 1961–2019 change in output per worker $Y(t)/P^w(t)$ into various margins. The baseline case maintains the calibrated parameter values given by Table 4. The counterfactual Scenarios 1–3 are defined in Section 3.3. The entry margin is negative when $y\left(\underline{a}^w, t\right) < Y(t)/P^w(t)$; the retirement margin is positive when $y\left(\bar{a}^w, t\right) < Y(t)/P^w(t)$.

## B.5 Welfare assessment

### B.5.1 Derivation of CEV decomposition (56)

For $a \in \left[0, \underline{a}^w\right)$, solving (15) with value-matching condition (16), we have

$$V^{\mathcal{Y}}(a, t+a) = \int_a^{\underline{a}^w} e^{-\int_a^{a'}[\rho+\xi(a'')]da''} \log s\left(t+a'\right) da' + e^{-\int_a^{\underline{a}^w}[\rho+\xi(a')]da'} \int_{-\infty}^{\infty} \left[\sigma V_{HN}\left(x, \underline{a}^w, t+\underline{a}^w\right) + (1-\sigma) V_{LN}\left(x, \underline{a}^w, t+\underline{a}^w\right)\right] f\left(x, t+\underline{a}^w\right) dx.$$

Therefore, the lifetime utility of a cohort-$t$ newborn is

$$\begin{aligned}
\mathcal{V}(t) &= \int_0^{\underline{a}^w} e^{-\int_0^{a'}[\rho+\xi(a'')]da''} \log s\left(t+a'\right) da' \\
&\quad + e^{-\int_0^{\underline{a}^w}[\rho+\xi(a')]da'} \int_{-\infty}^{\infty} \left[\sigma V_{HN}\left(x, \underline{a}^w, t+\underline{a}^w\right) + (1-\sigma) V_{LN}\left(x, \underline{a}^w, t+\underline{a}^w\right)\right] f\left(x, t+\underline{a}^w\right) dx \\
&= \int_0^{\underline{a}^w} e^{-\int_0^{a'}[\rho+\xi(a'')]da''} \log s\left(t+a'\right) da' \\
&\quad + e^{-\int_0^{\underline{a}^w}[\rho+\xi(a')]da'} \left[\Pi\left(\underline{a}^w, t+\underline{a}^w\right) \log \mathcal{Z}_{\underline{a}^w}\left(t+\underline{a}^w\right) + \Phi\left(\underline{a}^w, t+\underline{a}^w\right) + \Psi_H\left(\underline{a}^w, t+\underline{a}^w\right)\right] \\
&\quad + e^{-\int_0^{\underline{a}^w}[\rho+\xi(a')]da'} \left[\Pi\left(\underline{a}^w, t+\underline{a}^w\right) \int_{-\infty}^{\infty} \tilde{x} \tilde{f}(\tilde{x}) d\tilde{x} - (1-\sigma) \widehat{\Psi}\left(\underline{a}^w, t+\underline{a}^w\right)\right],
\end{aligned} \tag{122}$$

where we have used (59), (32), and Lemma 3. Note that $\gamma(t)$, $\theta(t)$, and $\kappa_j(\cdot, t)$ for $j \in \{M, N\}$ do not enter the last line of (122).

### B.5.2 Computation of CEV

The computation of cohort-specific CEV is straightforward using (56), except that we need to specify an initial condition for the pension payout to individuals retired before 1961. I assume that this initial pension payout equals 5% of the 1961 aggregate output, declining afterwards at a population-weighted average mortality rate $\bar{\xi}(t)$ given by

$$\bar{\xi}(t) = \int_{\bar{a}^w+t}^{\bar{a}} \xi(a,t) \frac{p(a,t)}{\int_{\bar{a}^w+t}^{\bar{a}} p(a,t)\, da} da.$$

### B.5.3 CEV decomposition

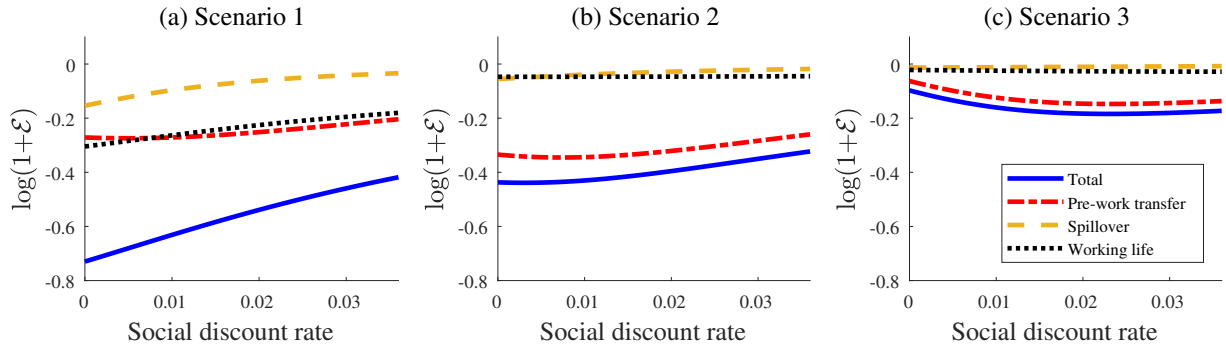



Figure 18: AGGREGATE CEV DECOMPOSITION, HISTORICAL COUNTERFACTUALS

*Notes:* This figure plots $\log(1+\mathcal{E})$, with blue lines, and its three components according to (56); $\mathcal{E}$ is the aggregate welfare change in terms of CEV. Given social discount rate, "Pre-work transfer", "Spillover", and "Working life" add up to "Total", i.e., $\log(1+\mathcal{E})$. Scenarios 1–3 refer to the three historical counterfactuals described in Section 3.3.

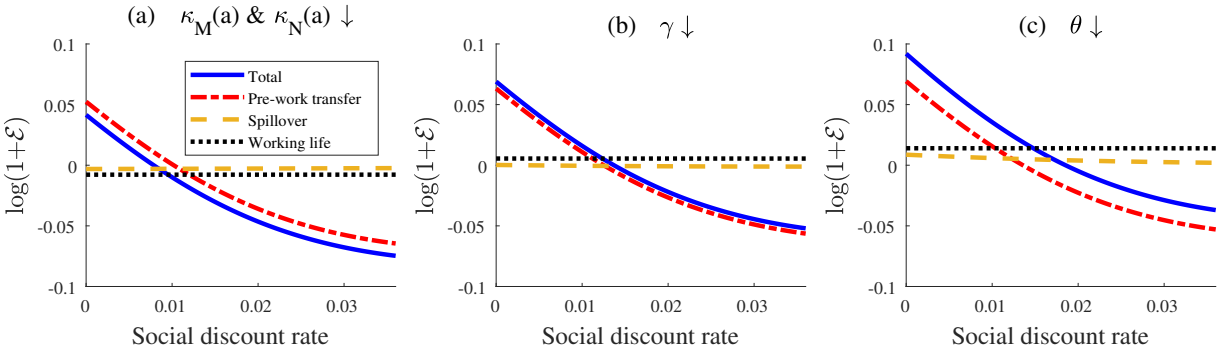



Figure 19: AGGREGATE CEV DECOMPOSITION, INTERVENED FUTURE TRAJECTORIES

*Notes:* This figure plots $\log(1+\mathcal{E})$, with blue lines, and its three components according to (56); $\mathcal{E}$ is the aggregate welfare change in terms of CEV. Given social discount rate, "Pre-work transfer", "Spillover", and "Working life" add up to "Total", i.e., $\log(1+\mathcal{E})$. The interventions correspond to the three one-time, permanent exogenous shocks described in Section 3.4, each calibrated to generate a long-run population growth rate of 0.88% per year.

# References


Carlson, Lauren J., and Natalie D. Shaw. 2019. "Development of Ovulatory Menstrual Cycles in Adolescent Girls." *Journal of Pediatric and Adolescent Gynecology* 32 (3): 249-253.

Edwards, Robert E. 1995. *Functional Analysis: Theory and Applications*. New York: Dover Publications.

Eijkemans, Marinus J.C., Frans van Poppel, Dik F. Habbema, Ken R. Smith, Henri Leridon, and Egbert R. te Velde. 2014. "Too Old to Have Children? Lessons from Natural Fertility Populations." *Human Reproduction* 29 (6): 1304-1312.

Flood, Sarah, Miriam King, Renae Rodgers, Steven Ruggles, J. Robert Warren, Daniel Backman, Etienne Breton, Grace Cooper, Julia A. Rivera Drew, Stephanie Richards, David Van Riper, and Kari C.W. Williams. 2025. IPUMS CPS: Version 13.0. University of Minnesota. Available at https://cps.ipums.org/cps/

Human Fertility Database. Max Planck Institute for Demographic Research and Vienna Institute of Demography. Available at https://www.humanfertility.org

Human Mortality Database. Max Planck Institute for Demographic Research, University of California, Berkeley, and French Institute for Demographic Studies. Available at https://www.mortality.org

Kolmogorov, A.N., and S.V. Fomin. 1975. *Introductory Real Analysis*. New York: Dover Publications.

Ruggles, Steven, Sarah Flood, Matthew Sobek, Daniel Backman, Grace Cooper, Julia A. Rivera Drew, Stephanie Richards, Renae Rodgers, Jonathan Schroeder, and Kari C.W. Williams. 2025. IPUMS USA: Version 16.0. University of Minnesota. Available at https://usa.ipums.org/usa/

Wang, Zifan, Gowtham Asokan, Jukka-Pekka Onnela, Donna D. Baird, Anne Marie Z. Jukic, Allen J. Wilcox, Christine L. Curry, Tyler Fischer-Colbrie, Michelle A. Williams, Russ Hauser, Brent A. Coull, Shruthi Mahalingaiah. 2024. "Menarche and Time to Cycle Regularity Among Individuals Born Between 1950 and 2005 in the US." *JAMA Network Open* 7 (5): e2412854.

Wesselink, Amelia K., Kenneth J. Rothman, Elizabeth E. Hatch, Ellen M. Mikkelsen, Henrik T. Sørensen, and Lauren A. Wise. 2017. "Age and Fecundability in a North American Preconception Cohort Study." *American Journal of Obstetrics and Gynecology* 217 (6): 667 e1-8.